

NM1-63

**Permit
Application**

Vol 3

Part 8 of 8

10/12/16

**APPLICATION FOR PERMIT
OWL LANDFILL SERVICES, LLC**

**VOLUME III: ENGINEERING DESIGN AND CALCULATIONS
SECTION 6: GEOSYNTHETICS APPLICATION AND
COMPATIBILITY DOCUMENTATION**

**ATTACHMENT III.6.F
PVC PIPE REFERENCE DOCUMENTATION**

PVC Chemical Resistance

KEY — E = Excellent G = Good L = Limited U = Unsuitable O = No test

Chemical	PVC I		PVC II		Chemical	PVC I		PVC II	
	72°F.	140°F.	72°F.	140°F.		72°F.	140°F.	72°F.	140°F.
Acetaldehyde	U	U	U	U	Beet - Sugar Liquor	E	E	E	E
Acetamide	O	O	U	U	Benzaldehyde	U	U	U	U
Acetate Solvents - Crude	U	U	U	U	Benzene	U	U	U	U
Acetate Solvents - Pure	U	U	U	U	Benzenesulfonic Acid - 10%	E	E	E	E
Acetic Acid 0-10%	E	E	G	L	Benzenesulfonic Acid	U	U	U	U
Acetic Acid 10-20%	E	E	G	L	Benzoic Acid	E	E	E	E
Acetic Acid 20-30%	E	G	G	L	Benzol	U	U	U	U
Acetic Acid 30-60%	E	E	G	L	Bismouth Carbonate	E	E	E	E
Acetic Acid 80%	G	L	L	L	Black Liquor (Paper Industry)	E	E	E	E
Acetic Acid - Glacial	G	U	L	U	Bleach - 12.5% Active Cl ₂	E	G	G	L
Acetic Acid - Vapors	E	U	U	U	Borax	E	E	E	E
Acetic Anhydride	U	U	U	U	Borax Liquors	E	E	E	E
Acetone	U	U	U	U	Boric Acid	E	E	E	E
Acetylene	L	L	U	U	Boron, TriFluoride	E	E	E	E
Adipic Acid	E	E	E	E	Breeder Pellets - Fish Deriv.	E	E	E	E
Alcohol - Allyl - 96%	G	L	L	U	Brine	E	E	E	E
Alcohol - Amyl	E	L	L	U	Bromic Acid	E	E	E	E
Alcohol - Butyl	E	G	L	U	Bromine - Liquid	U	U	U	U
Alcohol - Ethyl	E	E	L	G	Bromine (Gas) - 25%	U	U	U	U
Alcohol - Methyl	E	E	E	E	Bromine - Water	E	E	L	U
Alcohol - Propargyl	E	E	E	E	Butadiene	E	E	E	U
Alcohol - Propyl	E	E	E	G	Butane	E	E	E	E
Allyl - Chloride	U	U	U	U	Butane, Butylene	E	E	E	U
Alum	E	E	E	E	Butane, Diol	E	E	E	U
Alum, Ammonium	E	E	E	E	Butanol	E	U	U	U
Alum, Chrome	E	E	E	E	Butanol - Primary	E	E	U	U
Alum, Potassium	E	E	E	E	Butanol - Secondary	E	L	U	U
Aluminum Chloride	E	E	E	E	Butter milk	E	E	E	U
Aluminum Fluoride	E	E	E	E	Butyl Acetate	U	U	U	U
Aluminum Hydroxide	E	E	E	E	Butyl Phenol	E	U	L	U
Aluminum Oxychloride	E	E	E	E	Butylene	E	O	E	O
Aluminum Nitrate	E	E	E	E	Butynediol (Erthritol)	E	U	U	U
Aluminum Sulfate	E	E	E	E	Butyric Acid 20%	G	U	U	U
Ammonia - Dry Gas	E	E	E	E	Butyric Acid	E	U	L	U
Ammonia, Aqua (10%)	E	E	E	E	Calcium Bisulfide	E	E	E	E
Ammonia - Liquid	L	U	O	O	Calcium Bisulfite	E	E	E	E
Ammonium Acetate	E	E	E	E	Calcium Carbonate	E	E	E	E
Ammonium BiFluoride	E	E	E	E	Calcium Chlorate	E	E	E	E
Ammonium Carbonate	E	E	E	E	Calcium Chloride	E	E	E	E
Ammonium Chloride	E	E	E	E	Calcium Hydroxide	E	E	E	E
Ammonium Fluoride - 25%	E	L	U	U	Calcium Hypochlorite	E	E	E	E
Ammonium Hydroxide - 28%	E	E	E	E	Calcium Nitrate	E	E	E	E
Ammonium Metaphosphate	E	E	E	E	Calcium Oxide	E	E	E	U
Ammonium Monophosphate	E	E	E	E	Calcium Sulfate	E	E	E	E
Ammonium Nitrate	E	E	E	E	Cane Sugar Liquors	E	E	E	E
Ammonium Persulfate	E	E	E	E	Carbic Acid	E	U	E	U
Ammonium Phosphatel (Ammoniacal)	E	E	O	O	Carbon Bisulfide	U	U	U	U
Ammonium Phosphate - Neutral	E	E	E	E	Carbon Dioxide (Aqueous S.L.)	E	E	E	E
Ammonium Sulfate	E	E	E	E	Carbon Dioxide Gas (Wet)	E	E	E	E
Ammonium Sulfide	E	E	E	E	Carbon Monoxide	E	E	E	E
Ammonium Thiocyanate	U	U	U	U	Carbon Tetrachloride	L	U	U	U
Amyl Acetate	U	U	U	U	Carbonated Water	E	E	E	E
Amyl Chloride	U	U	U	U	Carbonic Acid	E	E	E	E
Aniline	U	U	U	U	Casein	E	E	E	E
Aniline Chlorohydrate	U	U	U	U	Castor Oil	E	E	E	E
Aniline Dyes	U	U	U	U	Caustic Potash	E	E	E	E
Aniline Hydrochloride	U	U	U	U	Caustic Soda	E	E	E	E
Anthraquinone	E	E	E	L	Cellosolve	G	L	L	U
Anthraquinonesulfonic Acid	E	E	E	E	Chloracetic Acid	E	E	E	U
Anitimony Trichloride	E	E	E	E	Chloral Hydrate	E	E	E	E
Aqua Regia	E	L	U	U	Chloric Acid 20%	E	E	E	E
Arsenic Acid - 80%	E	G	U	G	Chlorinated Solvents	U	U	U	U
Arylsulfonic Acid	E	E	L	E	Chlorine (Dry)	E	L	L	L
Asphalt	E	E	E	E	Chlorine Gas (Moist)	G	L	L	L
Barium Carbonate	E	E	E	E	Chlorine Water	E	E	E	E
Barium Chloride	E	E	E	E	Chloroacetic Acid	E	E	E	U
Barium Hydroxide	E	E	E	E	Chlorobenzene	U	U	U	U
Barium Sulfate	E	E	E	E	Chlorobenzyl Chloride	U	U	U	U
Barium Sulfide	E	E	E	E	Chloro Form	U	U	U	U
Beer	E	E	E	E	Chlorosulfonic Acid (100%)	E	U	O	O
					Chrome Alum	E	E	E	E

CertainTeed EI

Chemical	PVC I		PVC II		Chemical	PVC I		PVC II	
	72 °F.	140 °F.	72 °F.	140 °F.		72 °F.	140 °F.	72 °F.	140 °F.
Chromic Acid 10%	E	E	E	E	Gas - Natural (Wet)	E	E	E	E
Chromic Acid 25%	E	L	G	L	Gasoline (Leaded)	E	E	E	E
Chromic Acid 30%	E	L	G	L	Gasoline (unleaded)	E	E	E	E
Chromic Acid 40%	E	L	L	L	Gasoline - Refined	E	E	E	E
Chromic Acid 50%	E	L	L	L	Gasoline - Sour	E	E	E	E
Citric Acid	E	E	E	E	Gelatin	E	E	E	E
Coconut Oil	E	E	E	E	Glucose	E	E	E	E
Coke Oven Gas	E	E	E	E	Glycerine (Glycerol)	E	E	E	E
Copper Carbonate	E	E	E	E	Glycol	E	E	E	E
Copper Chloride	E	E	E	E	Glue	E	E	E	E
Copper Cyanide	E	E	E	E	Glycolic Acid 30%	E	E	E	E
Copper Fluoride	E	E	E	E	Green Liquor (Paper Industry)	E	E	E	E
Copper Nitrate	E	E	E	E	Heptane	E	G	L	U
Copper Sulfate	E	E	E	E	Hexane	E	L	L	U
Care Oils	E	E	E	E	Hexanol Tertiary	E	L	L	U
Corn Oil	E	E	E	E	Hydrobromic Acid - 20%	E	E	E	E
Corn Syrup	E	E	E	E	Hydrochloric Acid - 0-25%	E	G	E	E
Cottonseed Oil	E	E	E	E	Hydrochloric Acid - 25-40%	E	E	E	E
Cresol	U	U	U	U	Hydrocyanic Acid or				
Cresylic Acid 50%	U	U	L	U	Hydrogen Cyanide	E	E	E	E
Croton Aldehyde	U	U	U	U	Hydrofluoric Acid 4%	E	L	G	G
Crude Oil - Sour	E	E	E	E	Hydrofluoric Acid 10%	E	L	L	U
Crude Oil - Sweet	E	E	E	E	Hydrofluoric Acid 48%	E	L	G	U
Cuprous Chloride	E	E	E	E	Hydrofluoric Acid 60%	E	L	L	U
Cyclohexane	U	U	U	U	Hydrofluoric Acid 100%	G	L	G	U
Cyclohexanol	U	U	U	U	Hydrogen	E	E	E	E
Cyclohexanon	U	U	U	U	Hydrogen Peroxide - 30%	E	E	E	E
Demineralized Water	E	E	E	E	Hydrogen Peroxide - 50%	E	E	E	E
Dextrin	E	E	E	E	Hydrogen Peroxide - 90%	E	E	U	U
Dextrose	E	E	E	E	Hydrogen Sulfide - Aqueous				
Diazo Salts	E	E	E	E	Solution	E	E	E	E
Diesel Fuels	E	E	E	E	Hydrogen Sulfide - Dry	E	E	E	E
Diethy Amine	U	U	U	U	Hydroquinone	E	E	E	E
Diethylphthalate	U	U	U	U	Hydroxylamine Sulfate	E	E	E	E
Disodium Phosphate	U	U	U	U	Hypochlorous Acid	E	E	E	E
Diethyl Ether	U	U	U	U	Hypo-(Sodium Thiosulfate)	E	E	E	E
Diglycolic Acid	E	E	E	E	Iodine	U	U	U	U
Dioxane - 1,4	O	O	O	O	Iodine (in Alcohol)	U	U	U	U
Divinyl Benzene	O	O	O	O	Iodine Solution (10%)	U	U	U	U
Drying Oil	O	O	O	O	Iodoform	O	O	O	O
Ethers	U	U	U	U	Isopropylalcohol	E	E	E	E
Ethyl Acetate	U	U	U	U	Jet Fuels, JP4 & JP5	E	E	E	E
Ethyl Acrylate	U	U	U	U	Kerosene	E	E	E	E
Ethyl Chloride	U	U	U	U	Ketones	U	U	U	U
Ethyl Ether	U	U	U	U	Kraft Liquor (Paper Industry)	E	E	E	E
Ethylene Bromide	U	U	U	U	Lacquer Thinners	L	U	L	U
Ethylene Chlorohydrin	U	U	U	U	Lactic Acid 28%	E	E	E	E
Ethylene Dichloride	U	U	U	U	Lard Oil	E	E	E	E
Ethylene Glycol	E	E	E	E	Lauric Acid	E	E	E	E
Ethylene Oxide	U	U	U	U	Lauryl Chloride	E	E	E	E
Fatty Acide	E	E	E	E	Lauryl Sulfate	E	E	E	E
Ferric Chloride	E	E	E	E	Lead Acetate	E	E	E	E
Ferric Nitrate	E	E	E	E	Lime Sulfur	E	E	E	E
Ferric Sulfate	E	E	E	E	Linoleic Acid	E	E	E	E
Ferrous Nitrate	E	E	E	E	Linseed Oil	E	E	E	E
Fish Solubles	E	E	E	E	Liquers	E	E	E	E
Flourine Gas - Dry	L	U	U	U	Liquors	E	E	E	E
Flourine Gas - Wet	L	U	U	U	Lithium Bromide	E	E	E	E
Fluoroboric Acid - 25%	E	E	E	E	Lubricating Oil	E	E	E	E
Fluorosilicic Acid	E	E	E	E	Machine Oil	E	E	E	E
Formaldehyde	E	G	G	L	Magnesium Carbonate	E	E	E	E
Food Products such as Milk, Buttermilk, Molasses, Salad Oils, Fruit	E	E	E	E	Magnesium Chloride	E	E	E	E
Formic Acid	E	U	E	U	Magnesium Citrate	E	E	E	E
Freon - 12	E	G	E	G	Magnesium Hydroxide	E	E	E	E
Fructose	E	E	E	E	Magnesium Nitrate	E	E	E	E
Fruit Pulps and Juices	E	E	E	E	Magnesium Sulfate	E	E	E	E
Fuel Oil (containing H ₂ SO ₄)	E	E	E	E	Maleic Acid	E	E	E	E
Furfural	U	U	U	U	Malic Acid	E	E	E	E
Gallic Acid	E	E	E	E	Mercuric Chloride	E	E	G	G
Gas - Coke Oven	E	E	G	G	Mercuric Cyanide	E	E	G	G
Gas - Manufactured	U	U	U	U	Mercurous Nitrate	E	E	G	G
Gas - Natural (Dry)	E	E	E	E	Mercury	E	E	G	G

CertainTeed

Chemical	PVC I		PVC II		Chemical	PVC I		PVC II	
	72 °F.	140 °F.	72 °F.	140 °F.		72 °F.	140 °F.	72 °F.	140 °F.
Methane	E	E	E	E	Photographic Solutions	E	E	E	E
Methyl Bromide	U	U	U	U	Phthalic Acid	O	O	O	O
Methyl Cellosolve	U	U	U	U	Picric Acid	U	U	U	U
Methyl Chloride	U	U	U	U	Plating Solutions:				
Methyl Chloroform	U	U	U	U	Brass	E	E	E	E
Methyl Ethyl Ketone	U	U	U	U	Cadium	E	E	E	E
Methyl Iso-Butyl Ketone	U	U	U	U	Chromium	E	E	E	E
Methyl Salicylate	E	E	E	E	Copper	E	E	E	E
Methyl Sulfate	E	E	E	E	Gold	E	E	E	E
Methyl Sulfonic Acid	E	E	E	E	Iron	E	E	E	E
Methyl Sulfuric Acid	E	E	E	E	Judium	E	E	E	E
Methylene Chloride	E	E	E	E	Lead	E	E	E	E
Milk	E	E	E	E	Nickel	E	E	E	E
Mineral Oils	E	E	E	E	Rhodium	E	E	E	E
*Mixed Acids (H ₂ SO ₄ & HNO ₃)	E	E	E	E	Silver	E	E	E	E
Molasses	E	E	E	E	Tin	E	E	E	E
Monoethanolamine	E	E	E	E	Zinc	E	E	E	E
Muriatic Acid	E	E	E	E	Potassium Acid Sulfate	E	E	E	E
Naptha	E	E	E	E	Potassium Aluminum Sulfate	E	E	E	E
Napthalene	U	U	U	U	Potassium Alum	E	E	E	E
Natural Gas, Dry & Wet	E	E	E	E	Potassium Antimonate	E	E	E	E
Nickel Acetate	E	E	E	E	Potassium Bicarbonate	E	E	E	E
Nickel Chloride	E	E	E	E	Potassium Bichromate	E	E	E	E
Nickel Nitrate	E	E	E	E	Potassium Bisulfite	E	E	E	E
Nickel Sulfate	E	E	E	E	Potassium Borate 1%	E	E	E	E
Nickel Sulphate	E	E	E	E	Potassium Borate	E	E	E	E
Nicotine	E	E	E	E	Potassium Bromate 10%	E	E	E	E
Nicotine Acid	E	E	E	E	Potassium Bromate	E	E	E	E
Nitric Acid Anhydrous	U	U	U	U	Potassium Bromide	E	E	E	E
Nitric Acid 10%	E	E	E	E	Potassium Carbonate	E	E	E	E
Nitric Acid 20%	E	E	E	E	Potassium Chlorate (ag)	E	E	E	E
Nitric Acid 35%	E	E	E	E	Potassium Chlorate	E	E	E	E
Nitric Acid 40%	E	E	E	E	Potassium Chloride	E	E	E	E
Nitric Acid 60%	E	E	E	E	Potassium Chromate (Aln)	E	E	E	E
Nitric Acid 68%	E	E	E	E	Potassium Chromate (Neut.)	E	E	E	E
Nitric Acid 70%	E	E	E	E	Potassium Chromate 40%	E	E	E	E
Nitric Acid 100%	E	E	E	E	Potassium Cuprocyanide	E	E	E	E
Nitric Acid, Red Fuming	U	U	U	U	Potassium Cyanide	E	E	E	E
Nitrobenzene	U	U	U	U	Potassium Dichromate 40%	E	E	E	E
Nitropropane	U	U	U	U	Potassium Dichromate	E	E	E	E
Nitrous Acid (10%)	E	E	E	E	Potassium Dichrom (Alkaline)	E	E	E	E
Nitrous Oxide	E	E	E	E	Potassium Dichrom (Neutral)	E	E	E	E
Oenol (Unsaturated Alcohol)	E	E	E	E	Potassium Diphosphate	E	E	E	E
Oil and Fats	E	E	E	E	Potassium Ferricyanide	E	E	E	E
Oleic Acid	E	E	E	E	Potassium Ferrocyanide	E	E	E	E
Oleum	U	U	U	U	Potassium Fluoride	E	E	E	E
Oxalic Acid	E	E	E	E	Potassium Hydroxide	E	E	E	E
Oxygen	E	E	E	E	Potassium Hypochlorite	E	E	E	E
Ozone	G	L	U	U	Potassium Iodide	E	E	E	E
Palmitic Acid 10%	E	E	E	E	Potassium Nitrate	E	E	E	E
Palmitic Acid 70%	E	E	E	E	Potassium Perborate	E	E	E	E
Paraffin	E	E	E	E	Potassium Perchlorate	E	E	E	E
Pentane	O	O	O	O	Potassium Perchlorite	E	E	E	E
Paracetic Acid 40%	E	E	E	E	Potassium Permanganate 10%	E	E	E	E
Perchloric Acid 10%	E	E	E	E	Potassium Permanganate 25%	G	L	U	U
Perchloric Acid 15%	E	E	E	E	Potassium Persulfate	E	E	E	E
Perchloric Acid 70%	E	E	E	E	Potassium Sulfate	E	E	E	E
Perchloroethylene	O	O	O	O	Potassium Sulfide	E	E	E	E
Petrolatum	E	E	E	E	Potassium Thiosulfate	E	E	E	E
Phenol	E	E	E	E	Propane	E	E	E	E
Phenol (90%)	L	U	U	U	Propylene Dichloride	U	U	U	U
Phenylhydrazine	U	U	U	U	Propylene Glycol	E	E	E	E
Phenylhydrazine Hydrochloride	E	U	L	U	Pyrogalllic Acid	O	O	O	O
Phosgene (Gas)	E	U	L	U	Rayon Coagulating Bath	E	E	E	E
Phosgene (Liquid)	E	U	L	U	Rachelle Salts	E	E	E	E
Phosphoric Acid 0-25%	E	E	E	E	Sea Water	E	E	E	E
Phosphoric Acid 25-50%	E	E	E	E	Salen's Acid (Aqueous)	O	O	O	O
Phosphoric Acid 50-75%	E	E	E	E	Salicylaldehyde	O	O	O	O
Phosphoric Acid - 85%	E	E	E	E	Salt Water	E	E	E	E
Phosphorous (Yellow)	E	E	E	E	Selenic Acid	E	E	E	E
Phosphorous (Red)	E	E	E	E	Sewage	E	E	E	E
Phosphorous Pentoxide	E	E	E	E	Sillicic Acid	E	E	E	E
Phosphorous Trichloride	E	E	E	E	Silver Cyanide	E	E	E	E
Photographic Chemicals	E	E	E	E	Silver Nitrate	E	E	E	E
					Silver Sulfate	E	E	E	E
					Soap Solution	E	E	E	E

*Use PVC 1120

CertainTeed

Chemical	PVC I		PVC II		Chemical	PVC I		PVC II	
	72°F.	140°F.	72°F.	140°F.		72°F.	140°F.	72°F.	140°F.
Soaps	E	E	E	E	Sulphuric Acid 50-75%	E	E	E	G
Sodium Acetate	E	E	E	E	Sulphuric Acid 75-90%	E	E	L	L
Sodium Alum	E	E	E	E	Sulphuric Acid 95%	E	G	U	U
Sodium Acid Sulfate	E	E	E	E	Sulphurous Acid	G	U	L	U
Sodium Aluminate	E	E	E	E	Tan Oil	E	E	E	E
Sodium Antimonate	E	E	E	E	Tannic Acid	E	E	E	E
Sodium Arsenite	E	E	E	E	Tanning Liquors	E	E	E	E
Sodium Benzoate	E	E	E	E	Tartaric Acid	E	E	E	E
Sodium Bicarbonate	E	E	E	E	Tetrachloroethane	O	O	O	O
Sodium Bisulfate	E	E	E	E	Tetraethyl Lead	E	G	G	L
Sodium Bisulfite	E	E	E	E	Tetrahydro Furane	U	U	U	U
Sodium Borate	E	E	E	E	Thionyl Chloride	U	U	U	U
Sodium Bromide	E	E	E	E	Tepineol	G	L	G	L
Sodium Carbonate (Soda Ash)	E	E	E	E	Tin Chloride	E	E	E	E
Sodium Chlorate	E	G	G	L	Titanium Tetrachloride	E	U	U	U
Sodium Chloride	E	E	E	E	Toluol or Toluene	U	U	U	U
Sodium Chlorite	E	E	O	O	Toxaphene (90%)	O	O	O	O
Sodium Cyanide	E	E	E	E	Tributyl Phosphate	U	U	U	U
Sodium Dichromate	E	E	E	E	Trichloroacetic Acid	E	E	E	E
Sodium Dichromate (Neutral)	E	E	E	E	Trichloroethylene	U	U	U	U
Sodium Ferricyanide	E	E	E	E	Tricresylphosphate	U	U	U	U
Sodium Ferrocyanide	E	E	E	E	Triethanolamine	E	E	G	G
Sodium Fluoride	E	E	E	E	Triethylamine	E	G	G	L
Sodium Hydroxide 10%	E	E	E	E	Trimethyl Propane	E	E	E	E
Sodium Hydroxide 15%	E	E	E	E	Trisodium Phosphate	E	E	E	E
Sodium Hydroxide 35%	E	E	E	E	Turpentine	E	E	E	U
Sodium Hydroxide 70%	E	E	O	O	Urea	E	E	E	E
Sodium Hydroxide (Satr)	E	E	E	E	Urine	E	E	E	E
Sodium Hypochlorite	E	E	E	E	Vegetable Oil	E	E	E	E
Sodium Iodide	E	E	E	E	Vinegar	E	E	E	U
Sodium Nitrate	E	E	E	E	Vinyl Acetate	U	U	U	U
Sodium Nitrite	E	E	E	E	Water - Acid Mine	E	E	E	E
Sodium Perborate	E	E	O	O	Water - Distilled	E	E	E	E
Sodium Peroxide	E	E	E	E	Water - Fresh	E	E	E	E
Sodium Phosphate	E	E	E	E	Water - Salt	E	E	E	E
Sodium Phosphate - Acid	E	E	E	G	Water - Sewage	E	E	E	E
Sodium Silicate	E	E	E	E	Whiskey	E	E	E	E
Sodium Sulfate	E	E	E	E	White Gasoline	E	E	E	E
Sodium Sulfide	E	E	E	E	White Liquor (Paper Industry)	E	E	E	E
Sodium Sulfite	E	E	E	E	Wines	E	E	E	E
Sodium Thiosulfate (Hypo)	E	E	E	E	Xylene or Xylol	U	U	U	U
Sour Crude Oil	E	E	E	E	Zinc Chloride	E	E	E	E
Stannic Chloride	E	E	E	E	Zinc Chromate	E	E	E	E
Stannous Chloride (50%)	E	E	E	E	Zinc Cyanide	E	E	E	E
Stannous Chloride	E	G	E	E	Zinc Nitrate	E	E	E	E
Starch	E	E	E	E	Zinc Sulfate	E	E	E	E
Stearic Acid	E	E	E	E	Mixtures of Acids:				
Stoddards Solvent	E	E	U	U	Nitric 15%				
Sulfated Detergents	E	E	E	E	Hydrofluoric 4%	E	E	E	G
Sulfur	E	E	E	E	Sodium Dichromate 13%				
Sulfur Dioxide Gas - Dry	E	E	E	E	Nitric Acid 16				
*Sulfur Dioxide Gas - Wet	E	L	U	U	Water 71%	E	E	E	G
Sulfur Trioxide	E	E	E	G					
Sulphur Dioxide - Liquid	G	U	L	U					
Sulphuric Acid 0-10%	E	E	E	G					
Sulphuric Acid 10-30%	E	E	E	G					
Sulphuric Acid 30-50%	E	E	E	G					

*Use PVC 1120

This information has been obtained from reliable sources and can be used as a guide to assist in the proper application of PVC pipe. CertainTeed, however, cannot warrant its accuracy. It is suggested that you run your own tests for critical applications.

Pipe & Plastics Group

CertainTeed Corporation
P.O. Box 860
Valley Forge, PA 19482
(610) 341-6820
(610) 341-6837 Fax

Code No. 40-10-29

Printed in U.S.A.
0398

**APPLICATION FOR PERMIT
OWL LANDFILL SERVICES, LLC**

**VOLUME III: ENGINEERING DESIGN AND CALCULATIONS
SECTION 7: SETTLEMENT CALCULATIONS**

TABLE OF CONTENTS

Section No.	Title	Page
1.0	INTRODUCTION	III.7-1
1.1	Site Location	III.7-1
1.2	Description	III.7-1
2.0	DESIGN CRITERIA	III.7-2
3.0	FOUNDATION SOILS SETTLEMENT	III.7-2
4.0	WASTE SETTLEMENT CALCULATIONS	III.7-8
5.0	SOIL COVER SETTLEMENT CALCULATIONS.....	III.7-14
6.0	CONCLUSIONS.....	III.7-15

LIST OF FIGURES

Figure No.	Title	Page
III.7.1	SETTLEMENT POINTS.....	III.7-4

LIST OF TABLES

Table No.	Title	Page
III.7.1	SETTLEMENT AND ANGULAR DISTORTION OF FOUNDATION SOILS BETWEEN POINTS, CROSS SECTION A-A'	III.7-6
III.7.2	SETTLEMENT AND ANGULAR DISTORTION OF FOUNDATION SOILS BETWEEN POINTS, CROSS SECTION B-B'	III.7-7
III.7.3	TOTAL SETTLEMENT AND ANGULAR DISTORTION BETWEEN POINTS, CROSS SECTION A-A'	III.7-10
III.7.4	TOTAL SETTLEMENT AND ANGULAR DISTORTION BETWEEN POINTS, CROSS SECTION B-B'	III.7-12
III.7.5	TOTAL SETTLEMENT AND ANGULAR DISTORTION BETWEEN POINTS, CROSS SECTION A-A'	III.7-16
III.7.6	TOTAL SETTLEMENT AND ANGULAR DISTORTION BETWEEN POINTS, CROSS SECTION A-A'	III.7-18

**APPLICATION FOR PERMIT
OWL LANDFILL SERVICES, LLC**

**VOLUME III: ENGINEERING DESIGN AND CALCULATIONS
SECTION 7: SETTLEMENT CALCULATIONS**

LIST OF ATTACHMENTS

Attachment No.	Title
III.7.A	SUMMARY OF GEOTECHNICAL LABORATORY TESTING RESULTS
III.7.B	QIAN, XUEDE; KOERNER, ROBERT M.; AND GRAY, DONALD H. 2002. <i>GEOTECHNICAL ASPECTS OF LANDFILL DESIGN AND CONSTRUCTION</i> . NEW YORK: PRENTICE HALL.
III.7.C	CODUTO, DONALD P. 1998. <i>GEOTECHNICAL ENGINEERING PRINCIPLES AND PRACTICES</i> . NEW JERSEY: PRENTICE HILL.
III.7.D	SHARMA, HARI .D. AND SANGEETA P. LEWIS. 1994. <i>WASTE CONTAINMENT SYSTEMS, WASTE STABILIZATION AND LANDFILLS: DESIGN AND EVALUATION</i> . NEW YORK: JOHN WILEY AND SONS.
III.7.E	STEPHENS, DANIEL B.; HSU, KUO-CHIN; PRIEKSAT, MARK A.; ANKENY, MARK D.; BLANDFORD, NEIL; ROTH, TRACY L.; KELSEY, JAMES A.; WHITWORTH, JULIA R. 1997. A COMPARISON OF ESTIMATED AND CALCULATED EFFECTIVE POROSITY. <i>HYDROGEOLOGY JOURNAL</i> (1998) 6:156–165.

**APPLICATION FOR PERMIT
OWL LANDFILL SERVICES, LLC**

**VOLUME III: ENGINEERING DESIGN AND CALCULATIONS
SECTION 7 SETTLEMENT CALCULATIONS**

1.0 INTRODUCTION

OWL Landfill Services, LLC (OWL) is proposing to permit, construct, and operate a “Surface Waste Management Facility” for oil field waste processing and disposal services. The proposed OWL Facility is subject to regulation under the New Mexico (NM) Oil and Gas Rules, specifically 19.15.36 NMAC, administered by the Oil Conservation Division (OCD). The Facility has been designed in compliance with the requirements of 19.15.36 NMAC, and will be constructed, operated, and closed in compliance with a Surface Waste Management Facility Permit issued by the OCD.

The OWL Facility is one of the first designed to the new more stringent standards that, for instance, mandate double liners and leak detection for land disposal. The new services that OWL will provide fill a necessary void in the market for technologies that exceed current OCD requirements.

1.1 Site Location

The OWL site is located approximately 22 miles northwest of Jal, adjacent to the south of NM 128 in Lea County, NM. The OWL site is comprised of a 560-acre ± tract of land located within a portion of Section 23, Township 24 South, Range 33 East, Lea County, NM (**Figure IV.1.1**). Site access will be provided on the south side of NM 128. The coordinates for the approximate center of the OWL site are Latitude 32.203105577 and Longitude -103.543122319 (surface coordinates).

1.2 Description

The OWL Surface Waste Management Facility will comprise approximately 500 acres of the 560-acre site, and will include two main components: an oil field waste Processing Area and an oil field waste Landfill Disposal Area, as well as related infrastructure. Oil field wastes are anticipated to be delivered to the OWL Facility from oil and gas exploration and production operations in southeastern NM and west Texas. The Permit Plans (**Attachment III.1.A**) identify the locations of the Processing Area and Landfill Disposal Area.

2.0 DESIGN CRITERIA

The slope of the final cover, liner and leachate collection piping after settlement must be consistent with the performance specifications for leachate collection and stormwater control. That is, the final cover and leachate collection system must allow adequate stormwater to runoff to the management controls, and to convey generated leachate such that the head on the primary high density polyethylene (HDPE) flexible membrane liner (FML) does not exceed 12 inches (i.e., 30 centimeters).

3.0 FOUNDATION SOILS SETTLEMENT

The methodology for estimating floor potential settlement involves selecting points on the landfill floor surface, computing the settlement at each point, and evaluating the resultant change in surface elevation. Points were conservatively selected from a cross-section where the waste and fill material is thickest. Qian et al. (2002), present a method to determine landfill foundation settlement that evaluates elastic, primary, and secondary settlement. The foundation soils at the OWL site vary from clays at the deeper southern boundary of the cells to a mixture of poorly graded sand with varying amounts of silt fines and clay to the northern extent. Recent laboratory testing evaluated a mixture of sands and silty sands (i.e., USCS Classifications SP-SM) in the primary excavation area. **Attachment III.7.A** provides a summary of the laboratory testing results compiled from samples at applicable depths from geotechnical borings installed on-site. Foundation soils consisting of silty sands, sandy clays and a mixture of sands and silty sands, elastic settlement is conservatively assumed for this calculation. The elastic settlement is estimated using equation 12.20 from **Attachment III.7.B, p. 469**.

$$Z_e = \left(\frac{\Delta\sigma}{M_s} \right) H_o$$

Where:

- Z_e** = elastic settlement of soil layer (ft)
- H_o** = initial thickness of soil layer (ft)
- Δσ** = increment of vertical effective stress, lb/ft²
- M_s** = constrained modulus of soil, lb/ft²

The constrained modulus is provided in equation 12.21 from **Attachment III.7.B, p. 470**.

$$M_s = \frac{E_s(1 - \nu_s)}{(1 + \nu_s)(1 - 2\nu_s)}$$

Where:

M_s = constrained modulus of soil, lb/ft²

E_s = elastic modulus of soil (lb/ft²) **Attachment III.7.B, p. 310**

E_s was interpolated from the data from Table 9.5, p. 310 (**Attachment III.7.B**) for CL, MH, GC, SC soils between 85% and 95% standard Proctor dry density to determine E_s for 90% as specified in the subgrade soils. E_s = (800 psi + 1,500 psi)/2 = 1,150 psi x 144 in²/ft² = 165,600 lb/ft².

ν_s = Poisson's ratio for soil = 0.39, which was found using the same method to estimate the elastic modulus of soil.

Settlement is estimated at the select locations (Points A1 through A30, and Points B1 through B33) shown on the landfill cross-sections (**Figure III.7.1**). An example calculation is demonstrated at point A15 on Cross Section A-A', with a total overburden depth of 247 ft. (final cover + intermediate cover + waste + protective soil layer).

Point A15

Elastic Foundation Soil Settlement

Thickness of Waste = 241 ft. (assume entire thickness of waste from intermediate cover to top of protective soil layer; this provides a conservative analysis)

Unit Weight of Soil = 120.5 lb/ft³ Dry Density

Unit Weight of Waste = 74 lb/ft³

Δσ = (waste effective stress) + (protective soil layer effective stress) + (intermediate cover effective stress) + (final cover effective stress)

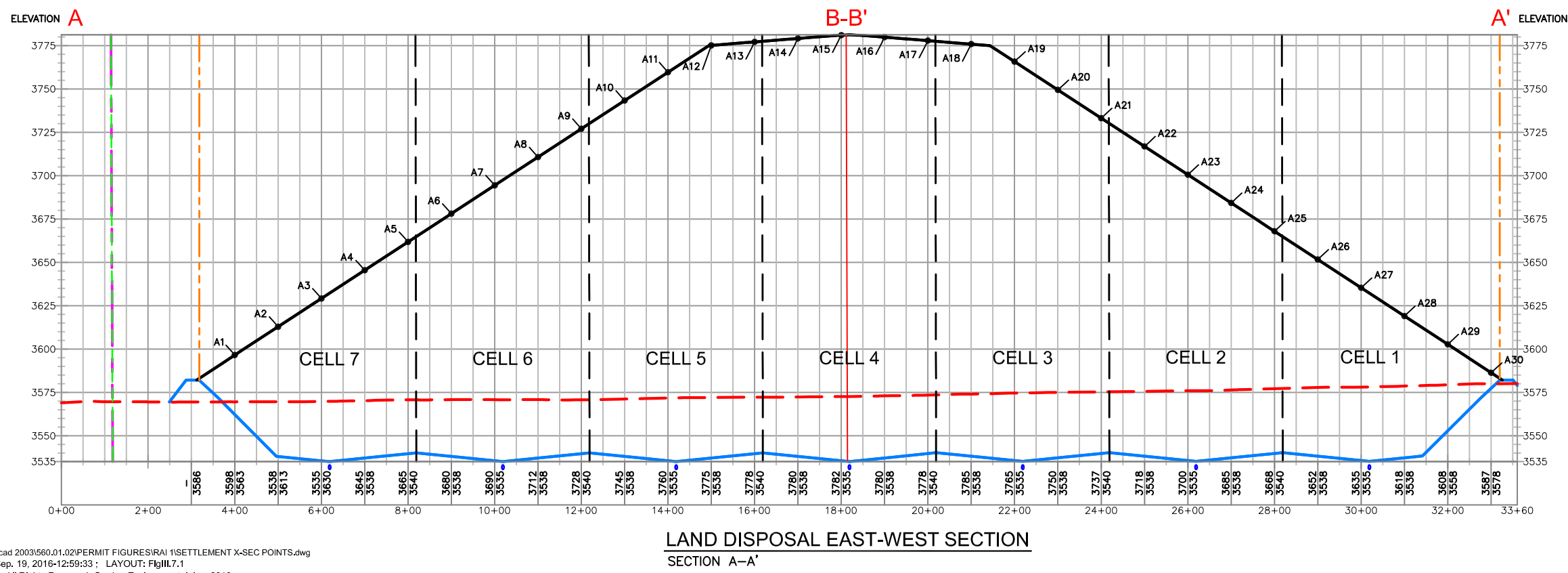
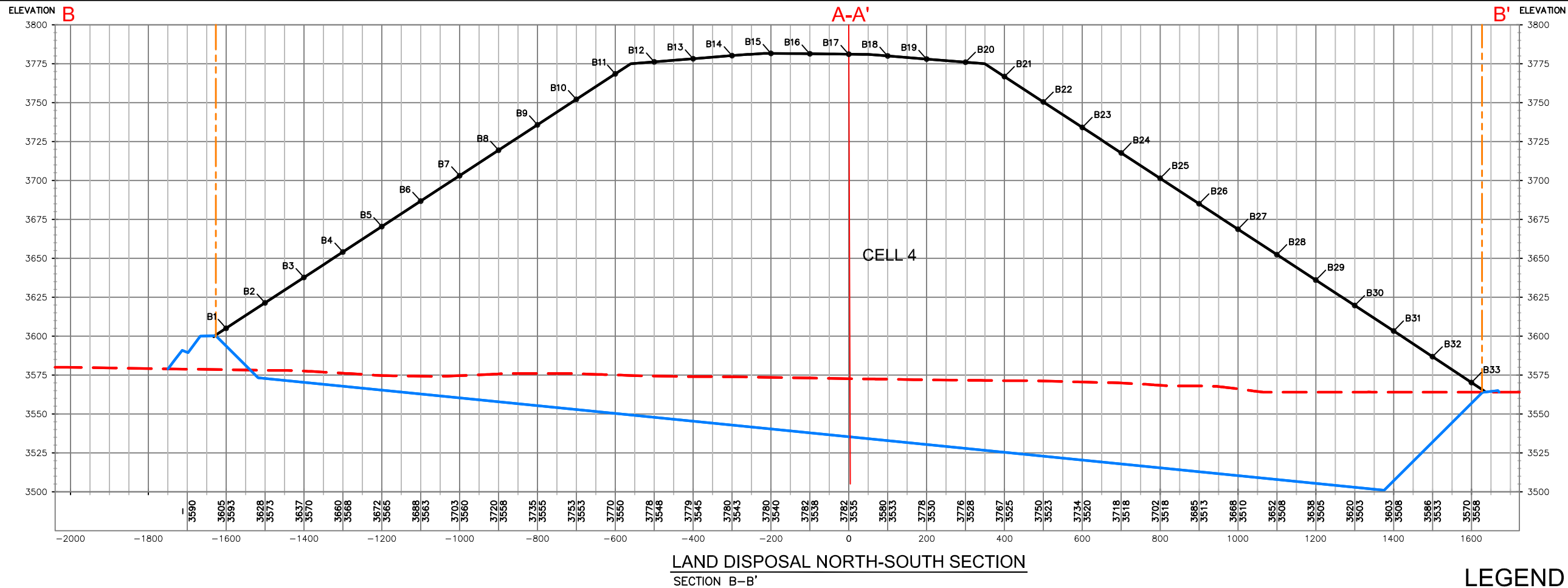
$$\Delta\sigma = (241 \text{ ft})(74 \text{ lb/ft}^3) + (2 \text{ ft})(120.5 \text{ lb/ft}^3) + (1 \text{ ft})(120.5 \text{ lb/ft}^3) + (3.0 \text{ ft})(120.5 \text{ lb/ft}^3) = 18,557 \text{ lb/ft}^2$$

$$M_s = \frac{165,600 \text{ lb/ft}^2 (1 - 0.39)}{(1 + 0.39)(1 - 2 * 0.39)} = 330,333.55 \text{ lb/ft}^2$$

H₀ = 241 ft. the full thickness of the compressible CL, MH, GC, SC soils; the compressible soil is considered incompressible at the depth of 45 ft.

$$Z_e = \left(\frac{18,557}{330,333.55} \right) 45 \text{ ft} = 2.53 \text{ ft}$$

Settlement between points A15 and A16 = 2.48 ft. - 2.53 ft. = - 0.05 ft.



LEGEND

- SITE BOUNDARY (559.5 ACRES±)
- FACILITY BOUNDARY (500 ACRES)
- DISPOSAL AREA/LIMIT OF WASTE (224.3 ACRES±)
- CELL BOUNDARY
- EXISTING GRADE
- BASE GRADE
- FINAL GRADE
- CROSS-SECTION POINT ELEVATIONS
- FINAL BASE
- CROSS-SECTION LOCATION

SETTLEMENT POINTS

OWL LANDFILL SERVICES, LLC
LEA COUNTY, NEW MEXICO

Gordon Environmental, Inc.
Consulting Engineers

213 S. Camino del Pueblo
Bernalillo, New Mexico, USA
Phone: 505-867-6990
Fax: 505-867-6991

DATE: 09/06/2016	CAD: SETTLEMENT POINTS.DWG	PROJECT #: 560.01.02
DRAWN BY: ASM	REVIEWED BY: CRK	
APPROVED BY: IKG	gei@gordonenvironmental.com	FIGURE III.7.1

Drawing: P:\acad 2003\560.01.02\PERMIT FIGURES\RAI 1\SETTLEMENT X-SEC POINTS.dwg
Date/Time: Sep. 19, 2016-12:59:33 : LAYOUT: FigIII.7.1
Copyright © All Rights Reserved, Gordon Environmental, Inc. 2016

Change in slope of base grade:

Elevation of base grade at point A15 = Approximately 3,535 ft.

Updated elevation of base grade at point A16 = 3,535 ft. – 2.53 ft. = 3,532.47 ft.

$$\text{Updated base grade slope} = \frac{(3,532.47 \text{ ft} - 3,535.52 \text{ ft})}{100 \text{ ft}} \times 100 = 3.05\%$$

Change in base grade slope = 3.0% - 3.05% = -0.05%

The angular distortion between points A15 and A16 is determined as follows:

$$\text{Distortion} = \frac{(\text{Settlement}_{A13} - \text{Settlement}_{A14})}{\text{distance}} * 100$$

$$\text{Distortion} = \frac{(2.53 \text{ ft} - 2.48 \text{ ft})}{100 \text{ ft}} * 100 = -0.05\%$$

A summary of potential foundation soils settlement is provided in **Tables III.7.1** and **III.7.2**. The angular distortion between each point is calculated as above. The maximum angular distortion of the foundation soils on the floor (i.e., settlement points A2 to A28 and B3 to B31) of the landfill is 0.25% between points B3 and B4 on Cross-Section B-B'. The minimum slope on the landfill floor; perpendicular to the leachate collection pipe is approximately 1.86% after settlement. Additionally, the minimum slope of the leachate collection pipe is 1.86% to the leachate collection sump. These slopes are adequate and will ensure that the design and performance standards for the leachate collection system will be met.

TABLE III.7.1
Settlement and Angular Distortion of Foundation Soils Between Points
Cross Section A-A'
OWL Landfill Services, LLC

Point Location	Total Settlement (feet)	Distance Between Points (feet)	Angular Distortion (%)	Distortion Direction	Design Base grade Elevation (feet)	Design Slope Between Point Locations (%)	Updated Base grade Elevation (feet)	Updated Slope Between Point Locations (%)
A1	0.25	100	0.542	▼	3563.00	25.00	3562.75	25.54
A2	0.79	100	0.202	▼	3538.00	3.00	3537.21	3.20
A3	1.00	100	0.121	▼	3535.00	3.00	3534.00	2.88
A4	1.12	100	0.181	▼	3538.00	2.00	3536.88	1.82
A5	1.30	100	0.171	▼	3540.00	2.00	3538.70	2.17
A6	1.47	100	0.131	▼	3538.00	3.00	3536.53	3.13
A7	1.60	100	0.192	▼	3535.00	3.00	3533.40	2.81
A8	1.79	100	0.141	▼	3538.00	2.00	3536.21	1.86
A9	1.93	100	0.192	▼	3540.00	2.00	3538.07	2.19
A10	2.12	100	0.181	▼	3538.00	3.00	3535.88	3.18
A11	2.31	100	0.121	▼	3535.00	3.00	3532.69	2.88
A12	2.43	100	0.010	▼	3538.00	2.00	3535.57	1.99
A13	2.44	100	0.040	▼	3540.00	2.00	3537.56	2.04
A14	2.48	100	0.050	▼	3538.00	3.00	3535.52	3.05
A15	2.53	100	-0.050	▲	3535.00	3.00	3532.47	3.05
A16	2.48	100	-0.040	▲	3538.00	2.00	3535.52	2.04
A17	2.44	100	-0.010	▲	3540.00	2.00	3537.56	1.99
A18	2.43	100	-0.071	▲	3538.00	3.00	3535.57	2.93
A19	2.36	100	-0.181	▲	3535.00	3.00	3532.64	3.18
A20	2.18	100	-0.151	▲	3538.00	2.00	3535.82	2.15
A21	2.02	100	-0.171	▲	3540.00	2.00	3537.98	1.83
A22	1.85	100	-0.151	▲	3538.00	3.00	3536.15	2.85
A23	1.70	100	-0.181	▲	3535.00	3.00	3533.30	3.18
A24	1.52	100	-0.192	▲	3538.00	2.00	3536.48	2.19
A25	1.33	100	-0.141	▲	3540.00	2.00	3538.67	1.86
A26	1.19	100	-0.141	▲	3538.00	3.00	3536.81	2.86
A27	1.05	100	-0.202	▲	3535.00	3.00	3533.95	3.20
A28	0.84	100	-0.302	▲	3538.00	20.00	3537.16	20.30
A29	0.54	100	-0.533	▲	3558.00	20.00	3557.46	20.53
A30	0.01	100	-0.009	▲	3578.00		3577.99	

Notes:

Points Correspond to Figure III.7.1

▲ = potential upward distortion

▼ = potential downward distortion

Elevations based on NM State Plan Coordinate System

TABLE III.7.2
Settlement and Angular Distortion of Foundation Soils Between Points
Cross Section B-B'
OWL Landfill Services, LLC

Point Location	Total Settlement (feet)	Distance Between Points (feet)	Angular Distortion (%)	Distortion Direction	Design Base grade Elevation (feet)	Design Slope Between Point Locations (%)	Updated Base grade Elevation (feet)	Updated Slope Between Point Locations (%)
B1	0.02	100	0.571	▼	3593.00	20.00	3592.98	20.57
B2	0.59	100	0.121	▼	3573.00	3.00	3572.41	3.12
B3	0.71	100	0.252	▼	3570.00	2.00	3569.29	2.25
B4	0.97	100	0.151	▼	3568.00	3.00	3567.03	3.15
B5	1.12	100	0.181	▼	3565.00	2.00	3563.88	2.18
B6	1.30	100	0.181	▼	3563.00	3.00	3561.70	3.18
B7	1.48	100	0.192	▼	3560.00	2.00	3558.52	2.19
B8	1.67	100	0.181	▼	3558.00	3.00	3556.33	3.18
B9	1.85	100	0.202	▼	3555.00	2.00	3553.15	2.20
B10	2.05	100	0.202	▼	3553.00	3.00	3550.95	3.20
B11	2.26	100	0.101	▼	3550.00	2.00	3547.74	2.10
B12	2.36	100	0.040	▼	3548.00	3.00	3545.64	3.04
B13	2.40	100	0.030	▼	3545.00	2.00	3542.60	2.03
B14	2.43	100	0.030	▼	3543.00	3.00	3540.57	3.03
B15	2.46	100	0.040	▼	3540.00	2.00	3537.54	2.04
B16	2.50	100	0.030	▼	3538.00	3.00	3535.50	3.03
B17	2.53	100	0.000	▼	3535.00	2.00	3532.47	2.00
B18	2.53	100	0.010	▼	3533.00	3.00	3530.47	3.01
B19	2.54	100	0.000	▼	3530.00	2.00	3527.46	2.00
B20	2.54	100	-0.060	▲	3528.00	3.00	3525.46	2.94
B21	2.48	100	-0.151	▲	3525.00	2.00	3522.52	1.85
B22	2.33	100	-0.131	▲	3523.00	3.00	3520.67	2.87
B23	2.20	100	-0.141	▲	3520.00	2.00	3517.80	1.86
B24	2.05	100	-0.131	▲	3518.00	3.00	3515.95	2.87
B25	1.92	100	-1.923	▲	3515.00	2.00	3513.08	1.85
B26	1.77	100	-1.772	▲	3513.00	3.00	3511.23	2.86
B27	1.63	100	-1.631	▲	3510.00	2.00	3508.37	1.86
B28	1.49	100	-1.490	▲	3508.00	3.00	3506.51	2.89
B29	1.38	100	-1.379	▲	3505.00	2.00	3503.62	1.84
B30	1.22	100	-1.217	▲	3503.00	5.00	3501.78	5.22
B31	1.00	100	-0.996	▲	3508.00	25.00	3507.00	25.42
B32	0.57	100	-0.572	▲	3533.00	25.00	3532.43	25.55
B33	0.02	100	-0.021	▲	3558.00		3557.98	

Notes:

Points Correspond to Figure III.7.1

▲ = potential upward distortion

▼ = potential downward distortion

Elevations based on NM State Plan Coordinate System

4.0 WASTE SETTLEMENT CALCULATIONS

The methodology to estimate waste settlement involves selecting key points on the final cover surface, computing the settlement at each point, and evaluating the resultant change in surface elevation. Points were selected from Cross-Sections A-A' and B-B' (**Figure III.7.1**). Qian et al. (2002; **Attachment III.7.B**) present a method developed by Sowers (1973) for determining settlement in landfills. This method is based on developed soils consolidation theory, which relates settlement to layer thickness and changes in void ratio.

The primary settlement is estimated using equation 12.4 (**Attachment III.7.B, p. 449**):

$$\Delta H_c = C_c \frac{H_o}{1 + e_o} \log \frac{\sigma_i}{\sigma_o}$$

Where:

- ΔH_c = primary settlement
- $C_c/(1+e_o)$ = 0.006 (**Attachment III.7.C, p. 393, $D_r = 80\%$**)
- H_o = initial thickness of the waste layer before settlement (assume entire thickness of waste from intermediate cover to the top of protective soil layer; this provides a conservative analysis) [**Figure III.7.1**] = 241 ft.
- σ_o = previously applied pressure in waste layer (assumed to equal the compaction pressure = 1,000 lbs/ft²)
- σ_i = total overburden pressure applied at the mid-level of the waste layer (lbs/ft²)

Long-term secondary settlement is estimated by equation 12.10 (**Attachment III.7.B, p.451**):

$$\Delta H_s = C_\alpha \frac{H_o}{1 + e_o} \log \frac{t_2}{t_1}$$

Where:

- ΔH_s = secondary settlement
- C_α = $\frac{1}{3} [C_c/(1+e_o)] = 0.002$ (**Attachment III.7.C, p. 393**)
- H_o = waste thickness at start of secondary settlement = $H - H_c$ (**Figure III.7.1**)
- t_1 = starting time of secondary settlement (1 year)
- t_2 = ending time of secondary settlement = Assume 30 years

Settlement is estimated at the key locations (Points A1 through A30 and Points B1 through B33) shown on the landfill Cross-Sections A-A' and B-B' (**Figures III.7.1**). An example calculation is demonstrated at point A15, the location of maximum waste depth for Cross-Sections A-A' (i.e., 241 ft).

Point A15

Primary Waste Settlement

Maximum Thickness of Waste = 241 ft.

$$\Delta H_c = C_c \frac{H_o}{1 + e_o} \log \frac{\sigma_i}{\sigma_o}$$

Where:

$$C_c / (1 + e_o) = 0.006 \text{ (Attachment III.7.C, p. 393, } D_r = 80\%)$$

$$H_o = 241 \text{ ft.}$$

$$\sigma_o = 1,000 \text{ lbs/ft}^2 \text{ (Typical compaction of waste as found in New Mexico)}$$

$$\sigma_i = 0.5[(241 \text{ ft.})(74 \text{ lbs/ft}^3) + 4.0 \text{ ft. (120.5 lbs /ft}^2)] = 9,158 \text{ lbs/ft}^2$$

$$\Delta H_c = 0.006 \times 241 \times \log \frac{9,158 \frac{\text{lbs}}{\text{ft}}}{1,000 \frac{\text{lbs}}{\text{ft}^2}}$$

$$\Delta H_c = 1.39 \text{ ft.}$$

Secondary Waste Settlement

$$H_o = 241 \text{ ft.} - 1.39 \text{ ft.} = 239.61 \text{ ft.}$$

$$\Delta H_s = 0.002 \times 241 \log \frac{30 \text{ years}}{1 \text{ years}} = 0.71 \text{ ft}$$

$$\text{Total waste settlement} = 1.39 \text{ ft.} + 0.71 \text{ ft.} = 2.10 \text{ ft.}$$

The maximum final settlement of waste is the sum of primary and secondary settlement at point A15. The waste settlement is 1.39 ft. + 0.71 ft. = 2.10 ft, which has nominal impact on the corresponding calculations for landfill cap slope, runoff, etc. A summary of potential waste settlement is provided in **Tables III.7.3** and **III.7.4**.

TABLE III.7.3
Waste Settlement and Angular Distortion Between Points
Cross Section A-A'
OWL Landfill Services, LLC

Point Location	Total Settlement (feet)	Distance Between Points (feet)	Angular Distortion (%)	Distortion Direction
A1	0.11	100	0.28	▼
A2	0.39	100	0.17	▼
A3	0.55	100	0.11	▼
A4	0.66	100	0.17	▼
A5	0.83	100	0.16	▼
A6	0.99	100	0.13	▼
A7	1.12	100	0.19	▼
A8	1.31	100	0.15	▼
A9	1.46	100	0.20	▼
A10	1.66	100	0.20	▼
A11	1.85	100	0.13	▼
A12	1.99	100	0.01	▼
A13	2.00	100	0.04	▼
A14	2.04	100	0.06	▼
A15	2.10	100	-0.06	▲
A16	2.04	100	-0.04	▲
A17	2.00	100	-0.01	▲
A18	1.99	100	-0.08	▲
A19	1.91	100	-0.20	▲
A20	1.71	100	-0.16	▲
A21	1.55	100	-0.18	▲
A22	1.37	100	-0.15	▲
A23	1.22	100	-0.18	▲
A24	1.04	100	-0.18	▲
A25	0.85	100	-0.13	▲

Notes:

Points Correspond to Figure III.7.1

▲ = potential upward distortion

▼ = potential downward distortion

Elevations based on NM State Plan Coordinate System

TABLE III.7.3
Waste Settlement and Angular Distortion Between Points
Cross Section A-A'
OWL Landfill Services, LLC

Point Location	Total Settlement (feet)	Distance Between Points (feet)	Angular Distortion (%)	Distortion Direction
A26	0.72	100	-0.13	▲
A27	0.60	100	-0.17	▲
A28	0.43	100	-0.23	▲
A29	0.20	100	-0.20	▲
A30	0.00	100	0.00	▲

Notes:

Points Correspond to Figure III.7.1

▲ = potential upward distortion

▼ = potential downward distortion

Elevations based on NM State Plan Coordinate System

TABLE III.7.4
Waste Settlement and Angular Distortion Between Points
Cross Section B-B'
OWL Landfill Services, LLC

Point Location	Total Settlement (feet)	Distance Between Points (feet)	Angular Distortion (%)	Distortion Direction
B1	0.01	100	0.23	▼
B2	0.24	100	0.09	▼
B3	0.33	100	0.20	▼
B4	0.53	100	0.13	▼
B5	0.66	100	0.17	▼
B6	0.83	100	0.17	▼
B7	1.00	100	0.19	▼
B8	1.19	100	0.18	▼
B9	1.37	100	0.21	▼
B10	1.58	100	0.22	▼
B11	1.80	100	0.11	▼
B12	1.91	100	0.04	▼
B13	1.95	100	0.03	▼
B14	1.99	100	0.03	▼
B15	2.02	100	0.04	▼
B16	2.06	100	0.03	▼
B17	2.10	100	0.00	▼
B18	2.10	100	0.01	▼
B19	2.11	100	0.00	▼
B20	2.11	100	-0.07	▲
B21	2.04	100	-0.17	▲
B22	1.88	100	-0.14	▲
B23	1.73	100	-0.15	▲
B24	1.58	100	-0.14	▲
B25	1.45	100	-0.16	▲
B26	1.29	100	-0.16	▲

Notes:

Points Correspond to Figure III.7.1

▲ = potential upward distortion

▼ = potential downward distortion

Elevations based on NM State Plan Coordinate System

TABLE III.7.4
Waste Settlement and Angular Distortion Between Points
Cross Section B-B'
OWL Landfill Services, LLC

Point Location	Total Settlement (feet)	Distance Between Points (feet)	Angular Distortion (%)	Distortion Direction
B27	1.15	100	-0.14	▲
B28	1.01	100	-0.11	▲
B29	0.90	100	-0.15	▲
B30	0.75	100	-0.20	▲
B31	0.55	100	-0.33	▲
B32	0.22	100	-0.22	▲
B33	0.01	100	-0.01	▲

Notes:

Points Correspond to Figure III.7.1

▲ = potential upward distortion

▼ = potential downward distortion

Elevations based on NM State Plan Coordinate System

5.0 SOIL COVER SETTLEMENT CALCULATIONS

The final cover soil layer consisting of vegetative, barrier, and intermediate cover layers will also experience nominal consolidation due to its own weight. The method for evaluating settlement of the soil cover and cushion layers is based on equation B.2 (**Attachment III.7.D, p. 569**).

Primary Soil Settlement

$$\Delta H_p = C_c \frac{H_p}{1 + e_s} \log \frac{P_o + \Delta P}{P_o}$$

$$C_c / (1 + e_o) = 0.006 \text{ (Attachment III.7.C, p. 393, } D_r = 80\%)$$

Thickness of Soil = H = 3.0 feet of final cover + 1 foot of intermediate cover soil + 2 feet of protective soil layer = 6 ft.

Unit Weight of Soil = 120.5 lb/ft³ Dry Density

$$\Delta P = (3.0 \text{ ft.}) (120.5 \text{ lb/ft}^3) + (1 \text{ ft.}) (120.5 \text{ lb/ft}^3) + (2.0 \text{ ft.}) (120.5 \text{ lb/ft}^3) = 723.0 \text{ lb/ft}^2$$

$$P_o = \frac{H}{2} (120.5 \text{ lb/ft}^3) = 3.0 (120.5) = 361.5 \text{ lb/ft}^2$$

$$\Delta H_p = (0.006)(6.0 \text{ ft.}) \log \left(\frac{361.5 \frac{\text{lbs}}{\text{ft}^2} + 723 \frac{\text{lbs}}{\text{ft}^2}}{361.5 \frac{\text{lbs}}{\text{ft}^2}} \right)$$

$$\Delta H_p = 0.017 \text{ ft}$$

Secondary Soil Cover Settlement

$$\Delta H_s = C_s \frac{H_o}{1 + e_s} \log \frac{t_2}{t_1}$$

$$C_s = \frac{1}{3} [C_c / (1 + e_o)] = 0.002 \text{ (Attachment III.7.C, p. 393)}$$

$$H_o = 6.0 \text{ ft.} - 0.017 \text{ ft.} = 5.98 \text{ ft.}$$

$$\Delta H_s = 0.002 (5.98 \text{ ft.}) \log \frac{30}{1} = 0.018 \text{ ft}$$

The maximum settlement of the final cover is the sum of primary and secondary settlement at point A15. The soil final cover layer settlement is equal to 0.017 ft. + 0.018 ft. = 0.035 ft. The maximum angular distortion at the level of the top of final cover occurs between points A14 and A15 and equals 0.06%. Therefore, after conservative assumptions for settlement, the minimum slope of the final cover (2% grade) will be $2\% - 0.06\% = 1.94\%$, which has nominal impacts on the slope and runoff calculations (see Section 6.0).

6.0 CONCLUSIONS

Settlement projections have been calculated for the landfill foundation, the waste mass and for the landfill final soil cover. Settlement estimates include elastic deformation and both primary and secondary consolidation in the foundations soils, in the waste, and in the cover materials. The greatest value of projected settlement in both the foundation soils and in the waste occurs where the waste thickness is greatest (Point A15).

The maximum final settlement of the landfill foundation, waste mass and landfill cover is the sum of primary and secondary settlement at point A15. The foundation soil settlement is equal to 2.53 ft, the waste settlement is equal to 1.39 ft. + 0.71 ft. = 2.10 ft, and the final cover layer settlement is calculated at 0.035 ft. Maximum total settlement that could occur on the final cover of the landfill is the sum of the foundation soil, waste, and cover settlement (i.e.: 2.52 ft + 2.10 ft + 0.035 ft = 4.67 ft). The methodology used to determine settlement at point A15 was used to find the settlement of points A1-A30 for Cross-Section A-A', and points B1-B33 for Cross-Section B-B'. The total settlement for the points on Cross-Sections A-A' and B-B' and the angular distortion between them, is provided on **Table III.7.5** through **Table III.7.6**.

The composite calculations demonstrate the slope of the final cover, liner and leachate collection piping following settlement does not compromise the design and performance specifications for the leachate collection system.

TABLE III.7.5
Total Settlement and Angular Distortion Between Points
Cross Section A-A'
OWL Landfill Services, LLC

Point Location	Total Settlement (feet)	Distance Between Points (feet)	Angular Distortion (%)	Distortion Direction	Design Final grade Elevation (feet)	Design Slope Between Point Locations (%)	Updated Final grade Elevation (feet)	Updated Slope Between Point Locations (%)
A1	0.393	100	0.824	▼	3598.00	15.00	3597.61	14.18
A2	1.217	100	0.368	▼	3613.00	17.00	3611.78	16.63
A3	1.586	100	0.227	▼	3630.00	15.00	3628.41	14.77
A4	1.812	100	0.347	▼	3645.00	20.00	3643.19	19.65
A5	2.159	100	0.334	▼	3665.00	15.00	3662.84	14.67
A6	2.494	100	0.259	▼	3680.00	10.00	3677.51	9.74
A7	2.753	100	0.384	▼	3690.00	22.00	3687.25	21.62
A8	3.137	100	0.287	▼	3712.00	16.00	3708.86	15.71
A9	3.424	100	0.394	▼	3728.00	17.00	3724.58	16.61
A10	3.818	100	0.377	▼	3745.00	15.00	3741.18	14.62
A11	4.195	100	0.254	▼	3760.00	15.00	3755.80	14.75
A12	4.449	100	0.021	▼	3775.00	3.00	3770.55	2.98
A13	4.470	100	0.085	▼	3778.00	2.00	3773.53	1.92
A14	4.555	100	0.106	▼	3780.00	2.00	3775.44	1.89
A15	4.662	100	-0.106	▲	3782.00	2.00	3777.34	1.89
A16	4.555	100	-0.085	▲	3780.00	2.00	3775.44	1.92
A17	4.470	100	-0.021	▲	3778.00	3.00	3773.53	2.98
A18	4.449	100	-0.148	▲	3775.00	10.00	3770.55	9.85
A19	4.301	100	-0.378	▲	3765.00	15.00	3760.70	14.62
A20	3.922	100	-0.312	▲	3750.00	13.00	3746.08	12.69
A21	3.610	100	-0.350	▲	3737.00	19.00	3733.39	18.65
A22	3.260	100	-0.305	▲	3718.00	18.00	3714.74	17.69
A23	2.955	100	-0.362	▼	3700.00	15.00	3697.05	14.64
A24	2.593	100	-0.375	▼	3685.00	17.00	3682.41	16.62
A25	2.218	100	-0.272	▼	3668.00	16.00	3665.78	15.73

Notes:

Points Correspond to Figure III.7.1

▲ = potential upward distortion

▼ = potential downward distortion

Elevations based on NM State Plan Coordinate System

TABLE III.7.5
Total Settlement and Angular Distortion Between Points
Cross Section A-A'
OWL Landfill Services, LLC

Point Location	Total Settlement (feet)	Distance Between Points (feet)	Angular Distortion (%)	Distortion Direction	Design Final grade Elevation (feet)	Design Slope Between Point Locations (%)	Updated Final grade Elevation (feet)	Updated Slope Between Point Locations (%)
A26	1.946	100	-0.267	▼	3652.00	17.00	3650.05	16.73
A27	1.680	100	-0.372	▼	3635.00	17.00	3633.32	16.63
A28	1.308	100	-0.529	▼	3618.00	10.00	3616.69	9.47
A29	0.779	100	-0.734	▼	3608.00	21.00	3607.22	20.27
A30	0.044	100	-0.044	▼	3587.00		3586.96	

Notes:

Points Correspond to Figure III.7.1

▲ = potential upward distortion

▼ = potential downward distortion

Elevations based on NM State Plan Coordinate System

TABLE III.7.6
Total Settlement and Angular Distortion Between Points
Cross Section B-B'
OWL Landfill Services, LLC

Point Location	Total Settlement (feet)	Distance Between Points (feet)	Angular Distortion (%)	Distortion Direction	Design Final grade Elevation (feet)	Design Slope Between Point Locations (%)	Updated Final grade Elevation (feet)	Updated Slope Between Point Locations (%)
B1	0.062	100	0.802	▼	3605.00	23.00	3604.94	22.20
B2	0.864	100	0.210	▼	3628.00	9.00	3627.14	8.79
B3	1.074	100	0.456	▼	3637.00	23.00	3635.93	22.54
B4	1.529	100	0.283	▼	3660.00	12.00	3658.47	11.72
B5	1.812	100	0.347	▼	3672.00	16.00	3670.19	15.65
B6	2.159	100	0.354	▼	3688.00	15.00	3685.84	14.65
B7	2.514	100	0.380	▼	3703.00	17.00	3700.49	16.62
B8	2.894	100	0.366	▼	3720.00	15.00	3717.11	14.63
B9	3.260	100	0.412	▼	3735.00	18.00	3731.74	17.59
B10	3.672	100	0.418	▼	3753.00	17.00	3749.33	16.58
B11	4.090	100	0.211	▼	3770.00	8.00	3765.91	7.79
B12	4.301	100	0.085	▼	3778.00	1.00	3773.70	0.92
B13	4.385	100	0.064	▼	3779.00	1.00	3774.61	0.94
B14	4.449	100	0.064	▼	3780.00	0.00	3775.55	0.06
B15	4.513	100	0.085	▼	3780.00	2.00	3775.49	1.91
B16	4.598	100	0.064	▼	3782.00	0.00	3777.40	0.06
B17	4.662	100	0.000	▲	3782.00	2.00	3777.34	2.00
B18	4.662	100	0.021	▲	3780.00	2.00	3775.34	2.02
B19	4.683	100	0.000	▲	3778.00	2.00	3773.32	2.00
B20	4.683	100	-0.128	▼	3776.00	9.00	3771.32	8.87
B21	4.555	100	-0.318	▼	3767.00	17.00	3762.44	16.68
B22	4.237	100	-0.273	▼	3750.00	16.00	3745.76	15.73
B23	3.964	100	-0.292	▼	3734.00	16.00	3730.04	15.71
B24	3.672	100	-0.269	▼	3718.00	16.00	3714.33	15.73
B25	3.404	100	-3.404	▼	3702.00	17.00	3698.60	16.69
B26	3.097	100	-0.283	▼	3685.00	17.00	3681.90	16.72

Notes:

Points Correspond to Figure III.7.1

▲ = potential upward distortion

▼ = potential downward distortion

Elevations based on NM State Plan Coordinate System

TABLE III.7.6
Total Settlement and Angular Distortion Between Points
Cross Section B-B'
OWL Landfill Services, LLC

Point Location	Total Settlement (feet)	Distance Between Points (feet)	Angular Distortion (%)	Distortion Direction	Design Final grade Elevation (feet)	Design Slope Between Point Locations (%)	Updated Final grade Elevation (feet)	Updated Slope Between Point Locations (%)
B27	2.813	100	-0.280	▼	3668.00	16.00	3665.19	15.72
B28	2.533	100	-0.217	▼	3652.00	14.00	3649.47	13.78
B29	2.316	100	-0.312	▼	3638.00	18.00	3635.68	17.69
B30	2.004	100	-0.419	▼	3620.00	17.00	3618.00	16.58
B31	1.586	100	-0.756	▼	3603.00	17.00	3601.41	16.24
B32	0.830	100	-0.768	▼	3586.00	16.00	3585.17	15.23
B33	0.062				3570.00		3569.94	

Notes:

Points Correspond to Figure III.7.1

▲ = potential upward distortion

▼ = potential downward distortion

Elevations based on NM State Plan Coordinate System

**APPLICATION FOR PERMIT
OWL LANDFILL SERVICES, LLC**

**VOLUME III: ENGINEERING DESIGN AND CALCULATIONS
SECTION 7: SETTLEMENT CALCULATIONS**

**ATTACHMENT III.7.A
SUMMARY OF GEOTECHNICAL LABORATORY TESTING RESULTS**

ATTACHMENT III.7.A

Soils Laboratory Analyses Summary OWL Landfill Services, LLC

Sample Number ¹	Sample Depth (ft bgs)	USCS Class ²	Grain Size Distribution			Atterberg Limits ³		Natural Moisture ⁴ (%)	Standard Proctor		Permeability (cm/sec)	Porosity (%) ⁵
			Pass #4 (%)	Pass #40 (%)	Pass #200 (%)	LL- PL	PI		Max Dry Density (PCF)	Optimum Moisture (%)		
BH1 - 3	15	SP-SM	82.1	39.7	8.3			5.99				38.39
BH1 - 12	82-85	SP-SM	99.0	70.6	6.0			3.68				37.13
BH1 Bucket	100	CL	100.0	71.0	51.2	31-15	16	4.90	130.4	10.6	2.87 x 10 ⁻⁸	44.39
BH2 - 6	29	SP	92.0	72.2	3.1			6.67				43.18
BH2 Bucket	50	SP	96.2	63.4	4.3							42.18
BH2 - 16	70	SC	100.0	55.5	30.8	37-20	17	17.52	120.5	12.4	4.23 x 10 ⁻⁵	40.75
BH3 - 5	20	SP-SM	100.0	97.9	6.6			8.38				33.15
BH3 Bucket	45	SP-SM	84.8	44.6	9.9				115.5	12.6	4.91 x 10 ⁻⁷	36.15
BH3 - 16	128	SP-SM	99.8	55.0	9.6			6.49				38.97
BH4 - 3	15	SP-SM	87.0	72.4	10.3			9.28				43.90
BH4 - Bucket	45	CL	100.0	94.0	72.6	39-24	15	13.50	104.3	19.1	4.56 x 10 ⁻⁷	
BH5 - 9	35	SP	96.2	61.5	4.0			10.37				43.06

Notes:

Blank field indicates test not conducted.

¹ See **Figure IV.2.6** for locations of borings and **Attachment IV.2.A** for boring logs.

² Unified Soil Classification System: SM = silty sand; SP = poorly graded sand; SC = clayey sand; ML = low-plasticity silt; CL = low-plasticity clay; CH = high-plasticity clay

³ LL = liquid limit; PL = plastic limit; PI = plasticity index

⁴ Gravimetric basis

⁵ Porosity = $(V_v/N) * 100$

**APPLICATION FOR PERMIT
OWL LANDFILL SERVICES, LLC**

**VOLUME III: ENGINEERING DESIGN AND CALCULATIONS
SECTION 7: SETTLEMENT CALCULATIONS**

ATTACHMENT III.7.B

**QIAN, XUEDE; KOERNER, ROBERT M.; AND GRAY, DONALD H. 2002.
GEOTECHNICAL ASPECTS OF LANDFILL DESIGN AND CONSTRUCTION.
NEW YORK: PRENTICE HALL.**

GEOTECHNICAL ASPECTS OF LANDFILL DESIGN AND CONSTRUCTION

Xuede Qian

*Geotechnical Engineering Specialist
Michigan Department of Environmental Quality*

Robert M. Koerner

*H. L. Bowman Professor of Civil Engineering, Drexel University
Director, Geosynthetic Research Institute*

Donald H. Gray

*Professor of Civil and Environmental Engineering
The University of Michigan*



PRENTICE HALL
Upper Saddle River, New Jersey 07458

TABLE 6.5 Index Properties of Solid Waste

Source	Unit Weight		Volumetric Moisture Content	Porosity	Void Ratio
	lb/ft ³	kN/m ³			
Rovers and Farquhar (1973)	59	9.3	0.16	-	-
Fungaroli (1979)	63	9.9	0.05	-	-
Wigh (1979)	73	11.5	0.08	-	-
Walsh and Kinman (1979)	90	14.1	0.17	-	-
Walsh and Kinman (1981)	89	14.0	0.17	-	-
Schroeder et al. (1984a, b)	-	-	0.28	0.52	1.08
Owels et al. (1990)	40 to 90	6.3 to 14.1	0.10 to 0.20	0.40 to 0.50	0.67 to 1.0
Schroeder et al. (1994a, b)	-	-	0.29	0.67	2.03
Zornberg et al. (1999)	64 to 95	10 to 15	0.30	0.49 to 0.62	1.02 to 1.65

Based on its constituent composition the average moisture content of the solid waste shown in Table 6.4 can be calculated as follows:

$$\begin{aligned}
 w_d &= [(60.0)(10.4) + (50.0)(19.1) + (20.0)(34.6) + (10.0)(6.0) + (15.0)(5.0) \\
 &\quad + (15.0)(9.5) + (2.0)(4.0) + (2.0)(7.2) + (8.0)(2.8) + (3.0)(1.4)]/100 \\
 &= (624 + 955 + 692 + 60 + 75 + 142.5 + 8 + 14.4 + 22.4 + 4.2)/100 \\
 &= 2597.5/100 \\
 &= \underline{26.0\%}
 \end{aligned}$$

Thus, the average dry gravimetric moisture content of the solid waste shown in Table 6.4 is 26.0%.

More information about the moisture content of solid waste can be found in Table 6.5. It should be noted that the values of moisture content listed in Table 6.5 are calculated on a volume basis and differ from those calculated on a weight basis, which is more common to geotechnical analyses.

6.4 POROSITY OF MUNICIPAL SOLID WASTE

Porosity is defined as the ratio of the volume of voids to the total volume occupied by a solid waste or soil. Void ratio is defined as the ratio of the volume of voids to the volume of solids. Porosity can be related to the void ratio by using the relationships

$$n = \frac{e}{1 + e} \quad (6.7)$$

and

$$e = \frac{n}{1 - n} \quad (6.8)$$

where n = porosity of solid waste; and
 e = void ratio of solid waste.

The porosity of MSW varies typically from 0.40 to 0.67 depending on the compaction and composition of the waste. For comparison, a typical compacted clay liner material will have a porosity of about 0.40. Table 6.5 shows a summary of the index properties of municipal solid waste, which includes initial volumetric moisture content, initial porosity, initial void ratio and unit weight data.

6.5 HYDRAULIC CONDUCTIVITY OF MUNICIPAL SOLID WASTE

Proper assessment of the hydraulic conductivity of municipal solid waste is important in the design of leachate collection systems and in leachate recirculation planning particularly for bioreactor landfills (see Chapter 15). The hydraulic conductivity can be measured using a field leachate pumping test and a large-scale percolation test in test pits or by using large-diameter permeameters in the laboratory.

Hydraulic conductivity measured in test pits at several landfills in Canada by Landva and Clark (1990) is plotted against unit weight in Figure 6.3. The values shown are based on an intermediate stage of water level recession, after the flow had stabilized and before any debris could clog the voids. The measured coefficients of hydraulic conductivity (1.0×10^{-3} to 4.0×10^{-2} cm/sec) correspond to those associated with clean sand and gravel. Qian (1994) used three-year field data from an active landfill in the state of Michigan to develop a relationship between precipitation and leachate volume from a primary leachate collection system with time. With this information, the hydraulic conductivity of the waste can be calculated based on the water travel time, hydraulic gradient, and waste thickness. The hydraulic conductivity calculated in this way was estimated to be about 9.2×10^{-4} to 1.1×10^{-3} cm/sec. Table 6.6 summarizes the hydraulic conductivity of different types of MSW taken from the

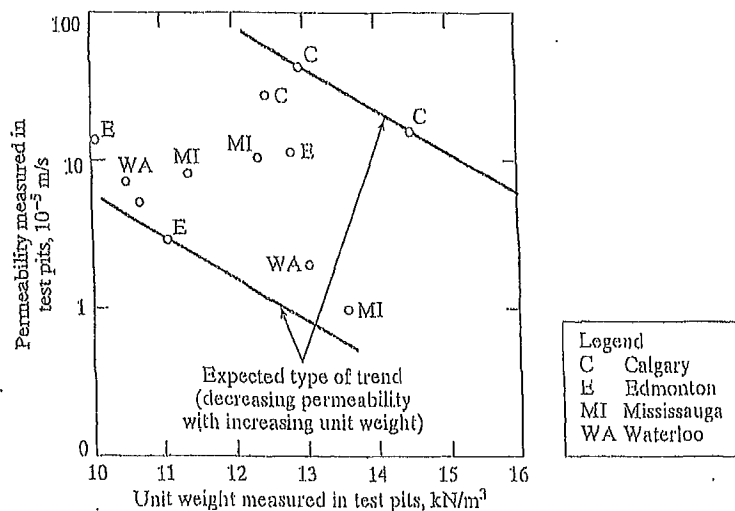
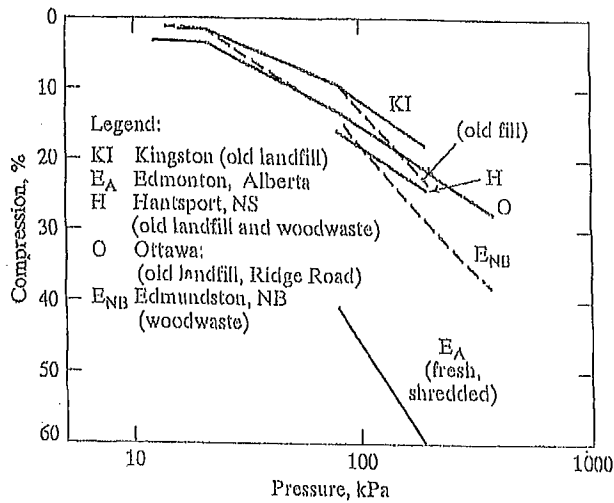


FIGURE 6.3 Unit Weight and Permeability (from Percolation) as Measured in Landfill Test Pits (Landva and Clark, 1990)

FIGURE 6.9 Compressive Strain versus Log Pressure for Various Landfills in Canada (Landva and Clark, 1990)

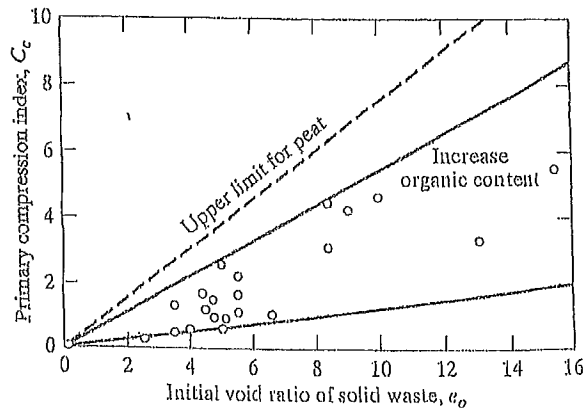


Legend:
 KI: $C_c' = 0.17$ ($p = 20 - 200$ kPa) O: $C_c' = 0.21$ ($p = 100 - 400$ kPa)
 EA: $C_c' = 0.35$ ($p = 80 - 200$ kPa) ENB: $C_c' = 0.36$ ($p = 100 - 400$ kPa)
 H: $C_c' = 0.22$ ($p = 80 - 200$ kPa)

cans; the lower values are for the less resilient materials. The maximum C_c for peat is about one-third greater than the maximum observed for waste fills.

Landva and Clark (1990) found that the coefficient of secondary consolidation, C_{α} , (the gradient of the compression versus log time relationship) was in the range 0.2 to 3.0 percent per log cycle time, depending on the type of waste involved. Field testing results using a settlement platform (Keene, 1977) showed that the coefficient of secondary consolidation, C_{α} , varies between 0.014 and 0.034. Too few tests have been carried out for any firm relationship to be established between the value of C_{α} and the type of waste, but it does appear that C_{α} increases with increasing organic content. Sowers (1973) pointed that the coefficient of secondary consolidation, C_{α} , is also a

FIGURE 6.10 Compressibility of MSW Landfills (Sowers, 1973)



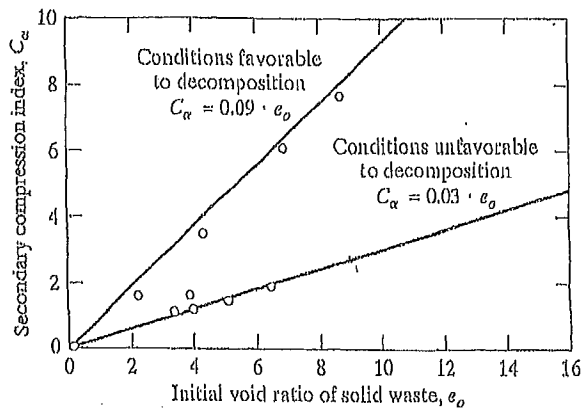


FIGURE 6.11 Secondary Compression of MSW Landfills (Sowers, 1973)

function of the void ratio, as shown in Figure 6.11. For any given void ratio, there is a large range in C_α , related to the potential for physico-chemical and bio-chemical decay. The value is high if the organic content subject to decay is large and the environment is favorable: namely, warm, moist, with fluctuating water table that pumps fresh air into the fill. The value is low for more inert materials and an unfavorable environment. More research and data are necessary before this relationship can be defined more closely.

The most widely reported compressibility parameter is the modified secondary compression index (C'_α). The reported values of C'_α range from 0.001 to 0.59. The lowest value represents the compressibility of a landfill that had been subjected to dynamic compaction. For typical landfills the lower limit of C'_α is generally around 0.01 to 0.03. This compares to 0.005 to 0.02 for common clays (Holtz and Kovacs, 1981). Fassett et al. (1994) observed that the typical upper limit of C'_α appears to be approximately 0.1.

According to Yen and Scanlon (1975), the settlement rate of waste increases with depth, hence larger values of C'_α should be associated with thicker fills. They observed that this effect leveled off at about 90 ft. and suggested that conditions within the landfill at great depths limit the biological activity to anaerobic decomposition, which is much slower than the aerobic decomposition believed to occur in shallower fills.

The values of C_α and C'_α , like C_v and C'_v , are dependent on the values used for e_0 or H_0 . The value of C'_α is also dependent on stress level, time, and on how the origin of time is selected. The waste placement or filling period for landfills is often long and should be taken into consideration for settlement rate analyses (Yen and Scanlon, 1975). The zero time selection has a large impact on C'_α particularly during earlier phases of a landfill (Fassett et al., 1994).

An additional problem with determining C'_α is the fact that this parameter is generally not constant. Edgers (1992) presents settlement log-time data from 22 case histories (shown in Figure 6.12). The majority of the curves show a relatively flat slope (i.e. low C'_α values) at small times, but at larger times the slope greatly increases (Figure 6.13). They attributed the higher slopes in the later stages of compression to increasing decomposition, but it may simply be an artifact of the log-time scale. It is

d = diameter of perforated hole or width of perforated slot on the pipe, in or m; and

n = number of perforated holes or slots per row per foot of pipe.

Pipe stiffness is measured according to ASTM D2412 (Standard Test Method for External Loading Properties of Plastic Pipe by Parallel-Plate Loading). The elastic modulus of the pipe material depends on the type of resin and formulation being used. Three formulas that can be used to calculate pipe stiffness are

$$PS = \frac{E \cdot I}{0.149 \cdot r^3} \quad (9.24)$$

$$PS = 0.559 \cdot E \cdot (t/r)^3 \quad (9.25)$$

and
$$PS = 4.47 \cdot \frac{E}{(SDR - 1)^3} \quad (9.26)$$

- where PS = pipe stiffness, lb/in² or kN/m²;
- E = elastic modulus of the pipe material, lb/in² or kN/m²;
- I = moment of inertia of the pipe wall per unit length,
 $I = t^3/12$, in⁴/in = in³ or m⁴/m = m³;
- r = mean radius of pipe, in or m;
- t = wall thickness of pipe, in or m; and
- SDR = standard dimension ratio, the same as the dimension ratio.

The allowable deflection ratios for a typical commercial polyethylene pipe are listed in Table 9.4.

Deflections of buried flexible pipe are commonly calculated using Equation 9.16 or 9.21. These equations use the soil reaction modulus, E' , as a surrogate parameter for soil stiffness. It should be noted that the values of E' in Table 9.3 only apply for soil fills of less than 50 ft (15 m). However, megafills built over leachate collection pipes often exceed 150 ft (46 m) in height. The soil reaction modulus is not a directly measurable soil parameter; instead it must be determined by back-calculation using observed pipe deflections. Research by Selig (1990) showed that E' is a function of the bedding condition and overburden pressure. Selig's studies were carried out to seek a correlation between the soil reaction modulus and soil stiffness parameters such as

TABLE 9.4 Allowable Deflection Ratio of Polyethylene Pipe

SDR	Allowable Deflection Ratio
11	2.7%
13.5	3.4%
15.5	3.9%
17	4.2%
19	4.7%
21	5.2%
26	6.5%
32.5	8.1%

Young's modulus of soil, E_s , and the constrained modulus of soil, M_s , where E_s and D_s are related through Poisson's ratio of soil, ν_s , by

$$M_s = \frac{E_s \cdot (1 - \nu_s)}{(1 + \nu_s)(1 - 2 \cdot \nu_s)} \quad (9.27)$$

where M_s = constrained modulus of soil, lb/ft² or kN/m²;
 E_s = elastic modulus of soil, lb/ft² or kN/m²; and
 ν_s = Poisson's ratio of soil.

The studies and analyses by Neilson (1967), Allgood and Takahashi (1972), and Hartely and Duncan (1987) indicated that for

$$E' = k \cdot M_s \quad (9.28)$$

the value of k may vary from 0.7 to 2.3. Using $k = 1.5$ as a representative value and $\nu_s = 0.3$, in addition to combining Equations 9.27 and 9.28 yields the following relationship between the elastic modulus of the pipe and soil (Selig, 1990):

$$E' = 2 \cdot E_s \quad (9.29)$$

The values of elastic parameters, E_s and ν_s , can be found in Table 9.5 according to different percents of density from a standard Proctor compaction test (ASTM D698).

TABLE 9.5 Elastic Soil Parameters (Selig, 1990)

Soil Type	Stress Level		85% Standard Density			95% Standard Density		
			E_s			E_s		
	psi	kPa	psi	MPa	ν_s	psi	MPa	ν_s
SW, SP, GW, GP	1	7	1,300	9	0.26	1,600	11	0.40
	5	35	2,100	14	0.21	4,100	28	0.29
	10	70	2,600	18	0.19	6,000	41	0.24
	20	140	3,300	23	0.19	8,600	59	0.23
	40	280	4,100	28	0.23	13,000	90	0.25
	60	420	4,700	32	0.28	16,000	110	0.29
GM, SM, ML, and GC, SC with < 20% fines	1	7	600	4	0.25	1,800	12	0.34
	5	35	700	5	0.24	2,500	17	0.29
	10	70	800	6	0.23	2,900	20	0.27
	20	140	850	6	0.30	3,200	22	0.29
	40	280	900	6	0.38	3,700	25	0.32
	60	420	1,000	7	0.41	4,100	28	0.35
CL, MH, GC, SC	1	7	100	1	0.33	400	3	0.42
	5	35	250	2	0.29	800	6	0.35
	10	70	400	3	0.28	1,100	8	0.32
	20	140	600	4	0.25	1,300	9	0.30
	40	280	700	5	0.35	1,400	10	0.35
	60	420	800	6	0.40	1,500	10	0.38

Table 12.2 Comparison of Settlement and Construction Period (Yen and Scanlon, 1975)

Range of Fill Depth H_f , feet, (meter)	Average Construction Period, t_c (month)	Total Time Required for Construction and Settlement (months)	Approximate Time Required for Settlement to Complete (month)
40 to 80 (12 to 24)	12	113	101
40 to 80 (12 to 24)	72	324	252
80 to 100 (24 to 30)	12	245	233
80 to 100 (24 to 30)	72	310	238

Used with permission of ASCE.

12.4 ESTIMATION OF LANDFILL SETTLEMENT

The usual laboratory tests for soil consolidation testing are not well suited for obtaining accurate consolidation parameters for solid waste that has a heterogeneous composition and extremely large particle sizes. By analyzing the field settlement data from some large-scale pilot landfill cells, Sowers (1973) proposed an alternative method to estimate the amount of the landfill settlement. In recent years, this method has been revised and refined several times by other investigators.

The settlement of solid waste includes primary settlement and long-term secondary compression. The total amount of settlement is given by the expression

$$\Delta H = \Delta H_c + \Delta H_\alpha \quad (12.3)$$

where ΔH = total settlement of solid waste;
 ΔH_c = primary settlement of solid waste;
 ΔH_α = long-term secondary settlement of solid waste.

12.4.1 Settlement of New Solid Waste

Based on the procedure proposed by Sowers (1973), the equations that follow can be used to calculate the settlement for new landfilled solid waste. The *Initial primary settlement* is given by

$$\Delta H_c = C_c \cdot \frac{H_0}{1 + e_0} \cdot \log \frac{\sigma_1}{\sigma_0} \quad (12.4)$$

or

$$\Delta H_c = C'_c \cdot H_0 \cdot \log \frac{\sigma_1}{\sigma_0} \quad (12.5)$$

where ΔH_c = primary settlement;
 e_0 = initial void ratio of the waste layer before settlement;
 H_0 = initial thickness of the waste layer before settlement;
 C_c = primary compression index (recall Figure 6.10);
 C'_c = modified primary compression index, $C'_c = 0.17 \sim 0.36$;
 σ_0 = previously applied pressure in the waste layer (assumed equal to the compaction pressure, $\sigma_0 = 1,000 \text{ lb/ft}^2$ or 48 kN/m^2);
 σ_1 = total overburden pressure applied at the mid level of the waste layer.

The previous compaction pressure applied on the solid waste layer during placement with compaction equipment is assumed to be 1,000 lb/ft² (48 kN/m²) based on 1973 compaction efforts for municipal solid waste landfills. In other words, the waste that has been placed in the landfill is essentially incompressible at normal pressure below 1,000 lb/ft² (48 kN/m²) due to the preconsolidation effect caused by previous compaction of the material. The value of the previously applied pressure, σ_o , should be changed during estimation of settlement if the compaction effort is much lower or higher than 1,000 lb/ft² (48 kN/m²) for a specific landfill project. Indeed, current practices of using waste compactors in the 100 to 150 U.S. tons (900 to 1,300 kN) range will significantly increase the value of σ_o .

The *long-term secondary settlement* can be obtained from

$$\Delta H_\alpha = C_\alpha \cdot \frac{H_o}{1 + e_o} \cdot \log \frac{t_2}{t_1} \quad (12.6)$$

or

$$\Delta H_\alpha = C'_\alpha \cdot H_o \cdot \log \frac{t_2}{t_1} \quad (12.7)$$

where ΔH_α = long-term secondary settlement;
 e_o = initial void ratio of the waste layer before settlement;
 H_o = initial thickness of the waste layer before settlement;
 C_α = secondary compression index (recall Figure 6.11);
 C'_α = modified secondary compression index, $C'_\alpha = 0.03 \sim 0.1$;
 t_1 = starting time of the time period for which long-term settlement of the layer is desired, $t_1 = 1$ month;
 t_2 = ending time of the time period for which long-term settlement of the layer is desired.

Because a standard consolidation test method for solid waste has not yet been developed, the selection of waste compression indices are mainly based on experience and limited field data. The value of the primary compression index C_c can be selected from Figure 6.10 based on the initial void ratio and organic content of the solid waste. The value of the secondary compression index C_α can be selected from Figure 6.1.1 based on the initial void ratio of the waste and the decomposition conditions.

Generally, the initial void ratio of municipal solid waste placed in a landfill after compaction is quite difficult to determine, and hence the values of the primary compression index C_c and the secondary compression index C_α cannot be estimated readily for settlement analysis. Accordingly, an alternative approach has been used in engineering practice—namely, the use of a “modified” primary compression index C'_c and a “modified” secondary compression index C'_α . Based on experience, the value of the modified primary compression index C'_c varies from 0.17 to 0.36, and the value of the modified secondary compression index C'_α varies from 0.03 to 0.1 for municipal solid waste (depending on the initial compaction effort and composition of the solid waste). The value of the modified secondary compression index C'_α for common clay ranges from 0.005 to 0.02. Therefore, the secondary settlement for municipal solid waste is approximately five to six times that of common clay.

12.4.2 Settlement of Existing Solid Waste

The following equations can be used to calculate the settlement of an existing solid waste landfill caused by vertical expansion (Chapter 14) or other additional extra loading, such as a light structure on a raft foundation.

The *primary settlement* is obtained by

$$\Delta H_c = C_c \cdot \frac{H_o}{1 + e_o} \cdot \log \frac{\sigma_o + \Delta\sigma}{\sigma_o} \quad (12.8)$$

or

$$\Delta H_c = C'_c \cdot H_o \cdot \log \frac{\sigma_o + \Delta\sigma}{\sigma_o} \quad (12.9)$$

where ΔH_c = primary settlement;
 e_o = initial void ratio of the waste layer before settlement;
 H_o = initial thickness of the waste layer of the existing landfill;
 C_c = primary compression index;
 C'_c = modified primary compression index, $C'_c = 0.17 \sim 0.36$;
 σ_o = existing overburden pressure acting at the mid level of the waste layer;
 $\Delta\sigma$ = increment of overburden pressure due to vertical expansion or other extra load.

The *long-term secondary settlement* is given by

$$\Delta H_\alpha = C_\alpha \cdot \frac{H_o}{1 + e_o} \cdot \log \frac{t_2}{t_1} \quad (12.10)$$

or

$$\Delta H_\alpha = C'_\alpha \cdot H_o \cdot \log \frac{t_2}{t_1} \quad (12.11)$$

where ΔH_α = secondary settlement;
 e_o = initial void ratio of the waste layer before starting secondary settlement;
 H_o = initial thickness of the waste layer before starting secondary settlement;
 C_α = secondary compression index;
 C'_α = modified secondary compression index, $C'_\alpha = 0.03 \sim 0.1$;
 t_1 = starting time of the secondary settlement. It is assumed to be equal to the age of the existing landfill for vertical expansion project;
 t_2 = ending time of the secondary settlement.

(e.g., temperature within landfill and oxygen reaching the waste) still is not entirely clear. These functions should be used with caution in engineering practice and should be supported by additional testing data and research.

12.7 ESTIMATION OF LANDFILL FOUNDATION SETTLEMENT

If the landfill is underlain by a soil layer, particularly a thick layer of soft, fine-grained soil, consolidation settlements may be large. In these cases, design analyses should consider settlement of the foundation clay layer. Both primary consolidation and long-term secondary settlement should be considered. Calculations are performed using conventional equations from soil mechanics theory and a time frame at least equal to the active life and postclosure care period of the landfill.

Excessive settlement of an underlying foundation clay layer will affect the performance of a landfill liner and leachate collection system. The purposes of analyzing the settlement of a foundation clay layer and overlying landfill liner and leachate collection/removal system are as follows:

- (i) Tensile strain induced in the liner system and leachate collection and removal system must be limited to a minimum allowable tensile strain for the components of these two systems. The compacted clay liner usually has the smallest allowable tensile strain value between 0.1% and 1.0% and an average allowable tensile strain of 0.5%.
- (ii) Post-settlement grades of the landfill cell subbase and the leachate collection pipes must be sufficient to maintain leachate performance to prevent grade reversal and leachate ponding in accordance with the rule requirements.

12.7.1 Total Settlement of Landfill Foundation

The total settlement of landfill foundation soil can be divided into three portions: elastic settlement, primary consolidation settlement, and secondary consolidation settlement. The settlement of sandy soils includes only elastic settlement. The settlement of clayey soils includes all three types of settlements. The total settlement of clayey soil is equal to the sum of the elastic settlement and the primary and secondary settlements. Because the permeability of clay is quite low, it takes a long time to complete the whole process of consolidation settlement. The settlement of clayey soil is usually much larger than the settlement of sandy soils.

Because the settlement of sandy soils includes only elastic settlement, the settlement of sand layer can be calculated from the Elastic Settlement equation, which is

$$Z_e = (\Delta\sigma/M_s)H_o \quad (12.20)$$

where Z_e = elastic settlement of soil layer, ft or m;
 H_o = initial thickness of soil layer, ft or m;
 $\Delta\sigma$ = increment of vertical effective stress, lb/ft² or kN/m²;
 M_s = constrained modulus of soil, lb/ft² or kN/m².

The constrained modulus is given by

$$M_s = \frac{E_s(1 - \nu_s)}{(1 + \nu_s)(1 - 2\nu_s)} \quad (12.21)$$

where M_s = constrained modulus of soil, lb/ft² or kN/m²;
 E_s = elastic modulus of soil, see Table 9.5, lb/ft² or kN/m²;
 ν_s = Poisson's ratio of soil, see Table 9.5.

The *primary consolidation settlement* is given by

$$Z_c = C_r \cdot \frac{H_{oi}}{1 + e_{oi}} \cdot \log \frac{p_c}{\sigma_o} + C_c \cdot \frac{H_o}{1 + e_{oi}} \cdot \log \frac{\sigma_o + \Delta\sigma}{p_c} \quad (12.22)$$

where Z_c = primary consolidation settlement of clay layer, ft or m;
 H_o = initial thickness of clay layer, ft or m; $= 2 \text{ ft}$
 e_{oi} = initial void ratio of clay layer;
 C_r = recompression index;
 C_c = primary compression index.
 σ_o = initial vertical effective stress, lb/ft² or kN/m²;
 p_c = preconsolidation pressure, lb/ft² or kN/m²;
 $\Delta\sigma$ = increment of vertical effective stress, lb/ft² or kN/m².

The *secondary compression settlement* is given by

$$Z_\alpha = C_\alpha \cdot \frac{H_{os}}{1 + e_{os}} \cdot \log \frac{t_2}{t_1} \quad (12.23)$$

where Z_α = long-term secondary compression settlement, ft or m;
 e_{os} = initial void ratio of clay layer before starting secondary consolidation settlement;
 C_α = secondary consolidation compression index;
 H_{os} = initial thickness of clay layer before starting secondary consolidation settlement, ft or m;
 t_1 = starting time of the time period for which long-term settlement of the layer is desired;
 t_2 = ending time of the time period for which long-term settlement of the layer is desired.

The total settlement of clay layer includes three portions: elastic settlement, primary consolidation settlement, and secondary consolidation settlement. These three types of settlement for clayey soil layers can be calculated from Equations 12.20, 12.22, and 12.23, respectively. The total settlement of clayey soil at point i can be determined from the equation

$$Z_i = (Z_e)_i + (Z_c)_i + (Z_\alpha)_i \quad (12.24)$$

where Z_i = total settlement of points i ;
 $(Z_e)_i$ = elastic settlement of point i ;
 $(Z_c)_i$ = primary consolidation settlement of point i ;
 $(Z_\alpha)_i$ = secondary consolidation settlement of point i .

**APPLICATION FOR PERMIT
OWL LANDFILL SERVICES, LLC**

**VOLUME III: ENGINEERING DESIGN AND CALCULATIONS
SECTION 7: SETTLEMENT CALCULATIONS**

ATTACHMENT III.7.C

CODUTO, DONALD P. 1998.

GEOTECHNICAL ENGINEERING PRINCIPLES AND PRACTICES.

NEW JERSEY: PRENTICE HALL.

Geotechnical Engineering

Principles and Practices

Donald P. Coduto

*Professor of Civil Engineering
California State Polytechnic University, Pomona*

PRENTICE HALL, Upper Saddle River, NJ 07458

where:

$(N_1)_{60}$ = corrected SPT N -value, as defined in Chapter 3

C_p = grain size correction factor

C_A = aging correction factor

C_{OCR} = overconsolidation correction factor

D_{50} = grain size at which 50 percent of the soil is finer (mm) as defined in Section 4.4

t = age of soil (time since deposition in years). If no age information data is available, use $t = 100$ yr.

OCR = overconsolidation ratio, as defined in Chapter 11. If no information is available to assess the OCR, use a value of 2.

q_c = cone resistance (kg/cm² or ton/ft²), as defined in Chapter 3

Q_c = compressibility factor

= 0.91 for highly compressible sands

= 1.00 for moderately compressible sands

= 1.09 for slightly compressible sands

For purposes of solving this formula, a sand with a high fines content or a high mica content is "highly compressible," whereas a pure quartz sand is "slightly compressible."

σ'_z = vertical effective stress (lb/ft²; kPa), as defined in Chapter 10

Many people confuse relative density with relative compaction. The latter is defined in Chapter 6. Although the names are similar, and they measure similar properties, these two parameters are numerically different. In addition, some people in other professions use the term "relative density" to describe what we call specific gravity! Geotechnical engineers should never use the term in this way.

Table 4.5 presents typical values of e_{min} and e_{max} for various sandy soils. These are not intended to be used in lieu of laboratory or in-situ tests, but could be used to check test results or for preliminary analyses.

TABLE 4.5 TYPICAL VALUES OF e_{min} AND e_{max} (Hough, 1969; Adapted by permission of John Wiley and Sons, Inc.)

Soil Description	e_{min} (dense)	e_{max} (loose)
Equal spheres (theoretical values)	0.35	0.92
Clean, poorly graded medium sand (Ottawa, Illinois)	0.50	0.80
Clean, fine-to-medium sand	0.40	1.0
Uniform inorganic silt	0.40	1.1
Silty sand	0.30	0.90
Clean fine-to-coarse sand	0.20	0.95
Micaceous sand	0.40	1.2
Silty sand and gravel	0.14	0.85

TABLE 11.3 TYPICAL CONSOLIDATION PROPERTIES OF SATURATED NORMALLY CONSOLIDATED SANDY SOILS AT VARIOUS RELATIVE DENSITIES (Adapted from Burmister, 1962)

Soil Type	$C_c / (1+e_0)$					
	$D_r = 0\%$	$D_r = 20\%$	$D_r = 40\%$	$D_r = 60\%$	$D_r = 80\%$	$D_r = 100\%$
Medium to coarse sand, some fine gravel (SW)	-	-	0.005	-	-	-
Medium to coarse sand (SW/SP)	0.010	0.008	0.006	0.005	0.003	0.002
Fine to coarse sand (SW)	0.011	0.009	0.007	0.005	0.003	0.002
Fine to medium sand (SW/SP)	0.012	0.010	0.008	0.006	0.004	0.003
Fine sand (SP)	0.015	0.013	0.010	0.008	0.005	0.003
Fine sand with trace fine to coarse silt (SP-SM)	-	-	0.011	-	-	-
Fine sand with little fine to coarse silt (SM)	0.017	0.014	0.012	0.009	0.006	0.003
Fine sand with some fine to coarse silt (SM)	-	-	0.012	-	-	-

For saturated overconsolidated sands, $C_c / (1+e_0)$ is typically about one-third of the values listed in Table 11.3, which makes such soils nearly incompressible. Compacted fills can be considered to be overconsolidated, as can soils that have clear geologic evidence of preloading, such as glacial tills. Therefore, many settlement analyses simply consider the compressibility of such soils to be zero. If it is unclear whether a soil is normally consolidated or overconsolidated, it is conservative to assume it is normally consolidated.

Very few consolidation tests have been performed on gravelly soils, but the compressibility of these soils is probably equal to or less than those for sand, as listed in Table 11.3.

Another characteristic of sands and gravels is their high hydraulic conductivity, which means any excess pore water drains very quickly. Thus, the rate of consolidation is very fast, and typically occurs nearly as fast as the load is applied. Thus, if the load is due to a fill, the consolidation of these soils may have little practical significance.

However, there are at least two cases where consolidation of coarse-grained soils can be very important and needs more careful consideration:

1. Loose sandy soils subjected to dynamic loads, such as those from an earthquake. They can experience very large and irregular settlements that can cause serious damage. Kramer (1996) discusses methods of evaluating this problem.

**APPLICATION FOR PERMIT
OWL LANDFILL SERVICES, LLC**

**VOLUME III: ENGINEERING DESIGN AND CALCULATIONS
SECTION 7: SETTLEMENT CALCULATIONS**

ATTACHMENT III.7.D

**SHARMA, HARI .D. AND SANGEETA P. LEWIS. 1994.
*WASTE CONTAINMENT SYSTEMS, WASTE STABILIZATION
AND LANDFILLS: DESIGN AND EVALUATION.*
NEW YORK: JOHN WILEY AND SONS.**

WASTE CONTAINMENT SYSTEMS, WASTE STABILIZATION, AND LANDFILLS: DESIGN AND EVALUATION

HARI D. SHARMA, PH.D., P.E.

Chief Engineer and Director
EMCON Associates
San Jose, California

SANGEETA P. LEWIS, P.E.

Project Manager
CH₂M Hill
Oakland, California



A Wiley-Interscience Publication

JOHN WILEY & SONS, INC.

New York / Chichester / Toronto / Brisbane / Singapore

APPENDIX B

SETTLEMENT ANALYSES

Landfill settlement analyses include both foundation and refuse settlements. Foundation settlements are important in designing appropriately graded LCRSs, since these are typically gravity-flow systems. Refuse settlements are important in final cover design and estimating final landfill capacity. Estimating refuse settlements has also been critical in designing vertical landfill expansions and structures constructed on closed landfills.

Foundation settlement analyses for landfills follow the same principle as traditional geotechnical engineering settlement analyses. In this appendix we therefore focus on refuse settlements. For ease in reference, however, a brief discussion of foundation settlements is provided. The reader is referred to introductory geotechnical engineering textbooks if explanation is required on soil settlement and consolidation theories.

B.1 FOUNDATION SETTLEMENT

B.1.1 Mechanisms

For cohesive soils, settlement is characterized by the following three mechanisms:

- Immediate settlement following load application
- Consolidation settlements, which occur gradually as excess pore pressure caused by the applied loads are dissipated
- Secondary compression of the soil skeleton

Consolidation and secondary compression occur over several years and are theoretically never complete.

For granular soils, settlement is caused primarily by the compression of the soil skeleton as the particles rearrange due to the applied loads. Due to the relatively high permeability of granular soils, excess pore pressures induced by the applied load are assumed to dissipate in a very short period of time, and settlement is assumed to occur within a short period following load application; this is sometimes called immediate settlement.

B.1.2 Calculation of Settlement

For cohesive soils the total amount of consolidation settlement can be calculated using the following equation:

$$s = \Delta H = \frac{\Delta e}{1 + e_0} H_t \quad (\text{B.1})$$

where s = settlement

ΔH = change in height of layer

Δe = change in void ratio

e_0 = initial void ratio

H_t = layer thickness

Equation (B.1) can be modified as follows to suit the parameters obtained from a consolidation test:

$$s = \Delta H = \frac{C_c H_t}{1 + e_0} \left(\log \frac{P_0 + \Delta P}{P_0} \right) \quad (\text{B.2})$$

where C_c = consolidation index or compression index

P_0 = initial stress

ΔP = change in stress

For an infinite layer of soil, the change in stress is relatively easy to calculate and is typically equal to the change in applied load or overburden. However, since most aboveground landfills may be considered embankment loads, the subsurface stress distribution may be calculated using the influence chart shown in Figure B.1 for embankments of infinite length (Osterberg, 1957; U.S. Dept. of the Navy, 1982).

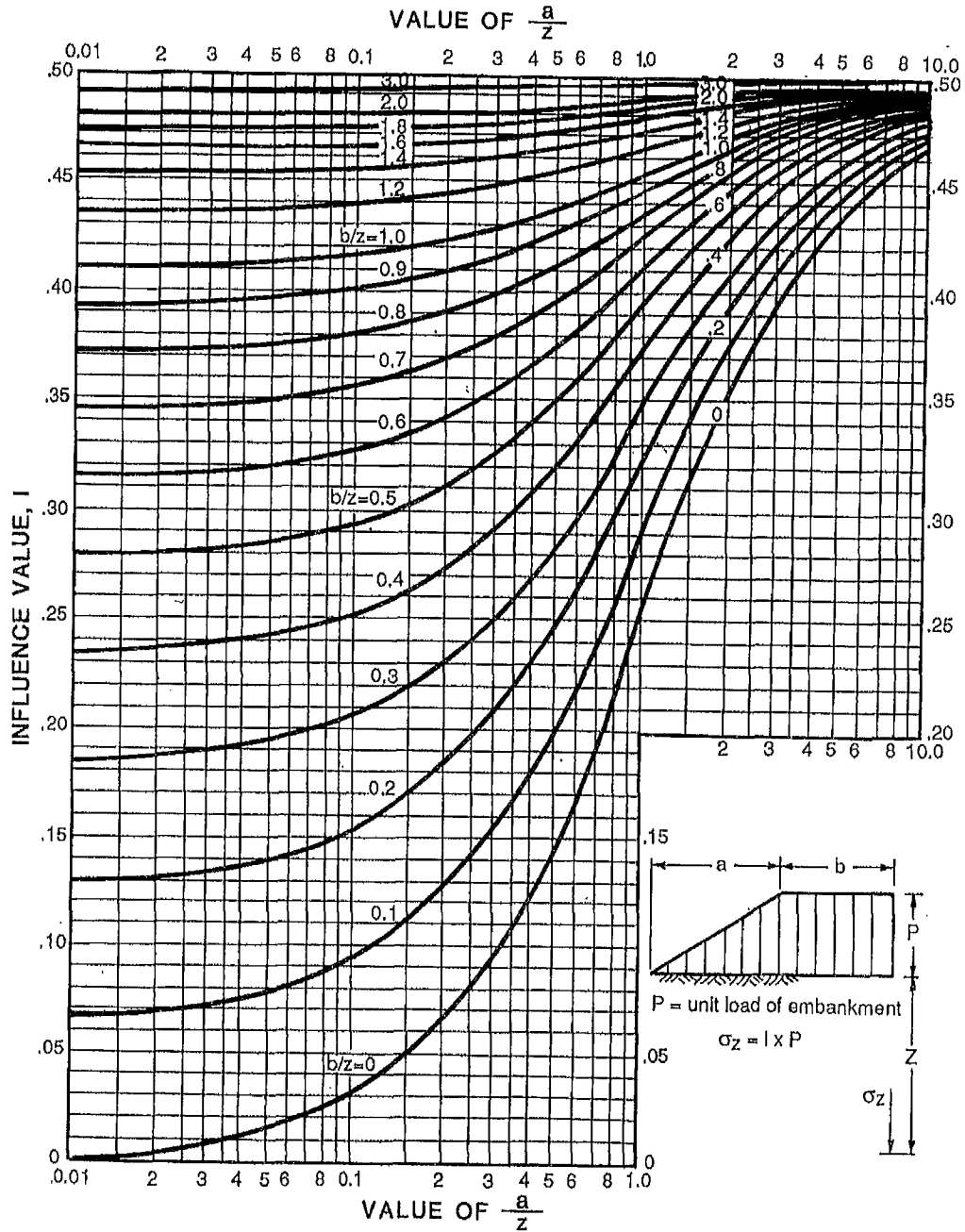


Figure B.1 Influence value for vertical stress under embankment load of infinite length. (From U.S. Dept. of the Navy, 1982.)

B.1.3 Liquefaction

B.1.3.1 Liquefaction Potential. In seismic regions, significant foundation settlements may also occur due to liquefaction of loose to medium-dense saturated cohesionless soils. Liquefaction is defined as a process where high shear deformations, typically induced by seismic activity, results in a progressive buildup of pore pressure. With limited drainage during the short period that the shear load is in-

**APPLICATION FOR PERMIT
OWL LANDFILL SERVICES, LLC**

**VOLUME III: ENGINEERING DESIGN AND CALCULATIONS
SECTION 7: SETTLEMENT CALCULATIONS**

ATTACHMENT III.7.E

**STEPHENS, DANIEL B.; HSU, KUO-CHIN; PRIEKSAT, MARK A.; ANKENY, MARK
D.; BLANDFORD, NEIL; ROTH, TRACY L.; KELSEY, JAMES A.; WHITWORTH,
JULIA R. 1997. A COMPARISON OF ESTIMATED AND CALCULATED EFFECTIVE
POROSITY. *HYDROGEOLOGY JOURNAL* (1998) 6:156–165.**

A comparison of estimated and calculated effective porosity

Daniel B. Stephens · Kuo-Chin Hsu
Mark A. Prieksat · Mark D. Ankeny
Neil Blandford · Tracy L. Roth · James A. Kelsey
Julia R. Whitworth

Abstract Effective porosity in solute-transport analyses is usually estimated rather than calculated from tracer tests in the field or laboratory. Calculated values of effective porosity in the laboratory on three different textured samples were compared to estimates derived from particle-size distributions and soil-water characteristic curves. The agreement was poor and it seems that no clear relationships exist between effective porosity calculated from laboratory tracer tests and effective porosity estimated from particle-size distributions and soil-water characteristic curves. A field tracer test in a sand-and-gravel aquifer produced a calculated effective porosity of approximately 0.17. By comparison, estimates of effective porosity from textural data, moisture retention, and published values were approximately 50–90% greater than the field calibrated value. Thus, estimation of effective porosity for chemical transport is highly dependent on the chosen transport model and is best obtained by laboratory or field tracer tests.

Résumé La porosité effective dans les analyses de transport de soluté est habituellement estimée, plutôt que calculée à partir d'expériences de traçage sur le terrain ou au laboratoire. Les valeurs calculées de la porosité effective au laboratoire sur trois échantillons de textures différentes ont été comparées aux estimations provenant de distributions de taille de particules et de courbes caractéristiques sol-eau. La concordance était plutôt faible et il semble qu'il n'existe aucune relation claire entre la porosité effective calculée à partir des expériences de traçage au laboratoire et la porosité effective estimée à partir des distributions de taille de parti-

cules et de courbes caractéristiques sol-eau. Une expérience de traçage de terrain dans un aquifère de sables et de graviers a fourni une porosité effective calculée d'environ 0,17. En comparaison, les estimations de porosité effective de données de texture, de teneur en eau et les valeurs publiées étaient environ 50 à 90% plus fortes que la valeur calibrée sur le terrain. Ainsi, l'estimation de la porosité effective pour le transport en solution dépend fortement du modèle de transport utilisé et est préférable lorsqu'elle est obtenue à partir d'expériences de traçage de laboratoire ou de terrain.

Resumen La porosidad efectiva en el análisis del transporte de solutos se suele estimar, en lugar de calcularse a partir de ensayos de trazadores en el campo o el laboratorio. Los valores calculados de la porosidad efectiva en el laboratorio en tres muestras de distintas texturas se compararon con las estimaciones realizadas a partir de las distribuciones de tamaño de partículas y de las curvas características suelo-agua. El ajuste fue bastante pobre y parece que no existe una relación clara entre los valores de la porosidad efectiva calculados mediante los tres métodos. Un ensayo de trazadores en el campo, en un acuífero formado por arenas y gravas, dio lugar a un valor de porosidad efectiva calculado de 0.17. Las estimaciones realizadas a partir de los datos de textura, humedad retenida y valores publicados eran entre un 50–90 por ciento mayores que el valor calibrado en el ensayo de campo. Así, la estimación del valor de la porosidad efectiva para el transporte químico depende mucho del modelo de transporte seleccionado y es mejor si se obtiene a partir de ensayos de laboratorio o de campo.

Received, March 1997
Revised, August 1997
Accepted, August 1997

Daniel B. Stephens (✉) · Kuo-Chin Hsu · Mark A. Prieksat
Mark D. Ankeny · Neil Blandford · Tracy L. Roth
James A. Kelsey
Daniel B. Stephens and Associates, Inc., 6020 Academy Road
NE, Albuquerque, New Mexico 87109, USA
Fax: + 505-822-8877
e-mail: dbsteph@dbstephens.com

Julia R. Whitworth
New Mexico Institute of Mining and Technology, Socorro,
New Mexico 87801, USA

Key words laboratory experiments measurements ·
tracer tests · unconsolidated sediments · numerical
modeling

Introduction

Modeling the transport of contaminants in groundwater has become a common and sometimes routine task for many practitioners in the field of hydrogeology over the past 15 years. Usually, hydraulic conductivity, and to a much lesser extent dispersivity, are the focus of field and laboratory data-collection efforts for models

that are based on the advection–dispersion equation (ADE). A third hydraulic parameter required for transport modeling is effective porosity. For aquifer simulations, it has become common practice to estimate effective porosity from one’s experience or the literature.

Effective porosity is generally defined for solute transport as that portion of the soil or rock through which chemicals move, or that portion of the media that contributes to flow (Fetter 1993; Domenico and Schwartz 1990). Horton et al. (1987) added some confusion by defining effective porosity as that part of the pore space where velocity is greater than the average fluid velocity. However, its in simplest and traditional form, effective porosity n_e is

$$n_e = \frac{q}{v} \quad (1)$$

where v is the mean velocity of a conservative tracer and q is the specific discharge, or Darcy velocity (e.g., Bear and Verruijt 1987). It is well recognized that effective porosity is less than the total porosity, because, even if the medium is fully saturated, not all of the water-filled pores are interconnected or contribute to flow. Therefore, terms such as mobile and immobile water or dead-end pores are also used in reference to the definition of effective porosity. In fact, Luckner and Schestakow (1991) equate effective porosity and mobile water content. In this paper we review some of the methods to derive effective porosity in the laboratory and field and assess their validity.

Determining effective porosity from tracer tests is not common practice. Field tracer tests are rare because of their expense, duration, and the impacts of the tracer on the aquifer may not be tolerated by regulators. Laboratory tracer tests are uncommon because the core samples are small and potentially unrepresentative of the aquifer at the scale of interest. Furthermore, laboratory cores are almost always vertical and perpendicular to the bedding, whereas aquifer flow and transport are predominantly horizontal; consequently, column tracer tests may poorly reproduce field conditions. Another reason that effective porosity is not often evaluated is that it has a small range of variability compared with hydraulic conductivity and dispersivity. Nevertheless, in the application of transport models, which in practice is often driven by environmental regulation and litigation, a need exists to justify the data that go into transport models with some type of measurement.

For the above reasons, effective porosity is most often obtained from other measured parameters, such as specific yield, or total porosity minus specific retention or residual water content. For example, Bear (1972, p. 484) defines effective porosity as the drainable porosity or the total porosity minus the field capacity. He indicates that for conditions of homogeneous soils and deep water tables, specific yield and effective porosity are identical. Practitioners in hydrogeology have been

attracted to this apparent identity, and they estimate effective porosity from the convenient relationship between particle size and specific yield, shown in *Figure 1*, that is included in most standard textbooks. Although effective porosity has been assigned two different definitions, many assume that the resulting two values are numerically equivalent. Unfortunately, many appear to have forgotten the caution issued by Bear (1972, p. 8) not to confuse effective porosity defined in the context of transport with effective porosity that pertains to drainage and capillary processes. Despite the obvious distinction, effective porosity defined by the latter is often used in simulating groundwater contamination and seems to have gained acceptance as a surrogate for the transport effective porosity without much challenge. For example, Boutwell et al. (1986) state “Most transport equations use effective porosity which does not include dead-end and unconnected pores. Effective porosity approximately equals specific yield.”

The purpose of this article is to evaluate the reliability of methods in estimating effective porosity from drainage and capillary measurements as well as particle size. Column tracer experiments were conducted in the laboratory to determine effective porosity, and these results were compared with estimates of effective porosity derived from soil–water characteristic curves and particle size. The second part of this article compares results of a field tracer test, where effective porosity was obtained by model calibration, to estimates of effective porosity derived from soil–water characteristic curves and particle size.

Calculating Effective Porosity for Transport

Effective porosity as required in groundwater transport models can be determined by laboratory and field techniques. Approaches to making these determinations are presented here, but the scope of the article precludes a comprehensive historical review or critique of

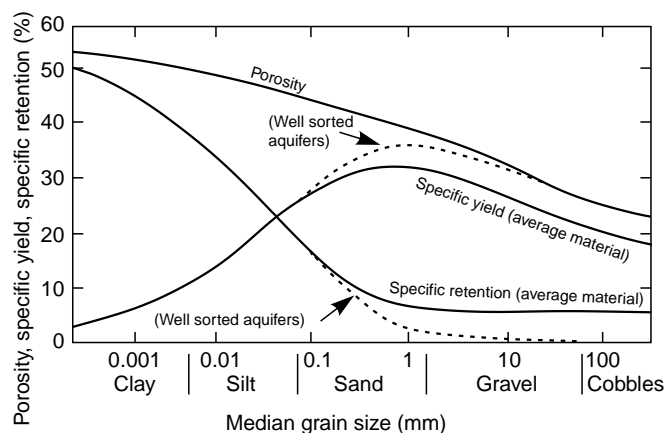


Fig. 1 Relationship between median grain size and water-storage properties of alluvium

all methods available. Such a thorough review has not been published to our knowledge, although excellent discussions of effective porosity in transport processes are in Norton and Knapp (1977), de Marsily (1986), Peyton et al. (1985), and elsewhere.

Laboratory Methods

For traditional solute-transport modeling, effective porosity (n_e) can be defined as the ratio between Darcy flux and seepage velocity, where q is experimental Darcy flux and v is seepage velocity (Eq. (1)). Laboratory apparatus for evaluating transport consists of a column packed with the media to be tested, fittings to maintain a constant flow rate through the column, fittings to inject tracers into the upstream end of the column, and a means to collect samples of outflow periodically for chemical analyses. Darcy flux can be calculated directly from the steady flow rate and column diameter, but seepage velocity depends on the conceptual transport model chosen.

If it is assumed that transport is a chemical and physical equilibrium process, solute transport can be modeled with a single porosity model described by the ADE

$$R \frac{\partial c}{\partial t} + v_i \frac{\partial c}{\partial x_i} = \frac{\partial}{\partial x_i} \left(D_{ij} \frac{\partial c}{\partial x_j} \right) \quad i, j = 1, 2, 3 \quad (2)$$

where R is the retardation factor, c is the solute concentration, v_i is the seepage velocity component in the x_i direction, and D_{ij} is the component of the dispersion coefficient tensor. This model assumes that degradation and chemical production are not significant. The mobile-flow pore space is represented by a single effective porosity and is used to estimate seepage velocity. Advective and diffusive processes are active within the pore space designated as effective porosity.

If it is assumed that there is no retardation, then the traditional column-testing approach can utilize the analytical solution of a one-dimensional version of Eq. (2) with constant inlet concentration, c_0 , and zero initial concentration

$$\frac{c}{c_0} = \frac{1}{2} \left[1 \pm \operatorname{erf} \left(\frac{x - vt}{2\sqrt{Dt}} \right) \right] \quad (3)$$

where erf is the error function. The relative concentration point ($c/c_0 = 0.5$) describes solute moving at the average velocity and for a nonreactive tracer $c/c_0 = 0.5$ should occur when one pore volume of solution has flowed from the column. Using the measured elapse time, $t_{0.5}$ at $c/c_0 = 0.5$, the known column length, L , and experimental Darcy flux, q , the effective porosity can be calculated as

$$n_e = \frac{L}{t_{0.5} q} \quad (4)$$

This approach is similar to determining n_e with Eq. (1), because $L/t_{0.5}$ is essentially the average solute velocity

eluting from the column. Luckner and Schestakow (1991) describe a three-step tracer test in short columns designed explicitly to quantify effective porosity.

Shackelford (1995) proposed a cumulative mass approach to derive effective porosity from breakthrough curves. A cumulative mass ratio (CMR) is calculated from

$$\text{CMR} = \frac{\sum \Delta m}{V_p c_0} = \frac{R_d}{2P_L} [(\xi_4 - \xi_2) \operatorname{erfc}(\xi_1) + (\xi_4 + \xi_2) \exp(\xi_2) \operatorname{erfc}(\xi_3)] \quad (5)$$

where

$$\xi_1 = \frac{R_d - T}{2\sqrt{\frac{TR_d}{P_L}}}; \quad \xi_2 = P_L; \quad \xi_3 = \frac{R_d + T}{2\sqrt{\frac{TR_d}{P_L}}};$$

and $\xi_4 = \frac{TP_L}{R_d}$ (6)

T is the number of pore volumes of flow, R_d is the retardation factor, and P_L is the column Péclet number. The CMR is plotted vs T and the slope of the plot during steady-state transport is unity, given by

$$\lim_{T \rightarrow \infty} \frac{d(\text{CMR})}{dT} = \lim_{T \rightarrow \infty} \frac{1}{2} [\operatorname{erfc}(\xi_1) + \exp(\xi_2) \operatorname{erfc}(\xi_3)] = 1 \quad (7)$$

The unit slope is plotted to determine the x -axis intercept and is designated as T_0 representing the retardation factor R_d . The measured value of T_0 for a nonreactive tracer ($R_d = 1$) represents the ratio of n_e/n . Thus, effective porosity is derived by multiplying this ratio by the total porosity.

Kinetic adsorption and heterogeneous flow regions cause chemical and physical non-equilibrium, respectively. Two-site/two-region transport models (van Genuchten and Wagenet 1989) have been proposed to describe non-equilibrium phenomenon. The two-site/two-region model can be described in dimensionless form as

$$\beta R \frac{\partial C_1}{\partial T} + \frac{\partial C_1}{\partial Z} = \frac{1}{P} \frac{\partial^2 C_1}{\partial Z^2} + \omega(C_1 - C_2) \quad (8)$$

$$(1 - \beta) R \frac{\partial C_2}{\partial T} = \omega(C_1 - C_2) \quad (9)$$

where β is the partition coefficient, P is the Péclet number (defined as vL/D), C_1 is the concentration at equilibrium site, C_2 is the concentration at non-equilibrium site, and ω is a dimensionless mass transfer coefficient. For the two-region model when $R = 1$, β is the ratio of the mobile-water region to total porosity. The pore space is divided into two parts, the mobile-water region, where equilibrium processes occur, and the immobile region, where non-equilibrium processes occur. Both advection and diffusion occur in the mobile region, but only first-order kinetic processes occur in the immobile region. Toride et al. (1995) present a versatile

software program, CXTFIT, for evaluating solute breakthrough curves. The program optimizes the parameters by fitting curves to measured data for a range of conceptual models, including the mobile/immobile water model presented in *Eqs. (8) and (9)*.

Breakthrough curves obtained from laboratory column tests can be described by a one-dimensional version of *Eq. (2)*, where v and D are viewed as constants or by *Eqs. (8) and (9)*. The decision to apply the equilibrium or non-equilibrium model may be judged using selection criteria presented by Carrera et al. (1990). The complex non-equilibrium model may be more representative of the soil system, but the equilibrium model is generally easier to use.

However, extrapolation of column-test results to field scales is still viewed with some skepticism. Therefore, several methods for determining effective porosity from field solute-transport experiments are presented.

Field Methods

Effective porosity can be obtained from field-scale well-tracer tests, in which a tracer is injected into a well and is pumped back from either the same injection well or from another well. For example, Hall et al. (1991) propose a method to estimate effective porosity in a homogeneous confined aquifer dominated by steady-state horizontal advective transport with a constant hydraulic gradient. They use Darcy's equation, with an added effective-porosity term from *Eq. (1)*.

$$V = \frac{KI}{n_e} \quad (10)$$

and a version of the equation for the drift and pump-back test described by Leap and Kaplan (1988).

$$V = \frac{(Qt/\pi n_e b)^{1/2}}{d} \quad (11)$$

where K is the horizontal hydraulic conductivity; I is the horizontal hydraulic gradient; Q is pumping rate during recovery of tracer, t is the time elapsed from the start of pumping until the center of mass of the tracer is recovered; b is the aquifer thickness; and d is the time elapsed from the injection of tracer until the center of the mass of tracer is recovered. From *Eqs. (11) and (12)*, effective porosity can be calculated as

$$n_e = \frac{\pi b K^2 I^2 d^2}{Qt} \quad (12)$$

A single-well borehole dilution test (Drost et al. 1968; Halevy et al. 1967; Grisak et al. 1977) can be conducted by injection and subsequent withdrawal of a tracer in a single well through a zone isolated by dual packers. Seepage velocity v can be calculated as

$$v = -\frac{V}{\beta A t} \ln\left(\frac{c}{c_0}\right) \quad (13)$$

where V is volume of the borehole interval with verti-

cal cross-sectional area A , β is a geometric factor ranging from 0.5–4.0, t is time, c is recovered tracer concentration, and c_0 is the concentration of introduced tracer. Effective porosity can then be calculated from *Eq. (1)* if specific discharge can be calculated from hydraulic conductivity K and hydraulic gradient I .

Two-well tests can be performed in both confined and unconfined aquifers (Gaspar and Oncescu 1972). One well is pumped at a constant flow rate Q , and when the flow rate is at a quasi-steady state, a tracer is injected into the other well at distance L from the pumping well. The concentration recovered from the pumping well is recorded over time. For a horizontal confined aquifer with thickness D , the effective porosity is calculated as

$$n_e = \frac{Qt_i}{\pi L^2 D} \quad (14)$$

where t_i is the travel time of the tracer between the injection and pumping wells. For an unconfined aquifer with negligible natural gradient, effective porosity can be calculated as

$$n_e = \frac{Qt_i}{\pi L^2 \left(h - \frac{Q}{4\pi k h} \right)} \quad (15)$$

where h is the hydraulic head in the well where the tracer was introduced. This method is effective if the wells span the thickness of the aquifer layer and if $L \gg h$ (Halevy and Nir 1962).

Another approach is to use solute-breakthrough data obtained from field tracer tests to calibrate the transport parameters of the model. However, since the numerical solution to most field-scale problems of non-reactive transport is non-unique (Molson and Frind 1990), the information obtained from model calibration may be valid only for the conceptual model used during calibration. Effective porosity is then a calibrated value that gives the best fit to measured solute breakthrough.

Laboratory Tracer Tests

Three soil materials (sand, silica flour, and a mixture of 75% fine sand and 25% silica flour) were chosen for testing. The sand, silica flour, and mixture columns were hand packed in the laboratory. Soil columns for the solute-breakthrough tests and hydraulic-properties tests were packed concurrently into a column comprised of brass cylinders to ensure that both columns would have similar physical and hydrologic characteristics.

Brass cylinders approximately 5 cm in diameter were cut to lengths of approximately 5 and 10 cm. The columns were prepared by securing one 5-cm-length and one 10-cm-length of brass cylinder together, end to end, using tape. The air-dry soil material was then poured

into the cylinder while gently tapping and shaking the cylinder, to insure uniform settling and packing, until the column was full. The cylinders were separated and trimmed flat on the ends. The 10-cm section was used for the solute-transport and breakthrough analysis, and the 5-cm portion was used for hydraulic-properties testing.

The repacked samples were placed in permeameters, and saturated hydraulic conductivities, K_s , were determined using constant and falling-head methods. Values of K_s are shown in *Table 1*. Soil-water characteristics for drainage were determined using hanging-column, pressure-plate, and thermocouple psychrometer analysis. Data from the moisture-retention analyses, shown in *Figure 2*, were fit using the RETC computer code (van Genuchten et al. 1991), and the results are shown in *Table 1*. The total porosity is equal to the saturated water content, θ_s , and is very close to the calculated porosity value obtained using the dry bulk density and an assumed particle density of 2.65 g/cm^3 .

Recognizing that the pressure potential used to determine residual moisture content will affect the moisture-retention analysis (Stephens and Rehfeldt 1985; Corey 1994), residual water contents (θ_r) were determined by using pressure potentials of -0.33 bar (Ahuja 1989) and -15 bar (*Table 1*).

Solute breakthrough tests, using a tritium tracer, were performed on the 10-cm-long repacked soil columns; results are shown in *Table 2*. The columns were oriented vertically and the flow direction was upward. A 0.05-M calcium sulfate-water solution was delivered from a reservoir to the columns using a peristaltic pump. The soil columns were periodically removed from the system and weighed to determine the extent of saturation. When the column weights were constant, the columns were considered to be saturated. Outflow solution was collected, using fraction collectors, for several days to determine column fluxes. After column fluxes had been determined, a tritium solute was then introduced into the influent solution. Activity of outflow samples and samples of the influent solutions were determined using a scintillation counter.

Solute-breakthrough data were analyzed using the CXTFIT (version 2.0) code (Toride et al. 1995). Both equilibrium and non-equilibrium models were fit to the tritium-breakthrough results. Effluent samples were assumed to represent flux-averaged concentrations. Because tritium approximates a conservative tracer, the retardation factor was set to 1 for all fitting procedures. The program was allowed to fit all other parameters, i.e., in the equilibrium model, mean pore velocity and dispersion are fitted, and in the non-equilibrium model two additional parameters, β and ω , are fitted. Measured data and fitted curves are shown in *Figure 3*. Calculated values of pore velocity and dispersion coefficient determined by fitting the equilibrium and non-equilibrium models are shown in *Table 3*. For the non-equilibrium model, $v = v_m$, the velocity through the mobile pores.

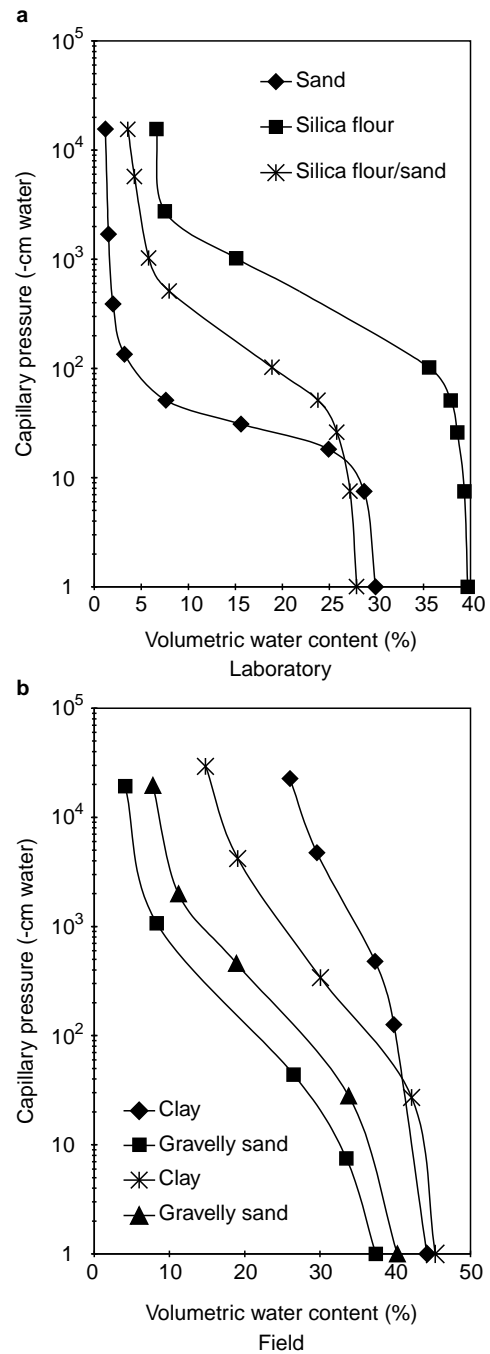


Fig. 2a,b Curves of soil-water characteristics

Effective porosity is calculated from *Eq. (1)* knowing q from the experimental flow rate (*Table 2*) and v obtained by analyses of the breakthrough curve using the CXTFIT program (*Table 3*). For the non-equilibrium model, one could presume that β , the mobile water content/porosity ratio, multiplied by the total porosity would also represent effective porosity.

Cumulative effluent solute mass was also measured for each column and the data were analyzed to compute effective porosity with Shackleford's cumulative-mass approach (*Eqs. (5)–(7)*).

Table 1 Laboratory hydraulic properties of soils used in the laboratory tracer tests and soils from the field site

Soil type	b (g/cm ³)	K_s (cm/sec)	θ_r (-1/3 bar) (cm ³ /cm ³)	θ_r (-15 bar) (cm ³ /cm ³)	θ_s (cm ³ /cm ³)	d_{50} (mm)
Sand	1.86	5.2×10^{-3}	0.024	0.011	0.300	0.13
Silica	1.60	1.6×10^{-5}	0.263	0.066	0.397	0.024
Sand/Silica Mixture	1.94	4.6×10^{-5}	0.124	0.036	0.279	0.091
Field 1 – Clay	1.48	2.0×10^{-8}	0.387	0.279	0.442	0.0065
Field 2 – Gravelly Sand	1.66	1.6×10^{-3}	0.157	0.046	0.374	8.7
Field 3 – Sandy Clay	1.45	2.3×10^{-6}	0.307	0.163	0.453	0.038
Field 4 – Gravelly Sand	1.58	4.7×10^{-4}	0.215	0.093	0.403	2.7

b : Bulk density
 K_s : Saturated hydraulic conductivity
 θ_r : Residual water content
 θ_s : Saturated water content
 d_{50} : Median grain size
Porosity

Table 2 Laboratory tracer test conditions

Soil Type	Flow rate, Q (cm ³ /hr)	Inlet Pulse Duration (hr)	Column Cross Section, A (cm ²)	Column Length, L (cm)	Darcy flux, q (cm/hr)
Sand	24.40	12.35	42.21	10.045	0.578
Silica	19.79	21.5	42.21	9.124	0.469
Sand/Silica Mixture	16.89	13.1	42.21	9.737	0.400

Table 3 Transport parameters from laboratory experiments

Soil Type	Equilibrium Model		Non-Equilibrium Model			
	v (cm/hr)	D (cm ² /hr)	v (cm/hr)	D (cm ² /hr)	β	ω
Sand	1.339	7.76	5.621	2.24	0.2665	1.556
Silica	1.139	12.29	1.674	6.60	0.3221	0.1612
Sand/Silica Mixture	1.15	2.197	18.67	6.6×10^{-3}	0.068	6.16

v = Pore-water velocity
D = Hydrodynamic dispersion coefficient
 β = θ_m/θ , where θ_m is the volumetric water content of mobile liquid phase and θ is total water content
 ω = $\alpha L/\theta v$, where L is characteristic length, and α is a first-order kinetic rate coefficient

Table 4 Estimated and calculated effective porosity in soil columns

Soil Type	Calculated			Estimated		
	Equilibrium Model	Non-Equilibrium Model	Cumulative Mass Approach	Particle Size	$n-\theta_r$ (0.3b)	$n-\theta_r$ (15b)
Sand	0.431	0.102	0.248	0.32	0.276	0.289
Silica	0.412	0.280	0.159	0.20	0.134	0.331
Sand/Silica Mixture	0.348	0.021	0.261	0.30	0.155	0.243

Table 4 summarizes the laboratory measured and estimated effective-porosity results. The equilibrium-model parameters resulted in effective porosity values that were greater than the total porosity (Table 1) for each soil and were deemed to be unreasonable. The non-equilibrium model gave the best fit to the experimental breakthrough data. However, the calculated effective porosity represented only approximately 33, 70, 7% of the saturated water content for the sand, silica,

and sand/silica mix, respectively. The cumulative-mass approach provided estimates of effective porosity that appear intuitively more reasonable, inasmuch as the effective porosity comprises approximately 83, 40, and 93% of the saturated water content for the sand, silica, and sand/silica mix.

The β parameter from the non-equilibrium model (Table 3), when multiplied by total porosity, θ_s (Table 1), gives θ_m , the mobile water content. The respec-

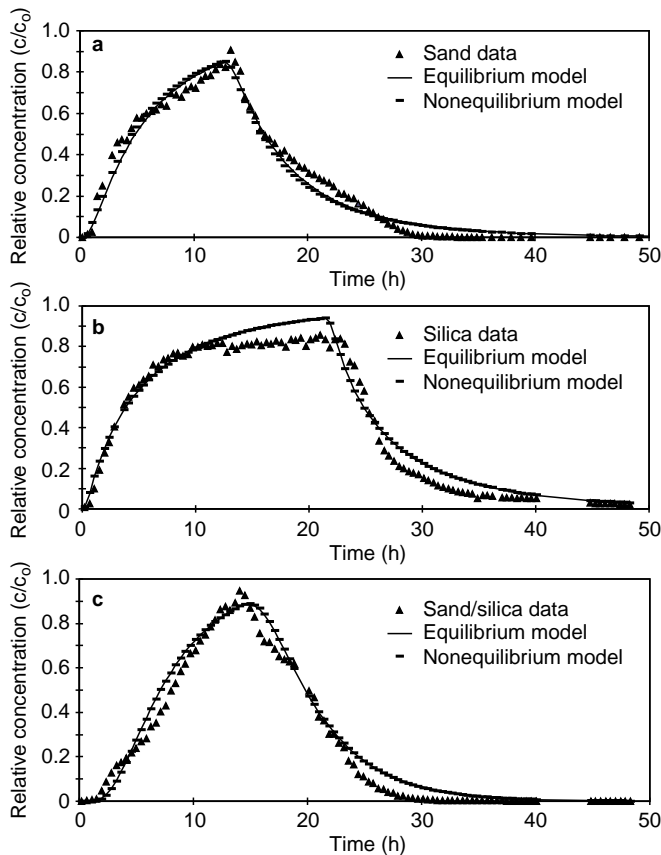


Fig. 3 Observed and fitted tritium breakthrough concentration for fine sand, silica flour, and sand/silica mixture

tive values of θ_m are 0.08 for sand, 0.128 for silica, and 0.02 for the sand/silica mix. The mobile water content is similar to the effective porosity calculated by *Eq. (1)*, except for silica. The reason for the poor agreement for silica is not clear.

Among the methods to estimate effective porosity of a specific soil, significant variability is evident. The estimated effective porosity from particle size (i.e., *Fig. 1*) tends to be most similar to effective porosity calculated by the cumulative-mass approach. The estimated effective porosity based on porosity minus the 0.33-bar water content gives reasonable agreement with calculated values from cumulative-mass approach, except for the sand/silica mix. The estimated effective porosity calculated as porosity minus the 15-bar water content gives fair agreement to effective porosity calculated for the sand and the sand/silica mix from the cumulative-mass approach; but for silica, porosity minus 15-bar water content overestimates the values from cumulative-mass approach by more than 100% and is actually closer to the effective porosity calculated from the non-equilibrium model.

Due to the scatter in calculated values of effective porosity for each soil, it is not possible to discern which model provided the most accurate estimate of effective porosity. The value of effective porosity appears to be

dependent on the conceptual model chosen for transport. Wide scatter also exists in the estimated values of effective porosity. Consequently, it is not possible based on these experiments to establish any relationship between estimated and calculated effective porosity, even for homogeneous soil.

Sources of uncertainty also exist in the analysis of the tracer experiments. For example, at the low Péclet numbers (0.9–5.2) in these short-column tests, the breakthrough curves are probably sensitive to boundary conditions. In the usual application of the equilibrium models, instead of obtaining v by fitting, one assumes that v is known from q/θ_s (Parker 1984). However, this would preclude us from obtaining effective porosity from *Eq. (1)*. Likewise, the velocity can be specified in the non-equilibrium model and effective porosity calculated from $\beta\theta_s$. Unfortunately, without constraints on more parameters, the calculated values of effective porosity from the popular code CXTFIT vary considerably. Perhaps special tracer tests, such as those described by Luckner and Schestakow (1991), would provide more definitive calculations of effective porosity in the laboratory.

Field Tracer Test

A groundwater reclamation system constructed to remediate contamination at the Tucson International Airport Superfund site (in Arizona, USA) afforded an opportunity to determine effective porosity in the field. The reclamation well field, which began operation in 1987, consists of extraction wells that pump contaminated water to a treatment plant where sulfuric acid is added to the treated water prior to reinjection. Sulfate in excess of background concentrations was considered as a conservative tracer in groundwater. Groundwater monitor wells were sampled periodically as part of the routine system performance assessment. A portion of the reclamation system consisting of the area near injection well R-5 and monitor well M-6 was used for analyzing the breakthrough data. This area and a geologic cross section are shown in *Figure 4*.

Effective porosity was obtained by calibrating a numerical flow and transport model. The flow code MODFLOW (McDonald and Harbaugh 1988) was used to generate the transient hydraulic-head field in two dimensions in the plan view (*Fig. 4*). The mesh consisted of grid blocks of 37 rows \times 31 columns having dimensions of 25 \times 25 feet. The injection-rate history is known from available metering records; rates ranged from 50–392 gpm. Hydraulic conductivity is 40 feet/day throughout this local domain and is consistent with the regional-scale conductivity field generated by geostatistical analysis of numerous well tests in the area. The storage coefficient is 0.25. The comparison of the model predicted and measured hydraulic head in the monitor well M-6 is presented in *Figure 5*.

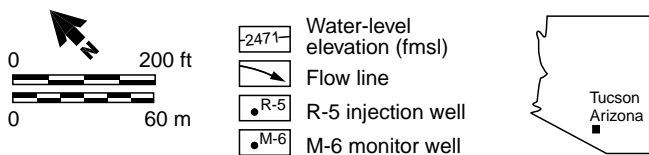
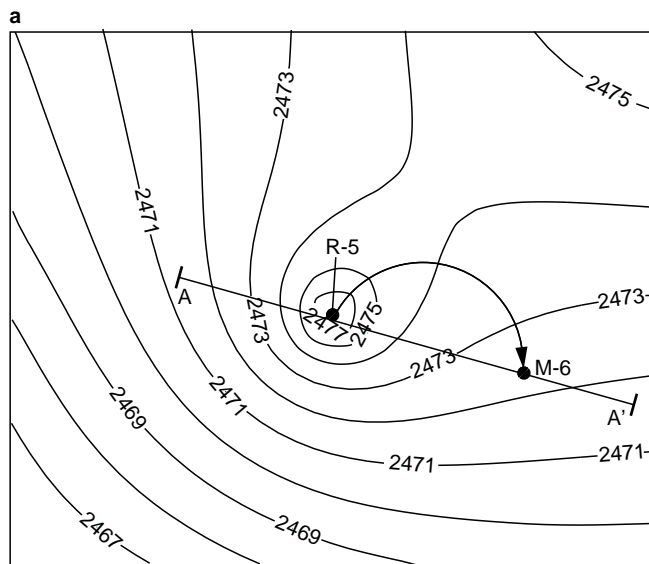


Fig. 4 **a** Water-level elevations and **b** geologic cross section through recharge well R-5 and monitor well M-6, Tucson International Airport Superfund Site, Arizona, USA

For transport, the solute-transport code SURFACT (Hydrogeologic, Inc. 1996) was used which accepted as input the velocity field produced by MODFLOW. Effective porosity was obtained in a trial-and-error process by adjusting the model-assigned effective porosity until a best fit to observed sulfate data was obtained. As part of the calibration process, longitudinal and

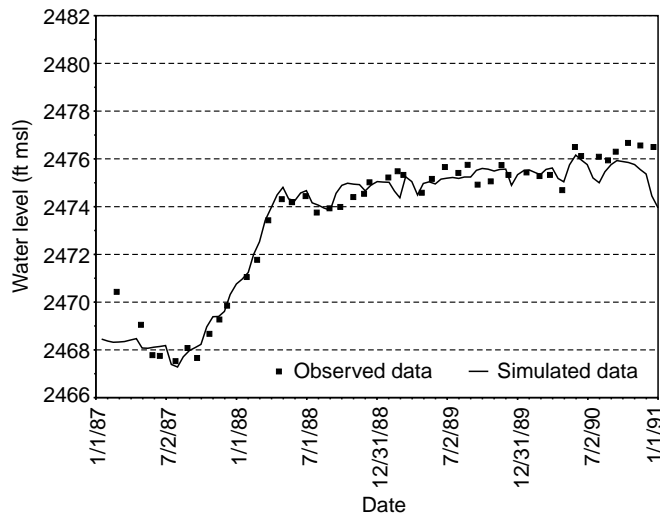


Fig. 5 Observed and predicted water levels in monitor well M-6

transverse dispersivity were also adjusted. The calibration criterion was the minimization of the root mean squared error in concentration

$$RMS = \left[\frac{1}{n} \sum_{i=1}^n (c_m - c_s)_i^2 \right]^{0.5} \tag{16}$$

where n is the number of monitoring data, c_m is the measured concentration, and c_s is the simulated concentration. The results are shown in *Figure 6*, which demonstrates that there is no unique solution, that the breakthrough curves are much more sensitive to effective porosity than dispersivity ratio, and that the best fit

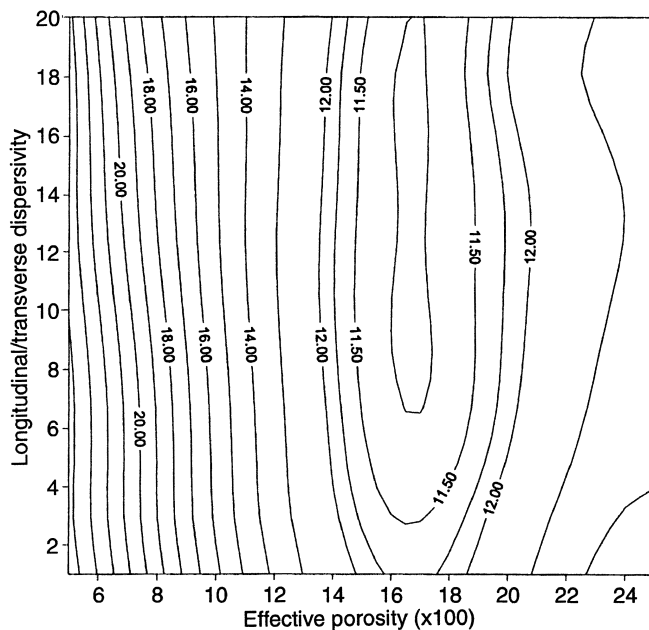


Fig. 6 RMS error from numerical simulation of sulfate breakthrough

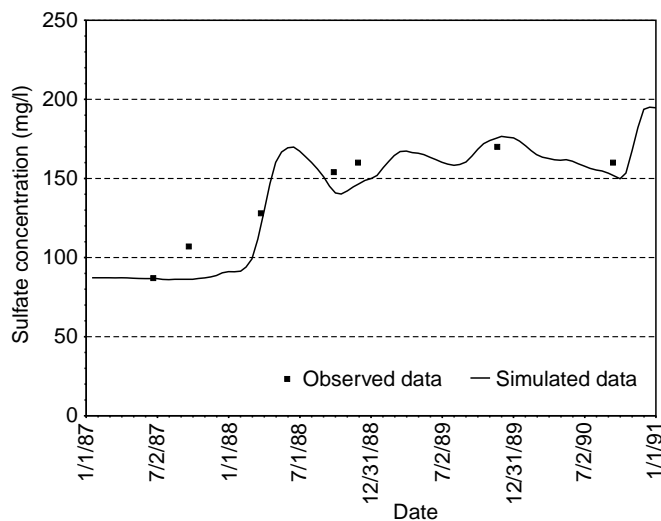


Fig. 7 Observed and predicted sulfate concentrations

to the measured concentration occurs when effective porosity is approximately 0.17. *Figure 7* shows the observed and simulated concentration history for the monitor well.

For comparison, the effective porosity also was inferred using *Figure 1* and estimated median particle size, based on geologic logs of the injection well. The aquifer consists of alluvium that is predominantly sand and gravel, with some layers of silt and clay (*Fig. 4*). Assuming transport occurs primarily in the gravelly sand, the effective porosity is estimated to be 0.32, based on a qualitative evaluation of soil texture. Measured physical properties from two core samples of similar gravelly sand field soils are given in *Table 1*. The measured median particle size by sieve analysis was used in *Figure 1* to determine specific yield. The estimated effective porosity is approximately 0.31.

The effective porosity was also estimated from measured soil-water characteristic curves on two samples of similar sand-and-gravel aquifer material from nearby borings (*Table 1*). For these samples effective porosity, estimated as porosity minus the 15-bar water content, ranges from 0.30–0.32. These values are consistent with effective porosity estimated from the specific yield determined with *Figure 1*, based on soil texture characterized both qualitatively from the geologic description and quantitatively from sieve analysis.

Groundwater models have also been constructed to simulate the regional transport of organic solvents over an area that encompasses this field tracer study area, as well as a plume one mile wide and five miles long. Each of the modelers estimated the effective porosity as 0.25, using professional judgment applied to the predominantly gravelly sand composition of the aquifer (Hargis and Montgomery 1982; Mock 1985; CH2M Hill 1987).

Table 5 summarizes the effective porosity values obtained at the field site. The estimates are approximately 50–90% greater than the measurements obtained from

Table 5 Estimated and calculated effective porosity at field site

Method		Effective Porosity
Calculated	Field Tracer Test	0.17
Estimated	Geologic Logs	0.32
	Measured Particle Size	0.31
	$n-\theta_r$ (15b)	0.32
	Mock (1985)	0.25
	CH2M Hill (1987)	0.25
	Hargis (1982)	0.25

the field tracer test. One practical implication of this result is that the predicted length of the regional TCE plume by the regional transport model using the smaller effective porosity would be at least 1.5 times longer than a plume predicted with the estimated, larger effective porosity.

Conclusion

A comparison of estimated and calculated effective porosity was done in this study. Calculated effective porosity from tracer tests in the laboratory is highly dependent on the chosen conceptual transport model and fitting approach. No consistent agreement was observed between estimated effective porosity and values calculated from laboratory tracer tests. Estimation methods tend to overestimate the transport effective porosity in a field tracer test conducted in a layered aquifer composed predominantly of gravelly sand. Effective porosity for transport cannot be reliably estimated from particle size and specific yield or from measurements of soil-water retention.

Field tracer tests provide the most direct method for obtaining effective porosity, but often they are relatively expensive and time-consuming. However, as in the case study here, model calibration may be a cost-effective approach to determine effective porosity using existing monitor-well time-series data.

Acknowledgment We are grateful to R. Bowman, Geoscience Department, New Mexico Institute of Mining Technology, Socorro, New Mexico, for conducting the laboratory tracer-breakthrough experiments and for his helpful suggestions in the interpretation of data.

References

- Ahuja LR, Cassel DK, Bruce RR, Barnes BB (1989) Evaluation of spatial distribution of hydraulic conductivity using effective porosity data. *Soil Sci Soc Am J* 148:404–411
- Bear J (1972) *Dynamics of fluids in porous media*. Elsevier, New York
- Bear J, Verruijt A (1987) *Modeling groundwater flow and pollution*. Reidel, Dordrecht

- Boutwell SH, Brown SM, Roberts BR, Atwood DF (1986) Modeling remedial actions at uncontrolled hazardous waste sites. Neyes Publications, Park Ridge, New Jersey
- CH2M-Hill (1987) Draft: assessment of the relative contribution to groundwater contamination from potential sources in the Tucson Airport area, Tucson, Arizona, EPA contract no. 68-01-7251, CH2M Hill, Santa Ana, California
- Carrera J, Samper J, Galarza G, Medina A (1990) An approach to process identification: application to solute transport through clays. In: ModelCARE 90: calibration and reliability in groundwater modeling. IAHS Publ 195:231-240
- Corey AT (1994) Mechanics of immiscible fluids in porous media. Water Resource Publication, Fort Collins, Colorado
- Marsily G de (1986) Quantitative hydrogeology: groundwater hydrology for engineers. Academic Press, San Diego, California
- Domenico PA, Schwartz FW (1990) Physical and chemical hydrogeology. Wiley, New York
- Drost W, Klotz D, Koch A, Moser M, Neumaier F, Rauer W (1968) Point dilution methods of investigating groundwater flow by means of radioisotopes. Water Resour Res 4:125-146
- Fetter CW (1993) Contaminant hydrogeology. MacMillan, New York
- Gaspar E, Oncescu M (1972) Radioactive tracers in hydrology. Elsevier, New York
- Grisak GE, Merriott WF, Williams DW (1977) A fluoride borehole dilution apparatus for groundwater velocity measurements. Can Geotech J 14:554-561
- Halevy E, Nir A (1962) The determination of aquifer parameters with the aid of radioactive tracers. J Geophys Res 67 (6): 403
- Halevy E, Moser H, Zellhofer O, Zuber A (1967) Borehole dilution techniques: a critical review. In: Isotopes in Hydrology, IAEA Proc Series, IAEA, Vienna
- Hall SH, Luttrell SP, Cronin WE (1991) A method for estimating effective porosity and ground-water velocity. Ground Water 29:171-174
- Hargis and Montgomery (1982) Digital simulation of contaminant transport in the regions aquifer systems, Tucson Report no. TR-C.4
- Horton R, Thompson ML, McBride JF (1987) Method of estimating the travel time of noninteracting solutes through compacted soil material. Soil Sci Soc Am J 51:48-53
- Hydrogeologic, Inc. (1996) MS-VNS users manual
- Leap DI, Kaplan PG (1988) A single-well tracing method for estimating regional advective velocity in a confined aquifer: theory and preliminary laboratory verification. Water Resour Res 24 (3): 993-998
- Luckner L, Schestakow WM (1991) Migration processes in the soil and groundwater zone. Lewis Publishers, Chelsea, Michigan
- McDonald MG, Harbaugh AW (1988) A modular three-dimension finite-difference groundwater flow model. USGS Open File Rep 83-875
- Mock PA, Travers BC, Williams CK (1985) Results of the Tucson Airport area remedial investigation, phase I, vol II. Tucson Report TR-B.1., pp 88-89
- Molson JW, Frind EO (1990) Perspectives on non-uniqueness in three-dimension transport simulations of biodegrading organic contaminants. In: ModelCARE 90: calibration and reliability in groundwater modeling. IAHS Publ 195:341-350
- Norton D, Knapp R (1977) Transport phenomena in hydrothermal systems: the nature of porosity. Am J Sci 277:913-936
- Parker JC (1984) Analysis of solute transport in column tracer studies. Soil Sci Soc Am J 48 (4): 719
- Peyton GR, Gibb JR, LeFaivre MH, Ritchey JD (1985) On the concept of effective porosity and its measurement in saturated fine-grained porous materials. In: Proc 2nd Canadian/American Conference of Hydrology, National Water Well Association, Dublin, Ohio
- Shackelford CD (1995) Cumulative mass approach for column testing. J Geotech Eng: 696-703
- Stephens DB, Rehfeldt KR (1985) Evaluation of closed-form analytical models to calculate conductivity in a fine sand. Soil Sci Soc Am J 49:12-19
- Toride N, Leij FJ, van Genuchten MTh (1995) The CXTFIT code for estimating transport parameters from laboratory and field tracer experiments. Version 2.0. U.S. Salinity Laboratory Research Rep no. 137
- van Genuchten MTh, Wagenet RJ (1989) Two-site/two-region models for pesticide transport and degradation: theoretical development and analytical solutions. Soil Sci Soc Am J 53:1303-1310
- van Genuchten MTh, Leij FJ, Yates SR (1991) The RETC code for quantifying the hydraulic functions of unsaturated soils. U.S. Salinity Laboratory Research Rep, 83 pp

**APPLICATION FOR PERMIT
OWL LANDFILL SERVICES, LLC**

**VOLUME III: ENGINEERING DESIGN AND CALCULATIONS
SECTION 8: EVAPORATION CALCULATIONS**

TABLE OF CONTENTS

Section No.	Title	Page
1.0	INTRODUCTION	III.8-1
1.1	Description	III.8-1
2.0	DESIGN CRITERIA	III.8-2
3.0	EVAPORATION POND DESIGN.....	III.8-5
3.1	Design Criteria	III.8-5
3.2	Design Concepts.....	III.8-6
3.3	Water Balance Modeling.....	III.8-7
3.4	Mechanical Evaporator Lateral Drift Analysis	III.8-10
4.0	SUMMARY	III.8-12

LIST OF FIGURES

Figure No.	Title	Page
III.8.1	WIND ROSE	III.8-4
III.8.2	EVAPORATION POND WATER BALANCE FLOW DIAGRAM	III.8-8
III.8.3	EVAPORATION POND MECHANICAL EVAPORATOR LOCATIONS	III.8-9
III.8.4	EFFECT OF HUMIDITY AND TEMPERATURE ON DRIFT	III.8-14

LIST OF TABLES

Table No.	Title	Page
III.8.1	EVAPORATOR WATER BALANCE.....	III.8-3
III.8.2	INFLUENCE OF DROPLET SIZE ON DRIFT DISTANCE.....	III.8-11
III.8.3	LATERAL DRIFT AT VARIOUS WINDSPEEDS	III.8-11
III.8.4	DRIFTSIM ANALYSIS RESULTS.....	III.8-13

**APPLICATION FOR PERMIT
OWL LANDFILL SERVICES, LLC**

**VOLUME III: ENGINEERING DESIGN AND CALCULATIONS
SECTION 8: EVAPORATION CALCULATIONS**

LIST OF ATTACHMENTS

Attachment No.	Title
III.8.A	EFFECTS OF MAJOR VARIABLES ON DRIFT DISTANCES OF SPRAY DROPLETS (OHIO STATE UNIVERSITY, 1998)
III.8.B	DRIFTSIM [®] : PREDICTING DRIFT DISTANCE OF SPRAY DROPLETS AND RESULTING EVAPORATION

**APPLICATION FOR PERMIT
OWL LANDFILL SERVICES, LLC**

**VOLUME III: ENGINEERING DESIGN AND CALCULATIONS
SECTION 8: EVAPORATION CALCULATIONS**

1.0 INTRODUCTION

OWL Landfill Services, LLC (OWL) is proposing to permit, construct, and operate a “Surface Waste Management Facility” for oil field waste processing and disposal services. The proposed OWL Facility is subject to regulation under the New Mexico (NM) Oil and Gas Rules, specifically 19.15.36 NMAC, administered by the Oil Conservation Division (OCD). The Facility has been designed in compliance with the requirements of 19.15.36 NMAC, and will be constructed, operated, and closed in compliance with a Surface Waste Management Facility Permit issued by the OCD.

The OWL Facility is one of the first designed to the new more stringent standards that, for instance, mandate double liners and leak detection for land disposal. The new services that OWL will provide fill a necessary void in the market for technologies that exceed current OCD requirements.

1.1 Description

The OWL Surface Waste Management Facility will comprise approximately 500 acres of the 560-acre site, and will include two main components: an oil field waste Processing Area and an oil field waste Landfill, as well as related infrastructure. Oil field wastes are anticipated to be delivered to the OWL Facility from oil and gas exploration and production operations in southeastern NM and west Texas. The Site Plan provided as **Figure II.1.2** identifies the locations of the Processing Area and Landfill facilities, which are further detailed on the **Permit Plans (Volume III.1)**. The proposed facilities are detailed in **Table II.1.2**, and are anticipated to be developed in four primary phases as described in **Table II.1.3**. The design of the OWL facilities shown on Figures and Permit Plans is preliminary; and construction plans and specifications for each major element will be submitted to OCD in advance of installation.

2.0 DESIGN CRITERIA

The Processing Area will include evaporation ponds for the disposal of Produced Water. The area and volume of the lined portion of each evaporation pond is 1.88 acres of water surface with a capacity of 9.5 acre-feet (ac-ft). OWL is considering the installation of approximately 12 ponds, which will provide a total of 18.80 surface acres for evaporation of 114 total acre-ft of pond capacity.

2.1 General Site Conditions

The site terrain is gently sloping toward the southwest with sparse vegetation. The macroclimate of the OWL area is classified by the Koppen Climate Classification System as a “BSk”, which indicates a semi-arid steppe with much of the characteristics of a desert. Meteorological climatic data was obtained from the Western Regional Climate Center for pan evaporation at Lake Avalon (north of Carlsbad) and precipitation at the Hobbs FAA Airport weather stations. The Hobbs climate summary provides a more conservative reporting point for this calculation than the Ochoa weather station reported in other Parts of this Application.

The evaluation of climate data for these nearby weather stations indicates that they are relatively similar and will likely provide reasonable precipitation estimates for the site (**Table III.8.1**). Climatic data available for the Lake Avalon weather station includes pan evaporation for the years of record from 1914 through 1979. The Hobbs FAA Airport weather station includes precipitation for the years of record from 1942 through 2006. The Lake Avalon pan evaporation data was used to estimate monthly evaporation values at the Facility. The observed pan evaporation values were scaled by a factor of 0.7 to represent actual pond evaporation. The average monthly evaporation and precipitation data used for design of this Facility’s evaporation ponds is summarized in **Table III.8.1**. Considering this climatic data, the annual evaporation exceeds annual precipitation on average by over six times.

The predominant wind directions for the site are from the southeast, with an average annual wind speed of 11 miles per hour (mph). The maximum sustained wind speed conservatively used for facility design is 12 mph. **Figure III.8.1** is the Wind Rose from the Paduca weather station located approximately 10 miles west of the facility.

**TABLE III.8.1
Produced Water Evaporation Ponds - Evaporator Water Balance
OWL Landfill Services, LLC**

All data in inches	January	February	March	April	May	June	July	August	September	October	November	December	Total
Rainfall	0.42	0.37	0.29	0.78	2.06	0.87	1.56	1.76	2.09	1.61	0.22	0.11	12.14
Pan Evaporation	4.49	5.33	9.42	12.36	14.31	15.16	14.14	12.33	9.25	7.26	4.68	4.2	112.93
Actual Evaporation	3.14	3.73	6.59	8.65	10.02	10.61	9.90	8.63	6.48	5.08	3.28	2.94	79.05
NET (Rainfall-Evaporation)	-2.72	-3.36	-6.30	-7.87	-7.96	-9.74	-8.34	-6.87	-4.39	-3.47	-3.06	-2.83	-66.91
Net Evaporation (bbl/pond)	3314	4090	7672	9580	9684	11856	10147	8362	5336	4225	3719	3444	81430

Mechanical Evaporation Analysis

% Mech Evap Potential 30% 32% 44% 50% 50% 50% 50% 50% 44% 40% 35% 34% 34%

BBL/D@75GPM 386 411 566 643 643 643 643 643 566 514 450 437

Assume 25% Mech Evap 25% 25% 25% 25% 25% 25% 25% 25% 25% 25% 25% 25%

BBL/D@75GPM 321 321 321 321 321 321 321 321 321 321 321 321 321

Evap Units Req:

1000 bbl/Pond 3 3 3 3 3 3 3 3 3 3 3 3 3

Phase I @3000 bbl 9 9 9 9 9 9 9 9 9 9 9 9 9

Ultimate @9000 bbl 28 28 28 28 28 28 28 28 28 28 28 28 28

bbl/day Factor of Safety (FS) 64 90 244 321 321 321 321 321 244 193 129 116 **224**

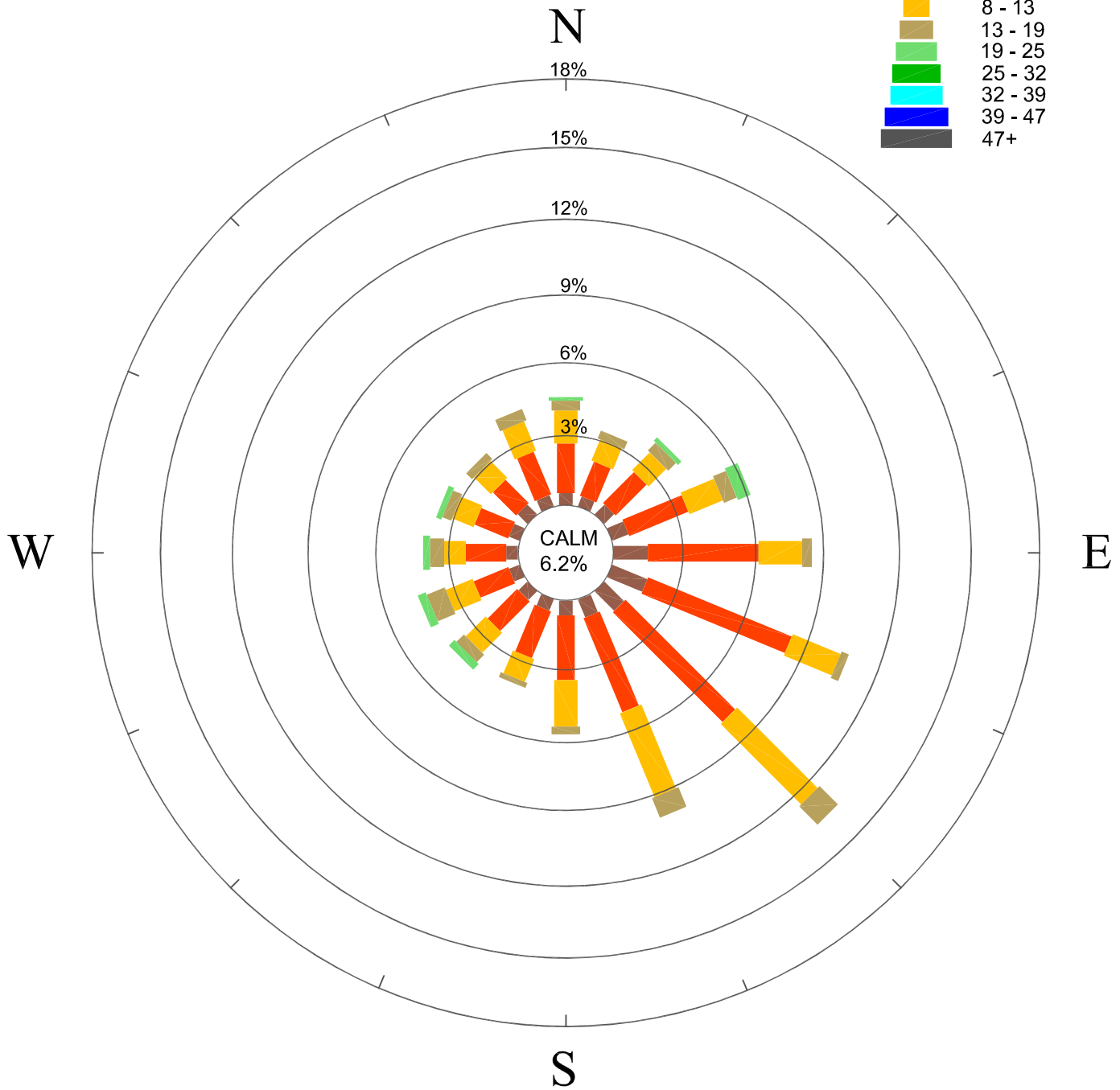
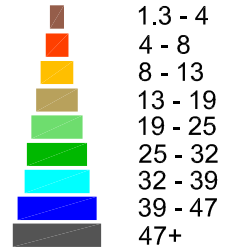
% FS 6% 9% 24% 32% 32% 32% 32% 32% 24% 19% 13% 12% 22%

Notes:

1. Rainfall obtained from Hobbs FAA Airport and reports average monthly rainfall from 1942-2006.
2. Input is the maximum monthly Produced Water that can be introduced to Evaporation Ponds based on Water Balance.
3. Evaporation rates obtained from Lake Avalon, New Mexico from 1914 -1979.
4. Actual Evaporation rates represent 70% of reported Pan Evaporation rate.
5. % Mech Evap Potential is the expected mechanical evaporation rate (%) for the pan Evaporation Rate per TurboMist calculation criteria
6. Assume 25% Mech Evap is the mechanical evaporation rate (%) minimum expected from SMI Evaporator 420F
7. BBL/D@75GPM is the flow rate for the SMI Evaporator Model 420F (assumes 12HRS of operation/day)
8. 1 BBL = 42 gallons (US, oil)

STATION: PADUCA, NEW MEXICO
 LATITUDE: 32° 10' 47" N
 LONGITUDE: -103° 43' 18" W
 ELEVATION: 3510 FT
 ELEMENT: WIND SPEED

MPH



START DATE: DEC. 1, 2005
 END DATE: DEC.31 2015
 # OF DAYS: 3683 OF 3683
 # OBS: Poss: 87196 of 88392
 WESTERN REGIONAL CLIMATE CENTER

Drawing:P:\acad 2003\560.01.02\PERMIT FIGURES\RAI 1\WINDROSE.dwg
 Date/Time: Sep. 19, 2016-12:54:46 ; LAYOUT: A (P)
 Copyright © All Rights Reserved, Gordon Environmental, Inc. 2016

<h2>WIND ROSE</h2>		
OWL LANDFILL SERVICES, LLC LEA COUNTY, NEW MEXICO		
 Gordon Environmental, Inc. <i>Consulting Engineers</i>		213 S. Camino del Pueblo Bernalillo, New Mexico, USA Phone: 505-867-6990 Fax: 505-867-6991
DATE: 09/06/2016	CAD: WIND ROSE.dwg	PROJECT #: 560.01.02
DRAWN BY: DMI	REVIEWED BY: DRT	FIGURE III.8.1
APPROVED BY: IKG	gei@gordonenvironmental.com	

3.0 EVAPORATION POND DESIGN

This section provides the engineering analyses and technical details to support design of the evaporation ponds for the OWL Facility with an average evaporation rate of 1,000 bbl per pond per day. The purpose of the design is to maintain potential drift (i.e., mist) within the pond boundary.

3.1 Design Criteria

3.1.1 Design Regulations

Regulations relevant to the design of the evaporation ponds presented here in Section 3.0 are summarized below.

Key Regulatory Agencies and Documents:

New Mexico Oil Conservation Division (OCD): Title 19 Natural Resources and Wildlife, Chapter 15 Oil and Gas, Part 36 Surface Waste Management Facilities, Section 17 Specific Requirements Applicable to Evaporation, Storage, Treatment and Skimmer Ponds, specifically B(12) which indicates that *“The maximum size of an evaporation or storage pond shall not exceed 10 acre-feet”*.

New Mexico Office of the State Engineer (NMOSE): Title 19 Natural Resources and Wildlife, Chapter 25 Administration and Use of Water – General Provisions, Part 12 Dam Design, Construction and Dam Safety, Section 7 Definitions, D. (1) Dams, (a) Jurisdictional Dam which indicates that *“A dam 25 feet or greater in height, which impounds more than 15 acre-feet of water or a dam that impounds 50 acre-feet or more of water and is 6 feet or greater in height.”* (b) Non-jurisdictional dam which indicates that *“Any dam not meeting the height and storage requirements of a jurisdictional dam.”* exempting this facility’s structures from this rule.

3.1.2 Project Design Criteria

Design criteria relevant to the analyses presented here in Section 3.0 are summarized below.

Geometry:

Process Operations: Design evaporation capacity of 1,000 barrels per day (bbl/d) of produced water per pond, with potential expansion capacity to 9,000 bbl/d.

Evaporation Pond Storage Capacity: Less than 10 acre-ft per pond, with potential expansion to 12 ponds. Developing an ultimate pond design configuration resulted in a 9.5 acre-foot pond capacity with a surface water area of 82,000 square feet (sq ft) and measuring 410 ft x 200 ft.

Maximum Evaporative Surface Area: for twelve ponds would be 984,000 square ft or 18.8 acres.

Process Design Life: 50 years.

Produced Water Properties:

Design Volumetric Flow Rate: 9,000 bbl/d or 263 gallons per minute (gpm).

System Requirements:

Evaporation Pond Liner System: Double layer liner system as follows (top to bottom): (1) upper (primary) 60 mil HDPE geomembrane liner; (2) leak detection system consisting of a 200 mil HDPE geonet; (3) lower (secondary) 60 mil HDPE geomembrane liner; underlain by (4) a density controlled compacted subgrade.

Leak Detection System: The leak detection system will meet the following requirements:(1) constructed with a bottom slope of at least two percent; (2) constructed with a 200 mil HDPE geonet with a transmissivity of $1 \times 10^{-3} \text{ m}^2/\text{sec}$ or greater; (3) constructed of materials that are chemically resistant to the waste and leachate; (4) designed and operated to minimize clogging during the active life; and (5) constructed with sumps and liquid removal methods (i.e., pumps).

3.2 Design Concepts

This section presents the general evaporation pond design concepts with the technical aspects discussed in detail in the following sections. The design of the OWL facilities shown on Figures and Permit Plans is preliminary; and construction plans and specifications for each major element will be submitted to OCD in advance of installation.

The OWL Facility is designed for start-up operations at 3,000 bbl/d routinely, with a potential to expand to 9,000 bbl/d on average. The design produced water flows from the Produced Water Tanks will be discharged to the evaporation ponds. The average design flow rates associated with the start-up and ultimate production rates are 88 and 263 gallons per minute (gpm), respectively.

The evaporation pond system is designed for construction in phases. Phase I includes 4 ponds, each with a surface dimension of 410 ft by 200 ft (i.e. 1.88 acres), designed to evaporate the inflows associated with the average receipt of 3,000 bbl/d. Similarly, Future Phases will include an additional 8 ponds with the same dimensions designed to evaporate the flows associated with an additional 6,000 bbl/d of produced water received daily (for a total of 9,000 bbl/day). All ponds are designed and constructed to provide contingency storage with additional freeboard (above the required design capacities). Pond berms with a minimum crest width of 15 ft are designed between ponds to allow access to all sides of the ponds, as well as operation and maintenance of the evaporation equipment. Two leak detection system (LDS)

sumps have been included in the design of each evaporation pond. Liquids collected in the LDS sumps will be pumped using a mobile pump, and returned to the evaporation ponds.

In order to improve performance of the evaporation pond system (i.e., enhance the evaporative capabilities), the design includes implementation of a mechanical evaporation system. The evaporators will be placed and sized to maximize evaporation and minimize the potential for wind-drift beyond the extents of the lined evaporation pond area. A continuous liner is designed over the entire evaporation pond area, including over the separation berms. A textured geomembrane will be extrusion welded on top of the berms between pond cells to facilitate access (i.e., pedestrian or ATV).

3.3 Water Balance Modeling

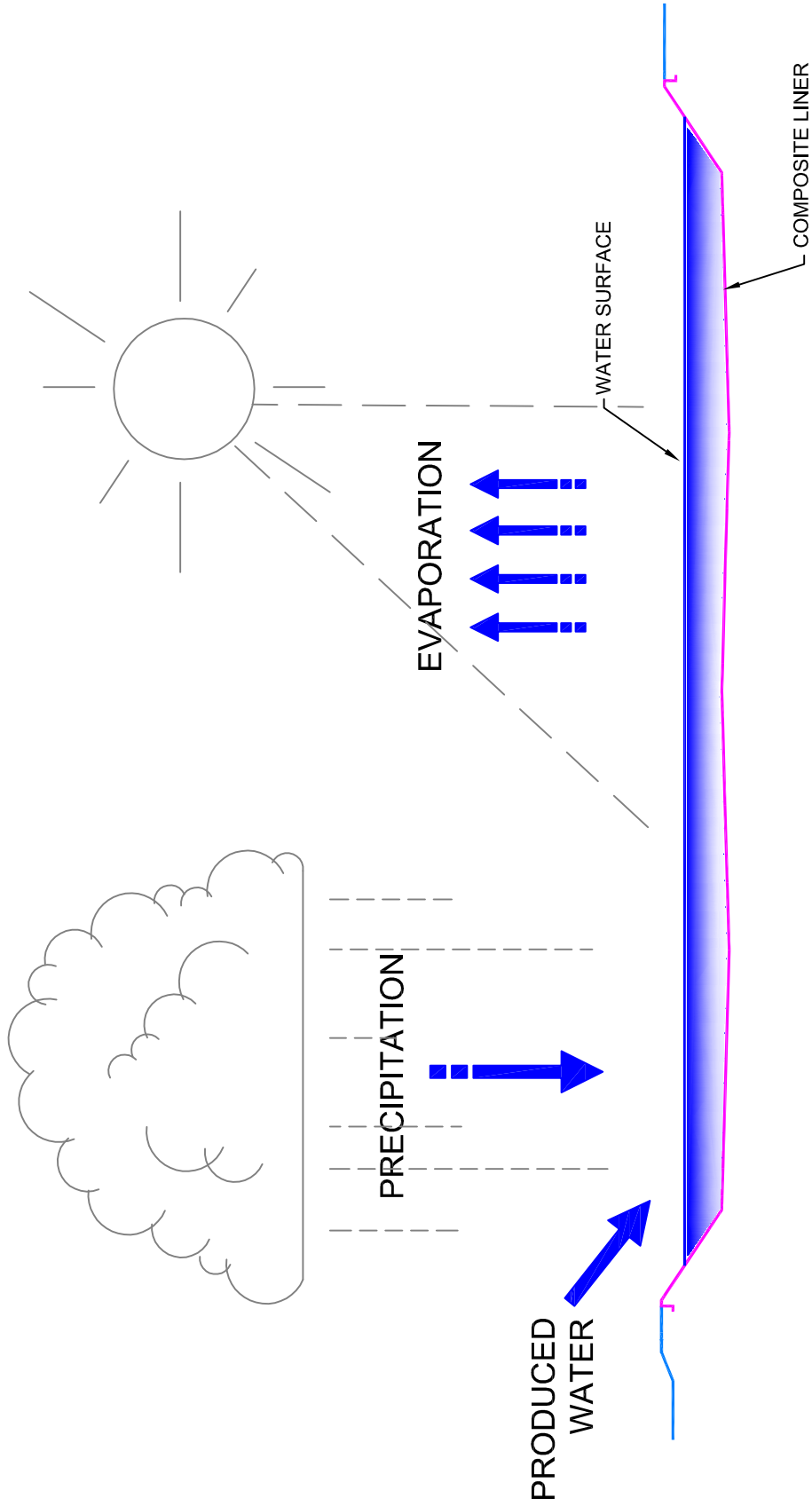
A probabilistic water balance model was developed to assist in determining the evaporation potential of the pond system (i.e., required evaporative surface area). Water balance calculations were performed to compare precipitation vs. evaporation (See **Table III.8.1**).

The following water balance components were considered:

- the amount of Produced Water entering the pond system from the Produced Water Tanks
- water entering the pond system through meteoric precipitation
- the amount of water released to the atmosphere through evaporation

Precipitation values are likely to exhibit the largest variations, and were therefore treated as stochastic inputs (i.e., probabilistic), while the other parameters were treated as deterministic variables. **Figure III.8.2** presents the process flow diagram for the evaporation pond water balance.

Preliminary analyses revealed a prohibitively large evaporation area for extreme precipitation events when considering evaporation losses solely from the pond surface. To reduce the required evaporative area, subsequent analyses included a mechanical evaporation system resulting in enhanced evaporation losses. All evaporators will be located at points within the ponds (as depicted in **Figure III.8.3**) and operated to minimize the probability of wind-drift blowing the produced water beyond the lined evaporation pond area.

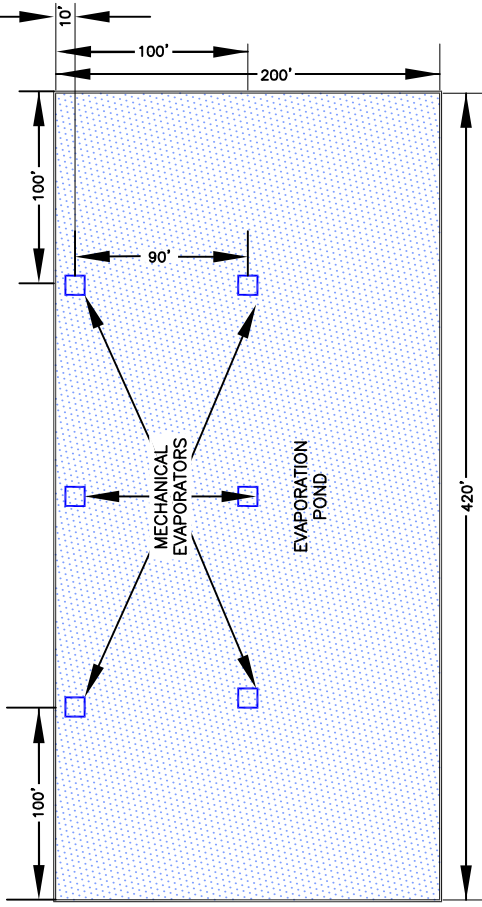
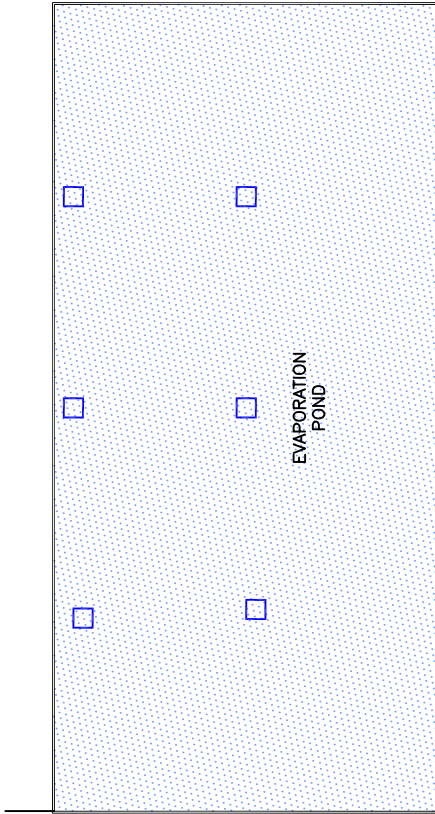
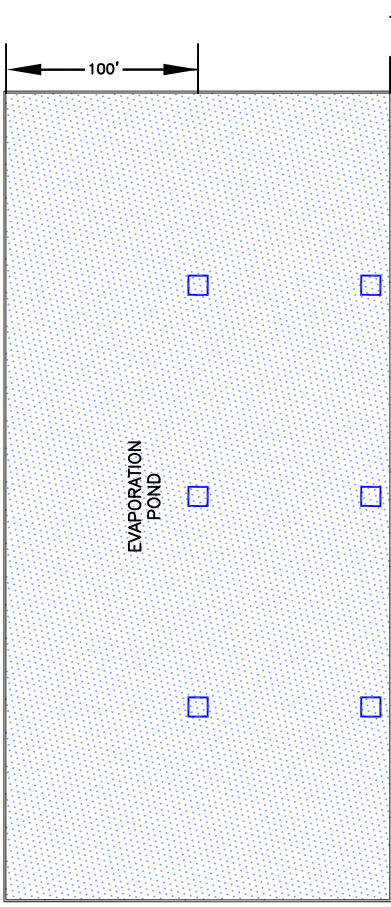
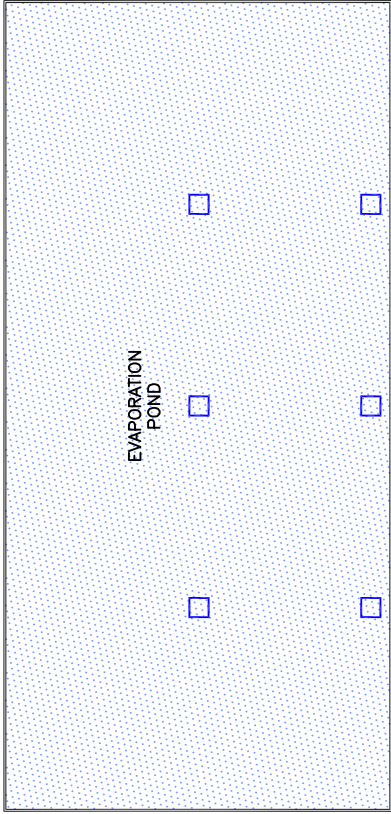


EVAPORATION POND WATER
BALANCE FLOW DIAGRAM
OWL LANDFILL SERVICES, LLC
LEA COUNTY, NEW MEXICO



213 S. Camino del Pueblo
Bernalillo, New Mexico, USA
Phone: 505-867-6990
Fax: 505-867-6991

DATE: 08/29/2016	CAD: EVAPORATION.dwg	PROJECT #: 560.01.02
DRAWN BY: DMI	REVIEWED BY: CWF	FIGURE III.8.2
APPROVED BY: IKG	iget@gordonenvironmental.com	



NOTE: SEE PERMIT PLANS FOR EVAPORATOR

Drawing: P:\acad 2003\560.01.02\PERMIT FIGURES\RAI 1\REVISED MECH EVAPORATORS.dwg
 Date/Time: Sep. 07, 2016-13:13:37
 Copyright © All Rights Reserved, Gordon Environmental, Inc. 2016

TYPICAL MECHANICAL EVAPORATOR LOCATION—PHASE I

OWL LANDFILL SERVICES, LLC.
 LEA COUNTY, NEW MEXICO



213 S. Camino del Pueblo
 Bernalillo, New Mexico, USA
 Phone: 505-867-6990
 Fax: 505-867-6991

DATE: 09/07/2016	CAD: MECH EVAPORATORS.dwg	PROJECT #: 530.06.01
DRAWN BY: DMI	REVIEWED BY: CWF	FIGURE III.8.3
APPROVED BY: IKG	ge@gordonenvironmental.com	

The results of the water balance for each pond were calculated assuming the average annual rainfall and the percentage of an average day when the wind speed is under 12 mph. The mechanical evaporators will be operating; limiting the flow rate to 10 gpm flow rate through the evaporators (even though extensive experience with this equipment indicates a greater evaporative expectation); and an input of 1,000 bbl/d of Produced Water. Based on these assumptions, the required number of mechanical evaporators per pond to evaporate 1,000 bbl/d is estimated to be three. The conservative assumption was made to discount the surface evaporation potential from the pond due to the micro-climate created by the mechanical evaporators. **Table III.8.1** details the evaporation potential per pond and identifies the additional evaporation potential that may be available based on extensive industry experience with this technology.

The influence of dissolved solids in the process water flow to the evaporation ponds may affect pond evaporation. It will be important to collect field evaporation measurements during the early years of pond operations to confirm the adequacy of this initial design. These field measurements will assist in refining expansion design potential of the evaporation ponds for an increase to 9,000 bbl/d average.

3.4 Mechanical Evaporator Lateral Drift Analysis

The proposed mechanical evaporators were analyzed for drift potential to ensure that all of the mist generated in the evaporation process would remain within the area of the lined pond area. The objective of this analysis was to determine the distance that the suspended solids would fall out with a given wind speed, droplet diameter and known level of Total Suspended Solids (TDS).

The higher the TDS the less lateral distance traveled and time the water droplet spends suspended in the air. For this analysis an 8% total TDS saturation was assumed. The proposed mechanical evaporator makes water droplet particle sizes of approximately 150 microns. This analysis assumes a droplet particle size of 150 microns for the drift calculations. Based on **Table III.8.2** the distance required for a 150 micron particle size to fall 10 ft is 10 seconds in a 3 mph wind is 39 feet.

TABLE III.8.2
Influence of Droplet Size on Potential Drift Distance
OWL Landfill Services, LLC

Droplet Diameter (Microns)	Type of droplets	Time required to fall 10 feet	Lateral distance Droplets travel in falling 10 feet in a 3 mph wind
5	Fog	66 minutes	3 miles
20	Very fine spray	4.2 minutes	1,100 feet
100	Fine spray	10 seconds	44 feet
150	Evaporator Standard	9 seconds	39 feet
240	Medium spray	6 seconds	28 feet
400	Course spray	2 seconds	8.5 feet
1,000	Fine rain	1 second	4.7 feet

Klingman, Glenn. 1961. Weed Control as a Science. John Wiley and Sons, New York, p. 67.

The proposed mechanical evaporator propels the water droplets 15 ft in the air, resulting in a 15 ft anticipated fall height for the water droplet particles generated. In this 3 mph wind the water droplet could drift 54 ft before falling back into the pond. Drift particles can travel up to 17 ft per mph in a strong wind (<12 mph). **Table III.8.3** provides a summary of anticipated lateral drift at different wind speeds for 150 micron water droplets falling from a height of 15 ft.

TABLE III.8.3
Lateral Drift at Various Windspeeds
OWL Landfill Services, LLC

Wind Speed MPH	Lateral Drift
2 MPH	39 ft
4 MPH	78 ft
6 MPH	117 ft
8 MPH	156 ft
10 MPH	195 ft
12 MPH	234 ft
14 MPH	273 ft

An analysis was performed with DRIFTSIM[®], a computer modeling program (**Attachment III.8.B**) that predicts the drift distance of spray droplets. This program was developed by Ohio State University, Food Agriculture, and Biological Engineering Department in coordination with the United States Department of Agriculture, Agricultural Research Service. The results from this model, utilizing a low TDS liquid (assuming greater drift), a 12 mph maximum wind speed (maximum average sustained wind speed onsite) and variable humidity's at various temperatures confirmed that based on the anticipated 150 micron droplet size, all lateral drift will fall back into the lined pond area. **Table III.8.4** and **Figure III.8.4** provide a summary of the output from this analysis.

The majority of the strong winds at this location originate from the southeast direction (see **Figure III.8.1**). Given the layout of the evaporation ponds, the proposed mechanical evaporators could operate in wind conditions up to 14 mph before the automation would need to shut the machines down relative to concerns that drift might escape the lined pond area.

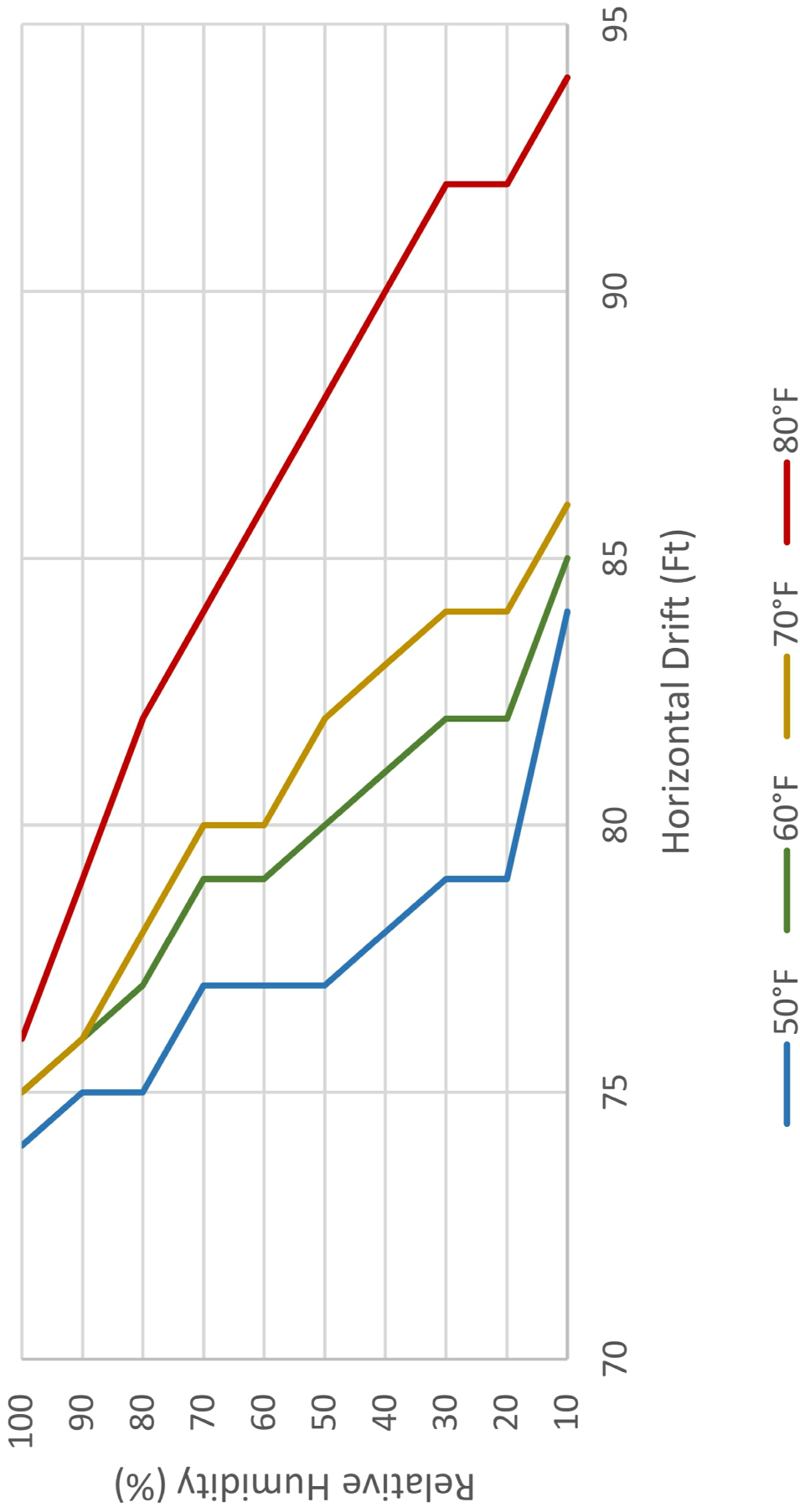
The mechanical evaporators will be controlled by a weather station with software designed to monitor wind speed; and to control (start and stop) the equipment to optimize evaporation hours and to minimize the potential for freezing during cold periods. This weather station will independently control each evaporator relative to wind speed and direction to minimize the potential for overspray and drift on windy days.

4.0 SUMMARY

The proposed evaporation ponds with mechanical evaporators will be able to evaporate the proposed volumes of Produced Waters that are anticipated for receipt in the various phases of this facility's development. The potential for drift can be managed to ensure that all materials remain within the lined area of the evaporation ponds. The phasing of evaporation pond installation will be based on the rates of Produced Water receipts, the characteristics of the material (e.g., TDS), and the observed efficacy of existing installations.

TABLE III.8.4
DRIFTSIM Analysis Results
(12 MPH Wind)
OWL Landfill Services, LLC

Temp	Drop Diameter	Humidity	Drift
50	150	10	84
50	150	20	79
50	150	30	79
50	150	40	78
50	150	50	77
50	150	60	77
50	150	70	77
50	150	80	75
50	150	90	75
50	150	100	74
60	150	10	85
60	150	20	82
60	150	30	82
60	150	40	81
60	150	50	80
60	150	60	79
60	150	70	79
60	150	80	77
60	150	90	76
60	150	100	75
70	150	10	86
70	150	20	84
70	150	30	84
70	150	40	83
70	150	50	82
70	150	60	80
70	150	70	80
70	150	80	78
70	150	90	76
70	150	100	75
80	150	10	94
80	150	20	92
80	150	30	92
80	150	40	90
80	150	50	88
80	150	60	86
80	150	70	84
80	150	80	82
80	150	90	79
80	150	100	76



EFFECT OF HUMIDITY AND TEMPERATURE ON DRIFT
 OWL LANDFILL SERVICES, LLC
 LEA COUNTY, NEW MEXICO


 Gordon Environmental, Inc.
Consulting Engineers

213 S. Camino del Pueblo
 Bernalillo, New Mexico, USA
 Phone: 505-867-6990
 Fax: 505-867-6991

DATE: 09/16/2016	CAD: DRIFT GRAPH.dwg	PROJECT #:	580.01.02
DRAWN BY: DMI	REVIEWED BY: CWF	FIGURE III.8.4	
APPROVED BY: IKG	gei@gordonenvironmental.com		

**APPLICATION FOR PERMIT
OWL LANDFILL SERVICES, LLC**

**VOLUME III: ENGINEERING DESIGN AND CALCULATIONS
SECTION 8: EVAPORATION CALCULATIONS**

**ATTACHMENT III.8.A
EFFECTS OF MAJOR VARIABLES ON DRIFT DISTANCES OF
SPRAY DROPLETS (OHIO STATE UNIVERSITY, 1998)**



FactSheet

Extension

Ohio State University Extension Fact Sheet

Food, Agricultural, and Biological Engineering

590 Woody Hayes Drive, Columbus, Ohio 43210

Effect of Major Variables on Drift Distances of Spray Droplets

AEX-525-98

Author

H. Erdal Ozkan

Professor
The Ohio State University
Food, Agricultural and Biological Engineering Department
590 Woody Hayes Drive
Columbus, OH 43210

Pesticide applications are required to ensure an adequate and high quality supply of many agricultural crops. Due to concerns for production costs, safety, and the environment, it is important to maximize the pesticide deposit on the target. One of the major problems challenging pesticide applicators is spray drift, which is defined as movement of pesticides by wind from the application site to an off-target site.

Spray drift occurs wherever liquid sprays are applied. Although complete elimination of spray drift is impossible, problems can be reduced significantly if the pesticide applicator is aware of major factors which influence drift, and takes precautions to minimize their influence on off-target movement of droplets.

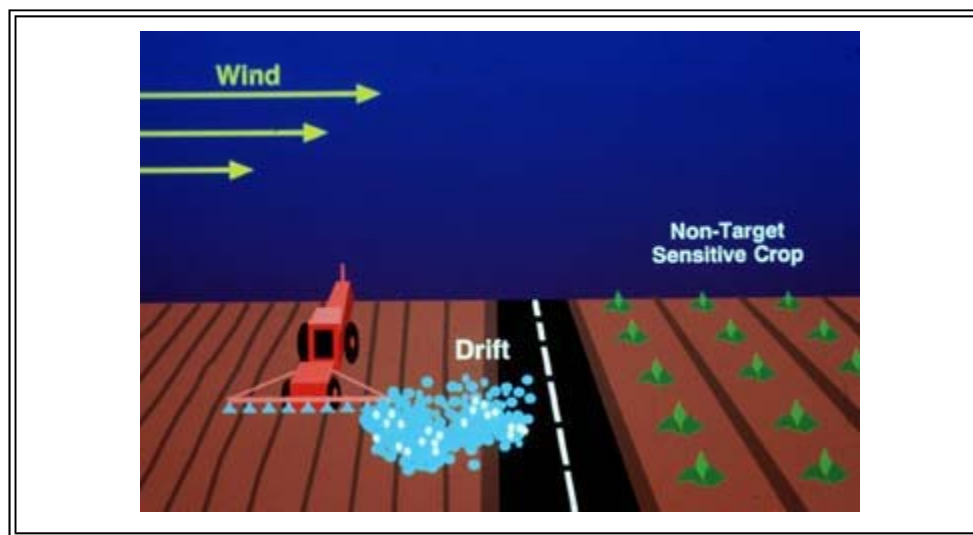
Drift is influenced by many factors that usually may be grouped into one of the following categories: 1) Spray characteristics, 2) Equipment and application techniques used, 3) Weather, and 4) Operator care and skill. A general discussion of these factors can be found in another publication by Ozkan (1991). In this publication, you will find specific information on how much influence some of these major factors

have on the drift distances of spray droplets.

The factors that significantly influence off-target movement of droplets are wind velocity and direction, droplet size and density, and distance from the atomizer to the target. Other factors that influence drift include droplet velocity and direction of discharge from the atomizer, volatility of the spray fluid, relative humidity, ambient temperature, and atmospheric turbulence intensity. Many scientists have conducted field tests to study influence of these variables on spray drift. Unfortunately, field tests have the limitation that weather conditions cannot be controlled and the variables that influence spray drift may interact and vary during a test. Computer simulations can allow determination of the effects of different values of variables such as droplet size and velocity, relative humidity, and wind velocity on spray drift. One such computer model was developed by Reichard et al.(1992a) in Ohio for modeling the effects of several variables on spray drift. Using the computer program, individual or mean droplet trajectories were determined for different values of several variables listed above. Experiments were also conducted to verify the accuracy of the computer model in predicting drift distances of water droplets in a wind tunnel. These tests revealed that the computer model can be used to accurately calculate spray drift distances for a wide range of spray droplet sizes and wind velocities (Reichard et. al., 1992b).

The major drift factors included in this publication are droplet size, wind velocity, relative humidity, ambient temperature, droplet discharge height, and initial droplet velocity. Although turbulence intensity is a major factor which influence drift, data related to this variable was not included in this publication because it is not something pesticide applicators can assess easily, and its magnitude can vary rapidly unlike the changes in other atmospheric conditions such as relative humidity and temperature. The affect of turbulence intensity on drift distances of droplets is discussed in the publication by Reichard et. al. (1992a). A turbulence intensity of 20% was assumed for all the computer simulation results reported in this publication,.

Although the accuracy of the drift data produced by computer simulation has been validated, one has to be cautious when drawing conclusions from the data presented in this publication. Due to the many variables that influence spray drift, it is extremely difficult to precisely predict drift distances of droplets for field conditions. Some of the variables that affect drift distances, such as wind turbulence, velocity and direction can vary considerably while a droplet is drifting. It is common for terrain and vegetation (size and density) to vary over the path of a drifting droplet and these influence local wind velocity and direction. The drift distance data presented in this publication are only valid for the constant conditions specified. The data presented are useful in comparing the relative effects of several factors on drift distances, but are not intended to precisely model variable field conditions.





Spray drift is the reason for the discoloration of part of the wheat crop shown in this photograph. The size of the area affected by drift and its severity depend on how adverse the weather conditions are and poor decisions made by the operator of the sprayer.

Droplet Size, Wind Velocity and Relative Humidity

Droplet size and wind velocity are the two most influential factors affecting drift. Relative humidity influences the evaporation rate of a droplet and hence its size, flight time, velocity and drift distance. Table 1 and Figure 1 show the simulated mean drift distances for various sizes of water droplets (50-200 micron diameter), wind velocities (2-8 mph), relative humidities (20-80%), and 75 degrees F ambient temperature. (Additional data are included in Tables in the publication by Zhu et al., 1994). Unless otherwise indicated, all simulated drift distances discussed in this publication are for droplets discharged downward with 65 ft/second (45 mph) velocity toward a target 18 inches below the point of discharge.



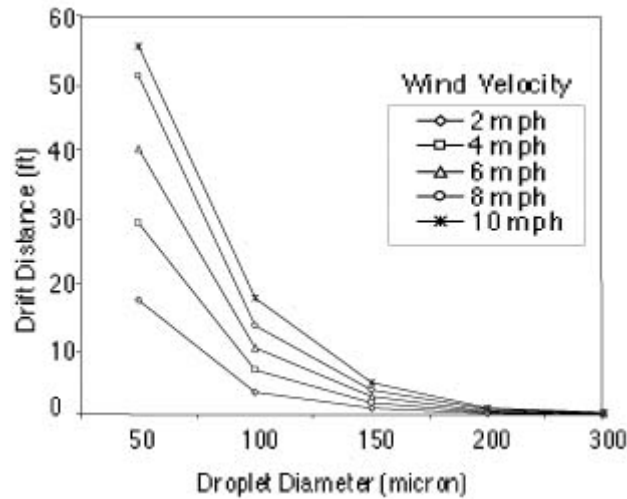


Figure 1. Effect of droplet diameter and wind velocity on drift distances of water droplets directed downward at 65 ft/second toward a target 18 inches below discharge point (Temperature = 75 degrees F; Relative Humidity = 60%).

Table 1. Effect of wind velocity and relative humidity on drift distances of droplets directed downward with initial velocity of 65 ft/second toward target 18 inches below discharge point. (Temperature = 75 degrees F; turbulence intensity = 20%)					
Initial droplet size (microns)	Wind velocity (mph)	20	40	60	80
20	2	3.03*	3.72*	6.41*	15.29*
20	4	6.00*	6.47*	10.24*	21.45*
20	6	6.57*	7.66*	11.87*	23.23*
20	8	7.96*	8.97*	13.29*	26.42*
20	10	8.99*	10.58*	15.06*	30.10*
50	2	10.70*	12.10	17.20*	25.30*
50	4	18.70*	21.00*	28.80*	41.70*
50	6	26.50*	30.00*	40.00*	55.60*
50	8	34.30*	38.20*	50.90*	69.00*
50	10	37.60*	42.00*	55.32*	87.24*
100	2	3.44	3.41	3.37	3.30
100	4	6.87	6.81	6.71	6.58
100	6	10.30	10.20	10.05	9.85
100	8	13.72	13.61	13.39	13.14
100	10	17.94	17.77	17.48	17.05
150	2	0.92	0.92	0.92	0.91

150	4	1.83	1.82	1.82	1.82
150	6	2.74	2.74	2.73	2.71
150	8	3.67	3.66	3.62	3.60
150	10	4.78	4.78	4.75	4.77
200	2	0.20	0.20	0.20	0.20
200	4	0.38	0.38	0.38	0.38
200	6	0.55	0.55	0.55	0.55
200	8	0.75	0.75	0.75	0.75
200	10	0.96	0.96	0.96	0.96
300	2	0.05	0.05	0.05	0.05
300	4	0.10	0.10	0.10	0.10
300	6	0.15	0.15	0.15	0.15
300	8	0.21	0.21	0.21	0.21
300	10	0.26	0.26	0.26	0.26
* Droplet completely evaporated before deposition.					

Water droplets with 50 micron diameter and smaller are highly susceptible to drift. All droplets 50 micron diameter and smaller completely evaporated before they reached 18 inches below point of discharge for wind velocities between 2.0 and 10.0 mph and relative humidities (RH) between 20 and 80% (Table 1). The mean drift distances of small droplets increased rapidly with increased wind velocity. For example, with 60% RH, 50 micron diameter droplets were displaced 17.2, 28.8, 40.0, 50.9, and 55.3 ft before they completely evaporated when wind velocities were 2, 4, 6, 8, and 10 mph, respectively.

The mean drift distances of 50 micron diameter water droplets and smaller increased with increased relative humidity because high relative humidity increased the lifetimes of the volatile droplets. Although both evaporated completely before deposition, the mean drift distances of 50 micron diameter droplets were greater than for 20 micron diameter droplets with the same relative humidity and wind velocity. This occurs because 50 micron diameter droplets have 15.6 times more volume and hence longer life than 20 micron diameter droplets. With 10 mph wind velocity and 60% RH, 20 and 50 micron diameter droplets drifted 15.1 and 55.3 ft downwind from the discharge point, respectively.

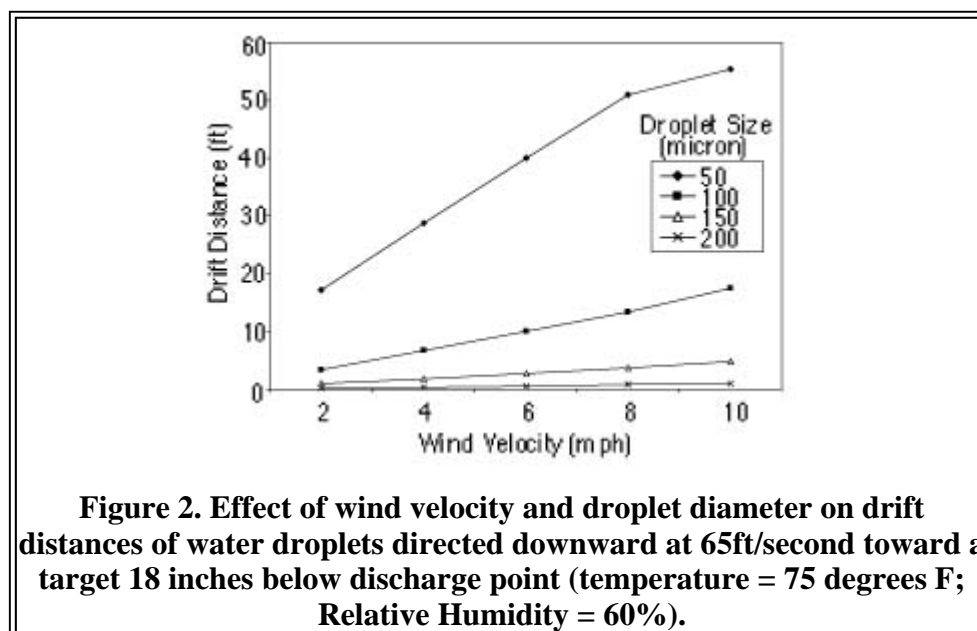
Most nozzles used for applying pesticides produce a large portion of the spray volume in 100 micron diameter droplets and larger. For example, our measurements of spray droplets from an XR 8002 VS nozzle (Spraying Systems Co., Wheaton, IL 60189) with 0.2 gpm flow rate when operated at 40 psi indicated that about 75% of the total spray volume was in droplets 100 micron diameter and larger. Computer simulation results indicate that all 100 micron and larger diameter water droplets reached 18 in below point of discharge at wind velocities up to 10 mph regardless of the relative humidity. However, due to affecting the evaporation rate, and hence droplet size, relative humidity significantly influenced the drift distances of 50 micron diameter droplets before they evaporated. With wind velocity of 10 mph, the mean drift distances of 50 micron diameter water droplets increased from 37.6 to 87.2 ft as relative humidity increased from 20% to 80%.

Data in Table 1 indicate that drift distances of droplets 200 micron diameter and larger are much less than for 100 micron diameter. For example, with 10 mph wind velocity and 60% RH, the mean drift

distance of 100 micron diameter droplets was about 18 times that of 200 micron diameter droplets (0.96 ft versus 17.48 ft). The mean drift distances of 200 micron diameter droplets were 0.20, 0.38, 0.55, 0.75, and 0.96 ft for wind velocities of 2, 4, 6, 8, and 10 mph, respectively. Relative humidity over a range of 20-80% had very little influence on the drift distances of 200 micron diameter droplets. The mean drift distances of all droplets 200 micron diameter and larger did not exceed 0.96 ft with wind velocities up to 10.0 mph.

Figure 1 illustrates the effect of water droplet size (50-300 micron diameter) on mean drift distance for wind velocities of 2.0, 4.0, 6.0, 8.0, and 10.0 mph, and 60% RH at 75 degrees F. All droplets 100 micron diameter or larger reached 18 in below point of discharge and deposited. The mean drift distances of the droplets increased with increased wind velocity but decreased as initial droplet size increased. The amount of droplet displacement that can be tolerated depends on several factors including the crop and surrounding area, and the pest control agent. If the target is a row crop that is sprayed from a nozzle centered over each row, then small amounts of droplet displacement by wind can result in large portions of the spray missing the target. It is also common for gusts with velocities two or more times the mean wind velocity to occur while spraying. Figure 1 indicates that drift is far less likely to be a problem when spraying with 200 micron diameter and larger droplets.

Figure 2 illustrates the simulated effect of wind velocities up to 10.0 mph on the mean drift distances for 100, 150, 200, and 300 micron diameter water droplets at 60% RH. Figure 2 and Table 1 both indicate that the influence of wind velocity on drift distance increases as droplet size decreases. Figure 2 shows that there is a nearly linear relationship between mean drift distance and wind velocity for each droplet size. The rate of change in drift distance with change in wind velocity was much greater for 100 than 200 micron diameter droplets. For example, over a range of 2 to 10 mph wind velocity the drift distances of 100 and 200 micron diameter droplets increased 1.8 and 0.01 ft per mph increase in wind velocity respectively.



Some spray carriers are oil or nonvolatile liquids. If the nonvolatile droplet density is close to the density of water, drift distances would be similar to drift distances in Table 1 for water droplets with 80% RH. Droplets 50 micron diameter or smaller can have very long drift distances with 100% RH. For example, the mean drift distances of 10 micron diameter droplets are beyond 650 ft with wind velocities of 5.5 mph and higher. For many pesticide applications, a small portion of the mixture is nonvolatile.

For small droplets that are still airborne when all of the water evaporates, there is potential for the small nonvolatile portion remaining to drift very long distances.

Temperature and Relative Humidity

Pesticides are applied over wide ranges of temperatures and relative humidities which influence the evaporation rates of droplets. Since evaporation of liquid from a droplet decreases its mass, it also influences the drift distance of the droplet. Table 2 shows the effects of temperatures (50, 68, and 86 degrees F) on droplet diameters at the end of droplet flights, and mean drift distances for water droplets with initial diameters ranging from 50 to 300 micron, wind velocities of 1 to 22 mph and 50% RH.

Table 2. Effect of temperature and wind velocity on droplet size at the end of flight of various size water droplets discharged downward at 65 ft/second toward a target 18 inches below point of discharge. (Relative humidity = 50%)							
Initial Droplet size (micron)	Wind Velocity (mph)	Final Droplet Size (micron) and Drift Distance (ft)					
		Temperature (degrees F)					
		50		68		86	
		DS#	DD##	DS#	DD##	DS#	DD##
50	1.1	0.0	11.58*	0.0	9.84*	0.0	9.74*
50	5.6	0.0	53.14*	0.0	32.8*	0.0	23.52*
50	11.1	0.0	105.94*	0.0	61.34*	0.0	41.32*
50	22.4	0.0	208.61*	0.0	117.75*	0.0	75.76*
70	1.1	59.4	5.18	43.6	6.30	0.0	12.50*
70	5.6	59.2	26.14	42.7	32.14	0.0	38.70*
70	11.1	59.0	52.48	41.9	64.61	0.0	70.19*
70	22.4	58.8	105.94	40.4	132.18	0.0	132.51*
100	1.1	96.7	2.13	93.7	2.13	88.7	2.36
100	5.6	96.7	10.53	93.7	10.73	88.7	11.64
100	11.1	96.7	19.48	93.7	21.48	88.6	23.39
100	22.4	96.6	42.97	93.5	43.62	88.3	47.56
150	1.1	149	0.59	148	0.59	147	0.59
150	5.6	149	2.72	148	2.85	147	2.98
150	11.1	149	5.58	148	5.74	147	6.04
150	22.4	149	11.97	148	12.27	147	12.82
200	1.1	200	0.13	199	0.13	199	0.13
200	5.6	200	0.56	199	0.56	199	0.56
200	11.1	200	1.18	199	1.18	199	1.18
200	22.4	200	2.69	199	2.69	199	2.69
300	1.1	300	0.03	300	0.03	299	0.03
300	11.1	300	0.33	300	0.33	299	0.33

300	22.4	300	0.69	300	0.69	299	0.69
* Droplet completely evaporated before deposition.							
# DS - Droplet diameter (micron) at end of flight.							
## DD - drift distance (ft).							

Table 2 indicates that ambient temperature had more influence on droplet sizes at end of flights for smaller droplets than larger droplets. For 70 micron diameter droplets, 5.6 mph wind velocity, and 50% RH, the mean droplet sizes at end of flights were 59.2, 42.7, and zero micron for ambient temperatures of 50, 68, and 86 degrees F, respectively. For 200 micron diameter droplets and the same conditions, the mean droplet sizes at times of deposition were 200, 199, and 199 micron. Over a temperature range of 50-86 degrees F, the volumes of 100 and 200 micron diameter water droplets changed about 20.9 and 1.5% respectively during flights when wind velocity was 1.1 m/s.

Table 2 also shows that wind velocities up to 22.4 mph had greater influence on droplet size change during flight on smaller than on larger droplets. For 70 micron diameter droplets at 68 degrees F and 50% RH, the droplet diameters at deposition were 43.6 and 40.4 micron with wind velocities of 1.1 and 22.4 mph, respectively. The 70 micron diameter water droplets lost 76 and 81% of their volume during flights with wind velocities of 1.1 and 22.4 mph, respectively. For 200 micron diameter droplets with the same conditions, the final droplet sizes at time of deposition were 199 micron for all wind velocities over a range of 1.1 to 22.4 mph.

Temperature can affect evaporation rate during flight and hence droplet size and drift distance. Because smaller droplets have greater surface area to volume ratios and longer flight times than larger droplets, temperature has greater influence on the drift distances of smaller droplets. With wind velocity of 5.6 mph and relative humidity of 50%, 50 micron diameter water droplets drifted 53.1 and 23.5 ft before completely evaporating at temperatures of 50 and 86 degrees F, respectively. With the same conditions, 100 micron diameter droplets drifted 10.5 and 11.6 ft before deposition at temperatures of 50 and 86 degrees F, respectively. Ambient temperatures within the range of 50 and 86 degrees F had very little influence on drift distances of 200 micron diameter and larger water droplets when wind velocity varied from 1.1 to 22.4 mph.

Figure 4 illustrates the simulated mean drift distances for 50, 100 and 200 micron diameter water droplets with 10 mph wind velocity, 50% RH and ambient temperatures of 55, 65, 75, and 85 degrees F. The curve for 50 micron droplets shows that drift distance decreased as temperature increased. The 50 micron diameter droplets completely evaporated before deposition. Small droplets tend to travel at speed close to wind velocity. When temperature, and hence evaporation rate increases, their travel distance over their lifetime tends to decrease. The curve for 100 micron diameter droplets shows that drift distance before deposition increased with increased temperature. The drift distance tended to increase with increased temperature because increased temperature resulted in faster evaporation rate, smaller droplet size and increased travel distance before deposition. Temperature over the range of 50 to 86 degrees F had little influence on drift distances of 200 micron diameter droplets. The data used to produce the curves on Figure 3 are presented in Table 3.



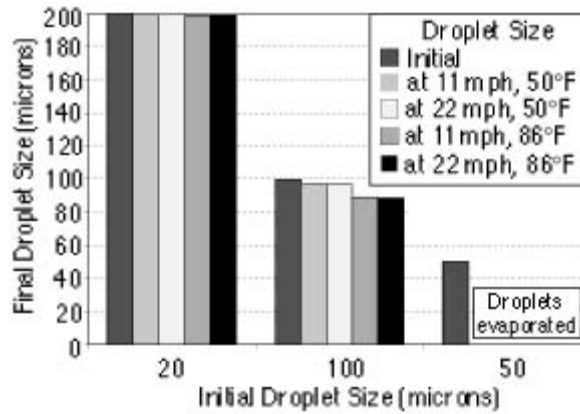


Figure 3. Effect of temperature and wind velocity on droplet sizes at the end of flight of 50, 100 and 200 micron diameter water droplets discharged down at 65 ft/second toward a target 18 inches below nozzle (RH=50%).

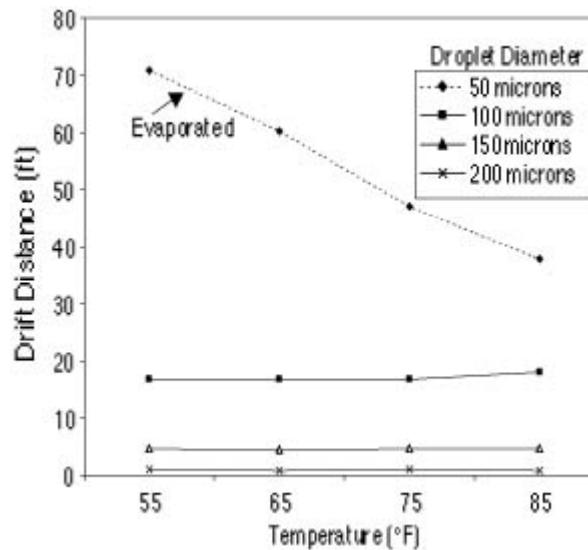


Figure 4. Mean drift distances for 50, 100 and 200 micron diameter water droplets with 10 mph wind velocity, 50% RH and ambient temperatures of 55, 65, 75 , and 85 degrees F.

Table 3. Effect of wind velocity and temperature on drift distances of droplets directed downward with initial velocity of 65 ft/second toward target 18 inches below discharge point. (Relative humidity = 50%; Turbulence intensity = 20%)

Initial Droplet size (micron)	Wind velocity (mph)	Drift Distance (ft)			
		Temperature (degrees F)			
		55	65	75	85
20	2	4.24*	4.47	4.64	4.79*
20	4	7.23*	7.33*	7.71*	7.79*

25	55	17.93*	20.37*	29.76*	56.43*	381.60
25	65	14.67*	16.63*	23.53*	43.18*	377.97
25	75	12.58*	14.41*	19.94*	37.95*	391.31
25	85	11.41*	12.77*	17.81*	33.25*	400.12
50	55	63.32*	60.87*	60.87*	119.73	76.78
50	65	48.21*	53.93*	63.82*	93.51*	76.05
50	75	37.58*	42.00*	55.32*	87.24*	78.82
50	85	30.81*	34.40*	44.81*	73.93*	80.34
100	55	16.90	16.82	16.63	16.43	16.20
100	65	16.97	16.88	16.64	16.36	15.99
100	75	17.94	17.77	17.48	17.05	16.46
100	85	18.55	18.28	17.88	17.34	16.55
150	55	4.65	4.64	4.62	4.62	4.59
150	65	4.58	4.57	4.56	4.54	4.50
150	75	4.78	4.78	4.72	4.72	4.66
150	85	4.76	4.73	4.70	4.64	4.58
200	55	0.98	0.98	0.95	0.95	0.95
200	65	0.95	0.95	0.94	0.94	0.94
200	75	0.96	0.96	0.96	0.96	0.96
200	85	0.93	0.93	0.93	0.93	0.93
300	55	0.98	0.98	0.95	0.95	0.95
300	65	0.95	0.95	0.94	0.94	0.94
300	75	0.96	0.96	0.96	0.96	0.96
300	85	0.93	0.93	0.93	0.93	0.93
* Droplet completely evaporated before deposition.						

Figure 5 illustrates the effect of relative humidity on mean drift distances of 25, 50, 100 and 200 micron size water droplets for 10 mph wind velocity. The ambient temperature was 65 degrees F for the simulations. The mean drift distances of 25 and 50 micron diameter water droplets, before complete evaporation, increased with increased relative humidity over the range of 20 to 80%. For the same conditions, but with 100% RH, 50 micron diameter droplets deposited 18 in below and 76 ft downwind from the point of discharge while 25 micron diameter droplets drifted beyond 378 ft. There was no change in drift distance of 200 micron diameter water droplets over the 10 to 80% range of relative humidity.



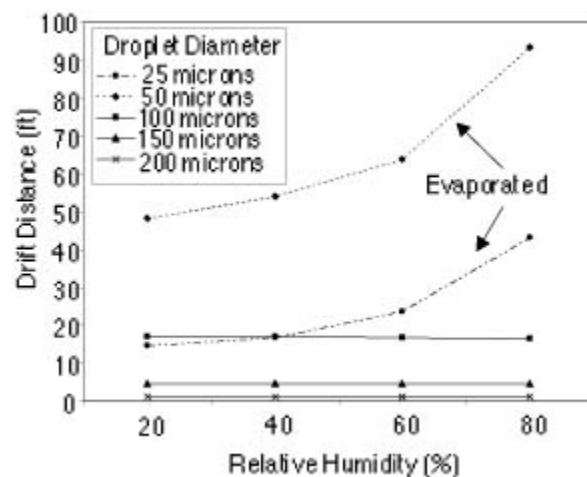


Figure 5. The effect of relative humidity on mean drift distances of 25, 50, 100 and 200 micron size water droplets for 10 mph wind velocity. (The ambient temperature= 65 degrees F).

Droplet Discharge Height

Agricultural pesticides are applied with a very wide range of nozzle heights above targets. Nozzle height depends on several factors including the sprayer setup, target and operating conditions. Table 5 shows the effects of discharge height (0.5-3.0 ft), droplet diameter (50-300 micron) and wind velocity (2.0-10.0 mph) on mean drift distances of water droplets directed downward with initial velocity of 65 ft/seconds. Relative humidity and ambient temperature were 50% and 70 degrees F, for all simulations. The mean drift distances of 50 micron diameter and smaller droplets were nearly constant with each wind velocity for the discharge height range of 0.5 to 3.0 ft. This occurs because these droplets have short life times and do not travel downward far enough to deposit before completely evaporating.

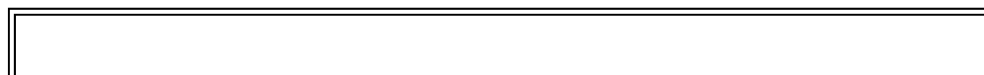
Initial Droplet size (micron)	Wind velocity (mph)	Drift distances (ft)					
		Nozzle height (ft)					
		0.5	1	1.5	2	2.5	3.0
50	2	0.43*	13.87*	14.02*	14.14*	14.22*	13.97*
50	4	14.28*	23.51*	23.72*	23.80*	23.83*	23.98*
50	6	19.96*	32.92*	33.41*	33.65*	33.78*	33.76*
50	8	25.61*	42.32*	43.18*	43.40*	43.39*	43.73*
50	10	31.20*	51.48*	52.29*	52.89*	53.37*	53.43*
100	2	0.50	1.50	3.37	5.40	7.51	9.85
100	4	0.99	2.99	6.76	10.82	15.02	19.72
100	6	1.48	4.47	10.15	16.23	22.54	29.62
100	8	1.98	5.97	13.51	21.63	30.05	39.51

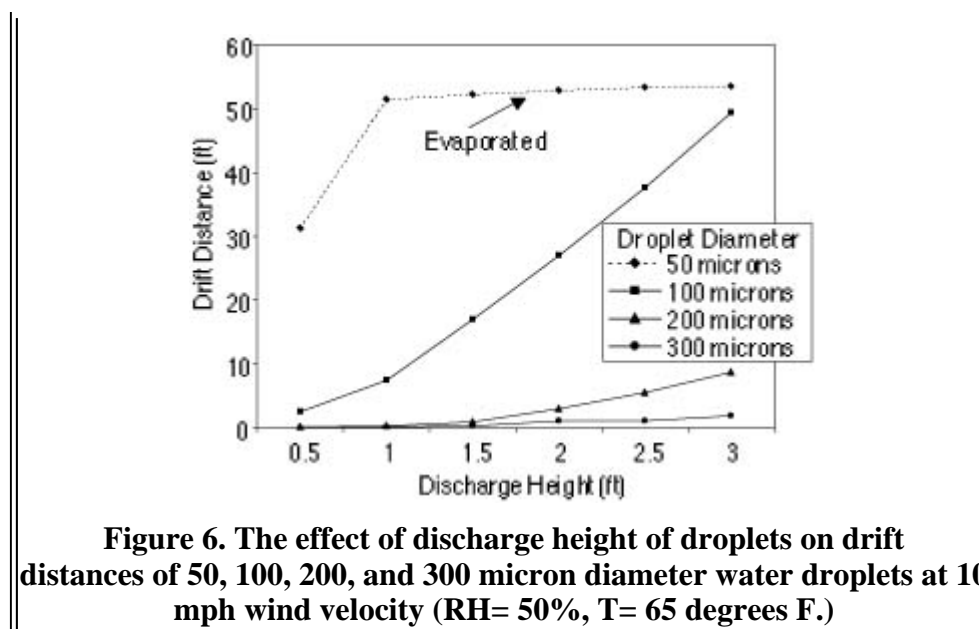
100	10	2.49	7.47	16.91	27.06	37.59	49.40
150	2	0.04	0.29	0.92	1.80	2.77	3.76
150	4	0.07	0.57	1.82	3.57	5.50	7.49
150	6	0.11	0.86	2.73	5.34	8.25	11.23
150	8	0.16	1.15	3.63	7.12	11.01	14.99
150	10	0.19	1.43	4.55	8.92	13.78	18.75
200	2	0.02	0.07	0.20	0.61	1.13	1.76
200	4	0.03	0.14	0.38	1.19	2.24	3.51
200	6	0.05	0.20	0.55	1.76	3.34	5.23
200	8	0.06	0.27	0.75	2.37	4.48	7.01
200	10	0.08	0.34	0.93	2.98	5.63	8.79
300	2	0.00	0.01	0.05	0.11	0.20	0.38
300	4	0.02	0.05	0.10	0.24	0.41	0.79
300	6	0.02	0.07	0.15	0.35	0.62	1.17
300	8	0.02	0.08	0.21	0.46	0.80	1.56
300	10	0.04	0.12	0.26	1.04	1.04	1.97
* Droplet completely evaporated before deposition.							

Increased discharge height resulted in increased drift distances for 100 micron diameter and larger water droplets (Table 5). For example, with 10 mph wind velocity and 65 ft/second initial droplet velocity, when discharge height increased from 0.5 to 3.0 ft, the mean drift distance of 200 and 300 micron diameter droplets increased from 2.49 to 49.40 ft and 0.08 to 8.79 ft, respectively. When the discharge height increased from 0.5 to 3.0 ft, the mean drift distance of 100 micron diameter droplets increased from 1.98 to 39.51 ft and kept increasing until the discharge height of 10 ft is reached. When the discharge height is increased beyond 10 ft, the drift distance remained constant (217 ft) because the 100 micron diameter water droplets completely evaporated before deposition.

When simulations for large size droplets were performed, results indicated that if the discharge height becomes too large, even the large droplets have tendency to drift under high wind velocity conditions. For example, the mean drift distance of 1000 micron diameter droplets was 5 ft for wind velocity and discharge height of 22 mph and 10 ft, respectively. Computer simulation also indicated that the mean drift distances of 1000 and 2000 micron diameter droplets were 57 and 19 ft, respectively, before impaction 13 ft below the point of discharge for 22 mph wind velocity, 50% relative humidity, and zero mph initial droplet velocity.

Figure 6 illustrates the effect of discharge height of droplets on the mean drift distances of 50, 100, 200, and 300 micron diameter water droplets for 10 mph wind velocity, 50% RH and 65 degrees F. The graph shows that increasing discharge height above 0.5 ft had no affect on the mean drift distance of 50 micron diameter droplets because they completely evaporated before depositing. However, increasing discharge height of 100 micron diameter and larger droplets affects their mean drift distances. Changes in discharge heights have less effect on mean drift distances as droplet size increases above 200 micron diameter.





Initial Droplet Velocity

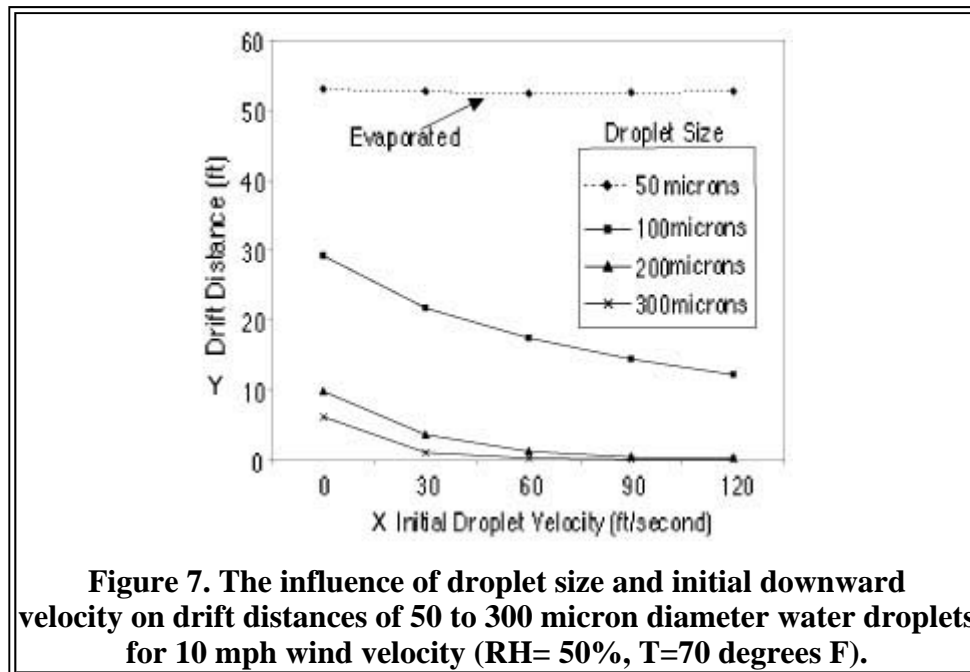
Pesticides are applied with many different types of nozzles. The velocity of droplets delivered by nozzles depends on the configuration of the nozzle, and operating pressure. Table 6 shows the effects of initial droplet velocity (0-120 ft/second) and wind velocity (2.5-10.0 mph) on the mean drift distances of various size water droplets directed downward toward a target 1.5 ft below the point of discharge. Relative humidity and ambient temperature were 50% and 70 degrees F, for all simulations. The data indicate that increasing the initial downward droplet velocity can decrease the mean drift distances before deposition of 75 micron diameter and larger droplets. When spray is directed downward from a nozzle centered over a row of plants, for example, it is important to maximize spray deposition on the target. Even for 30 ft/second initial droplet velocities, the drift distances of 100 micron diameter and smaller water droplets would be excessive when spraying row crops if the droplets were exposed to crosswinds with velocities of only 1 mph. Also, for many applications where the spray is exposed to crosswinds, the drift distances of 200 micron diameter droplets would be excessive for droplets directed downward with slow velocities. For example, the mean drift distances of 200 micron diameter droplets in 2.5 mph crosswinds are 2.4 and 0.9 ft for droplets directed downward with 0 and 30 ft/sec velocities, respectively. When wind velocity was 10 mph, the mean drift distance of 200 micron diameter droplets decreased from 9.88 to 0.28 ft as the initial downward droplet velocity increased from 0 to 120 ft/s. Some applicators use large droplets to reduce spray drift potential. With no initial downward droplet velocity (zero ft/second) and 18 in discharge height, the mean drift distances of 1000 micron diameter droplets were 0.24, 0.63, 1.08, and 1.62 ft when wind velocities were 2.5, 5.0, 7.5, and 10.0 mph, respectively. With 60 ft/sec instead of 0 m/s initial velocity, the mean drift distance of the 1000 micron diameter drops was only 0.04 ft when wind velocity was 10 mph. Table 6 also illustrates that initial droplet velocities had no effect on drift distances of 50 micron diameter water droplets. None of the 50micron diameter and smaller droplets reached 18 in below the point of discharge before complete evaporation for a range of initial droplet velocities from zero to 120 ft/second and wind velocities from 2.5 to 10.0 mph.

Table 6. Effect of initial droplet velocity and wind velocity on drift distances of various size water droplets directed downward toward a target 18 inches below point of droplet discharge. (Temperature: 70 degrees F;

Relative Humidity = 50%)						
Droplet size (micron)	Wind velocity (mph)	Drift Distances (ft)				
		Initial Droplet Velocity (ft/second)				
		0	30	60	90	120
50	2.5	16.50*	16.42*	16.40*	16.53*	16.50*
50	5.0	28.80*	28.74*	28.62*	28.67*	28.67
50	7.5	40.76*	40.73	40.74	40.70	40.54*
50	10.0	52.98*	52.70*	52.43*	52.48*	52.67*
75	2.5	17.86	13.05	11.35	10.29	9.09
75	5.0	33.83	25.82	22.19	20.03	18.31
75	7.5	49.58	38.64	33.03	29.74	27.17
75	10.0	65.28	52.26	44.00	39.49	36.01
100	2.5	5.39	5.39	4.37	3.64	3.06
100	5.0	14.51	10.79	8.75	7.26	6.10
100	7.5	21.84	16.25	13.11	10.88	9.12
100	10.0	29.25	21.75	17.51	14.48	12.15
150	2.5	3.64	2.05	1.26	0.73	0.39
150	5.0	7.34	4.10	2.49	1.45	0.76
150	7.5	11.07	6.19	3.73	2.15	1.12
150	10.0	14.83	8.34	5.00	2.87	1.49
200	2.5	2.36	0.89	0.31	0.13	0.07
200	5.0	4.82	1.79	0.58	0.25	0.15
200	7.5	7.34	2.72	0.89	0.82	0.20
200	10.0	9.88	3.72	1.20	0.52	0.28
300	2.5	1.39	0.24	0.08	0.04	0.03
300	5.0	2.91	0.49	0.15	0.08	0.5
300	7.5	4.56	0.76	0.22	0.12	0.07
300	10.0	6.23	1.06	0.31	0.17	0.11
500	2.5	0.67	0.08	0.03	0.01	0.00
500	5.0	1.52	0.16	0.05	0.03	0.03
500	7.5	2.49	0.25	0.09	0.05	0.03
500	10.0	3.58	0.34	0.11	0.06	0.04
1000	2.5	0.24	0.03	0.00	0.00	0.00
1000	5.0	0.63	0.05	0.03	0.01	0.00
1000	7.5	1.08	0.08	0.03	0.03	0.01
1000	10.0	1.62	0.11	0.04	0.03	0.03

* Droplet completely evaporated before deposition.

Figure 7 illustrates the influence of droplet size and initial downward velocity on drift distances of 50 to 300 micron diameter water droplets for 10 mph wind velocity. The relative humidity and ambient temperature were 50% and 70 degrees F for all simulations. As evident from the data presented on Figure 7, for 10 mph wind velocity, drift distances are greatly influenced by both droplet size and the initial downward velocity of the droplet. The drift distances of 100 micron diameter and larger droplets decreased with increased initial droplet velocity. Figure 7 also illustrates the large difference in drift distances between 100 and 200 micron diameter water droplets.



Conclusions

The following conclusions are based on the computer simulations of mean drift distances of water droplets within the range of variables discussed in this publication.

1. Changes in wind velocity, discharge height, ambient temperature and relative humidity had much greater influence on the drift distances of droplets 100 micron diameter or less than on 200 micron diameter and larger droplets. For droplets that did not evaporate before deposition, there was a nearly linear relationship between wind velocity and drift distance.
2. With 100% RH, 10 micron diameter droplets drifted beyond 650 ft when wind velocity exceeded 5.5 mph.
3. Droplets 50 micron diameter and smaller completely evaporated before reaching 18 inches below the discharge point, regardless of initial velocity, for relative humidities 60% and lower and temperatures between 55 and 85 degrees F. Also, the mean drift distances of these droplets increased with increased droplet size.
4. Mean drift distances of 100 micron diameter and larger droplets increased with increased wind velocity and discharge height, but decreased with increased droplet size and discharge velocity.
5. Drift distances of water droplets as large as 200 micron diameter were influenced by initial

droplet velocity and height of discharge.

6. 6. For 10 mph wind velocity, 20% turbulence intensity, 50% RH, 70 degrees F ambient temperature, 60 ft/second initial downward droplet velocity and 18 inches discharge height, the mean drift distances of 100, 200, and 500 micron diameter droplets were 17.5, 1.2, and 0.11 ft, respectively.
7. 7. The drift potential of 200 micron diameter droplets is considerably less than for 100 micron diameter droplets. Unless some means such as shields or air jets are used, drift reduction techniques should be directed toward reducing the portion of spray volume contained in droplets less than 200 micron diameter for applications where minimizing drift is important. For some applications, such as with high nozzles and slow initial downward velocity and high wind velocity, droplets larger than 200 micron diameter may be needed to satisfactorily reduce drift.

Acknowledgment

Most of the information presented in this publication was adapted from the following publication.

Zhu, H., D.L. Reichard, R.D. Fox, R.D. Brazee and H.E. Ozkan. 1994. Simulation of drift of discrete sizes of water droplets from field sprayers. Transactions of the ASAE 37(5):1401-1407.

References

Ozkan, H.E. 1991. Reducing spray drift. OSU Extension Bulletin 816. Ohio State University Extension, Columbus, Ohio.

Reichard, D.L., H. Zhu, R.D. Fox and R.D. Brazee. 1992a. Computer simulation of spray drift that influence spray drift. Transactions of the ASAE 35(5):1401-1407.

Reichard, D.L., H. Zhu, R.D. Fox and R.D. Brazee. 1992b. Wind tunnel evaluation of a computer program to model spray drift. Transactions of the ASAE 35(3):755-758.

NOTE: Disclaimer - This publication may contain pesticide recommendations that are subject to change at any time. These recommendations are provided only as a guide. It is always the pesticide applicator's responsibility, by law, to read and follow all current label directions for the specific pesticide being used. Due to constantly changing labels and product registrations, some of the recommendations given in this writing may no longer be legal by the time you read them. If any information in these recommendations disagrees with the label, the recommendation must be disregarded. No endorsement is intended for products mentioned, nor is criticism meant for products not mentioned. The author and Ohio State University Extension assume no liability resulting from the use of these recommendations.

All educational programs conducted by Ohio State University Extension are available to clientele on a nondiscriminatory basis without regard to race, color, creed, religion, sexual orientation, national origin, gender, age, disability or Vietnam-era veteran status.

Keith L. Smith, Associate Vice President for Ag. Adm. and Director, OSU Extension.

TDD No. 800-589-8292 (Ohio only) or 614-292-1868

**APPLICATION FOR PERMIT
OWL LANDFILL SERVICES, LLC**

**VOLUME III: ENGINEERING DESIGN AND CALCULATIONS
SECTION 8: EVAPORATION CALCULATIONS**

**ATTACHMENT III.8.B
DRIFTSIM[®]: PREDICTING DRIFT DISTANCE OF SPRAY DROPLETS
AND RESULTING EVAPORATION**



DRIFTSIM—Predicting Drift Distances of Spray Droplets

Heping Zhu and Robert D. Fox

Agricultural Engineers

USDA-ARS

Application Technology Research Unit

Wooster, OH 44691

H. Erdal Ozkan

Professor and Extension Agricultural Engineer

Food, Agricultural, and Biological

Engineering Department

The Ohio State University

Columbus, OH 43210

Introduction

Spray drift, movement of pesticide droplets through air during or after application to a site other than the intended targets of application, is one of the most critical problems pesticide applicators have to deal with. For example, three-fourths of agriculture-related complaints investigated by the Ohio Department of Agriculture involved drift issues; two-thirds of the total complaints in a five-year period brought to the attention of Iowa Department of Agriculture were related to drift problems; about one-third of court cases due to spray misapplications reported by a major insurance company involved drift damages. Drift problems will become even more critical in the future when farmers use more genetically modified crops which restrict use of non-selective herbicides because even a small amount of these herbicides can cause serious damage to neighboring crops.

Although complete elimination of spray drift is impossible, problems can be minimized if chemicals are applied with the proper equipment and methods under favorable weather conditions. Increased awareness of environmental quality and better understanding of the causes of spray drift can help operators make reasonable judgments for safer, more efficient applications.

Factors that significantly influence off-target movement of droplets are wind velocity and direction, droplet size and density, and distance from the atomizer to the target. Other factors that influence drift include droplet velocity, and direction of discharge from the atomizer, volatility of the spray fluid, relative humidity, ambient temperature, and atmospheric turbulence intensity. Many scientists have conducted field tests to study

influence of these variables on spray drift. Unfortunately, field tests have the limitation that weather conditions cannot be controlled and the variables that influence spray drift may interact and vary during a test.

Computer simulations can allow determination of effects of different variables such as droplet size and velocity, relative humidity, and wind velocity on spray drift. One such computer model or commercially available computational fluid dynamics (CFD) program was evaluated by Reichard et al. (1992) in Ohio for modeling the effects of several variables on spray drift. Experiments were conducted to verify the accuracy of the computer model in predicting drift distances of water droplets in a wind tunnel with a single size droplet generator. These tests revealed that the computer model could be used to accurately calculate spray drift distances for a wide range of spray droplet sizes and wind velocities. With the computer model, individual or mean droplet trajectories were determined for different values of several variables listed above (Zhu et al., 1994). However, the model is very expensive and requires special operator skills and a high-speed computer with a large memory space to operate. It also takes long time to calculate a drift distance even for a single simulation condition.

DRIFTSIM is a simplified and user-friendly version of a computer model developed with a visual BASIC language program to interpolate values from a large database of drift distances originally calculated from the CFD model evaluated by Reichard et al. (1992). Detailed information on DRIFTSIM is given in a publication by Zhu et al. (1995). DRIFTSIM can be used to determine effects of major drift-causing factors on the mean drift distances up to 656 feet from the release point for individual water droplets or classes of droplets. These factors or variables used in DRIFTSIM are listed in Table 1, with the limiting values acceptable to DRIFTSIM.

Table 1. Variables and their ranges used in DRIFTSIM program				
Variable	Range			
	American Unit		Metric Unit	
Wind velocity	0-22	mph	0-10	m/s
Droplet size	10-2000	Micron (μm)	10-2000	μm
Droplet velocity	0-110	mph	0-50	m/s
Discharge height	0-6.5	ft	0-2.0	m
Temperature	50-86	$^{\circ}\text{F}$	10-30	$^{\circ}\text{C}$
Relative humidity	10-100	%	10-100	%

Turbulence intensity is another important factor indicating how much the wind velocity varies about the mean. It can vary considerably in field conditions, but based on the frequency of nearly 20% turbulence intensity observed in many of the field measurements conducted in Ohio, a constant value of 20% turbulence intensity was used in DRIFTSIM for all calculations.

For classes of droplets in this version of DRIFTSIM, the upper-limit log normal (ULLN) method (Goering and Smith, 1978) was used to calculate the drop-size distribution produced by a nozzle. The ULLN method used three size measurements, $D_{V,1}$, $D_{V,5}$, and $D_{V,9}$ to estimate the volume of spray in droplets less than a selected droplet size. The $D_{V,1}$, $D_{V,5}$, and $D_{V,9}$ for the droplet size spectra produced by a specific nozzle can be measured with most modern droplet sizing instruments. DRIFTSIM computes the drift distance for the average of lower and upper droplet size for each size class. It also computes the portion of spray in each size class.

Terms used in DRIFTSIM program

Single size droplets: For the program to calculate a mean drift distance of a given size droplets with other variables

Array of droplets (DVs): For the program to calculate drift distances with the portion of volume for many size classes of droplets by entering $D_{v,1}$, $D_{v,5}$ and $D_{v,9}$

$D_{v,1}$: Droplet diameter such that 10% of total liquid volume that is in droplets smaller than $D_{v,1}$ (micron or μm)

$D_{v,5}$: Droplet diameter such that 50% of total liquid volume that is in droplets smaller than $D_{v,5}$ (micron or μm)

$D_{v,9}$: Droplet diameter such that 90% of total liquid volume that is in droplets smaller than $D_{v,9}$ (micron or μm)

Array of droplets (nozzle): For the program to calculate drift distances with the portion of volume for many size classes of droplets by selecting nozzle type [**Note:** In DRIFTSIM, data is available for only a limited number of nozzles]

Temperature: Ambient air temperature during spray operation ($^{\circ}\text{F}$ in American unit or $^{\circ}\text{C}$ in Metric unit)

Relative humidity: Relative humidity of ambient air (%)

Wind velocity: Wind speed at nozzle level during the spray application (mph in American unit or m/s in Metric unit)

Discharge height: Nozzle orifice height above the ground (ft in American unit or m in Metric unit)

Droplet velocity: Velocity of droplets near the outlet of the nozzle orifice (mph in American unit or m/s in Metric unit)

Droplet diameter: Droplet diameter near the outlet of the nozzle orifice (micron or μm)

Operating pressure: Liquid pressure acting on the nozzle orifice (psi or kPa)

Operating DRIFTSIM

To operate DRIFTSIM, minimum requirements for a computer are Pentium PC with a CD drive, MS-Windows version 3.1 or later, 8 MB of memory, 30 MB free hard drive space, and a mouse.

DRIFTSIM is compact enough to fit on a CD. It can be operated from either a CD or a computer hard drive. DRIFTSIM automatically starts running when the CD containing DRIFTSIM is inserted in the CD drive of the computer. To operate the program from the computer hard drive, DRIFTSIM files and program should be first copied onto the hard drive, and then the user should execute DRIFTSIM.exe file to start the program. The program may run somewhat faster from a hard drive than a CD.

After the program starts, it gives three on-screen boxes for choosing units and droplet size types and entering values of simulation variables. A selection of units or droplet size types can be changed at any time during the operation without needing to exit the program. To change the value of any variable, simply click on the input area next to the variable, and enter a value that is within the acceptable range defined in Table 1. Only two screens appear during the whole calculation process: input and result screens.

Steps to run DRIFTSIM from a CD

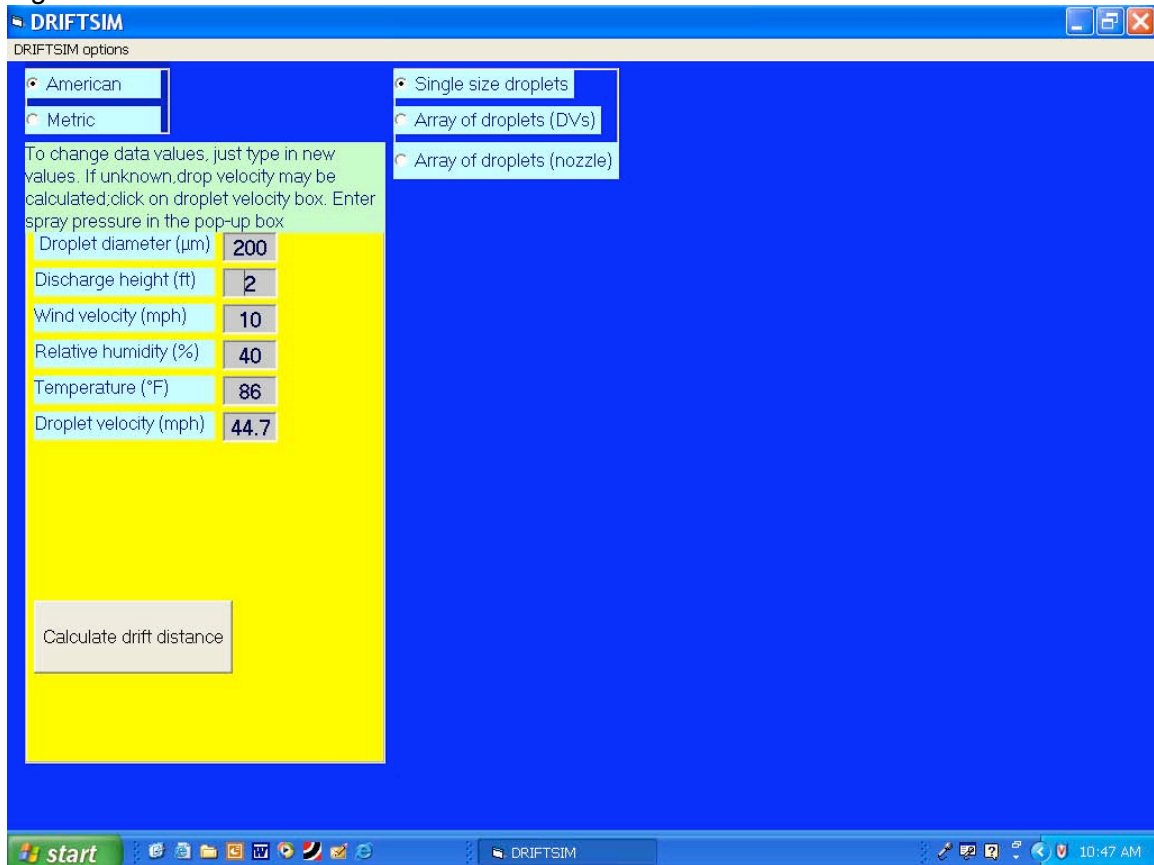
- (1) Insert CD in the computer.
- (2) Introductory information for DRIFTSIM as shown in Figure 1 appears on the screen.

Figure 1



- (3) Click on the “*Start Driftsim*” box. Three on-screen boxes for choosing and entering simulation conditions appear on the screen as shown in Figure 2. [**Note:** initial values for drift variables shown on the screen are built into DRIFTSIM. These values are only examples, not recommended values.]

Figure 2

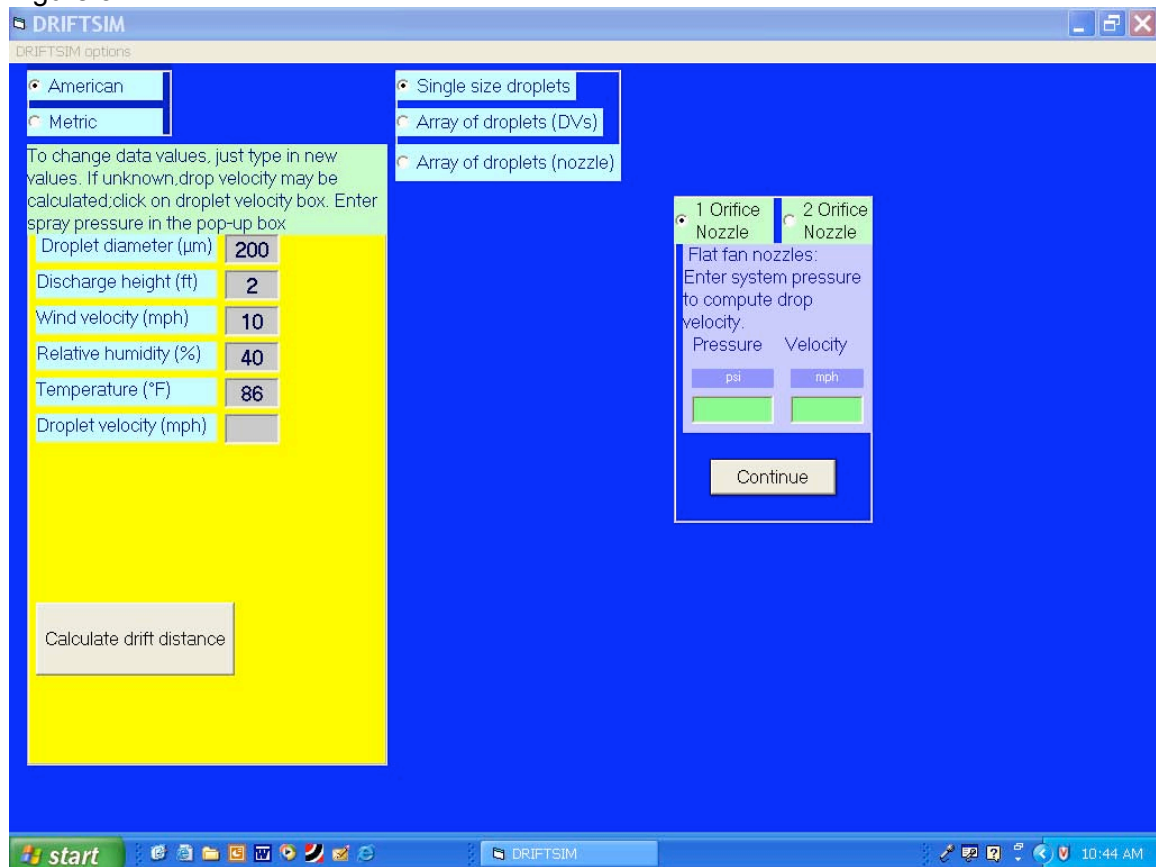


- (4) Select either "American" or "Metric" unit for calculation.
- (5) Select one of the three choices as a type of input for the droplet size: "Single size droplets", "Array of droplets (DVs)", or "Array of droplets (nozzle)".
- (6) For "Single size droplets", follow steps (7) to (11); for "Array of droplets (DVs)", follow steps (12) to (17); for "Array of droplets (nozzle)", follow steps (19) to (23).

[Note: Steps (7) to (11) are for "Single size droplets" only]

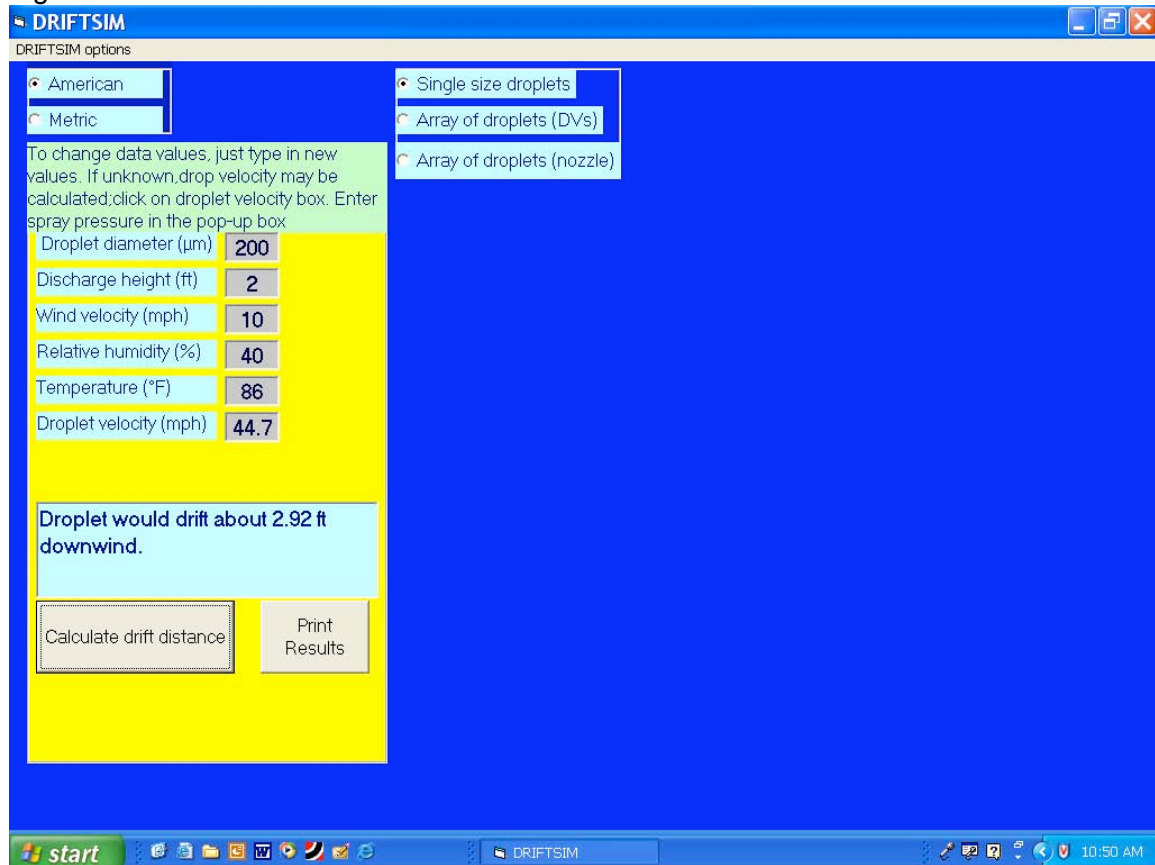
- (7) Enter or change values for "Droplet diameter", "Wind velocity", "Discharge height", "Droplet velocity", "Temperature", "Relative humidity" for inputs of variables. The value of "Droplet velocity" can be entered either by the user, or automatically by the program once the user enters a value for the operating pressure on the box which pops up on the screen as shown in Figure 3 after the user empties the "Droplet velocity" box. A red error message appears in the box under the variables if the value of an individual variable is outside the range defined in Table 1.

Figure 3



- (8) Click on "Compute drift distance" to obtain the results on the screen as shown in Figure 4.

Figure 4

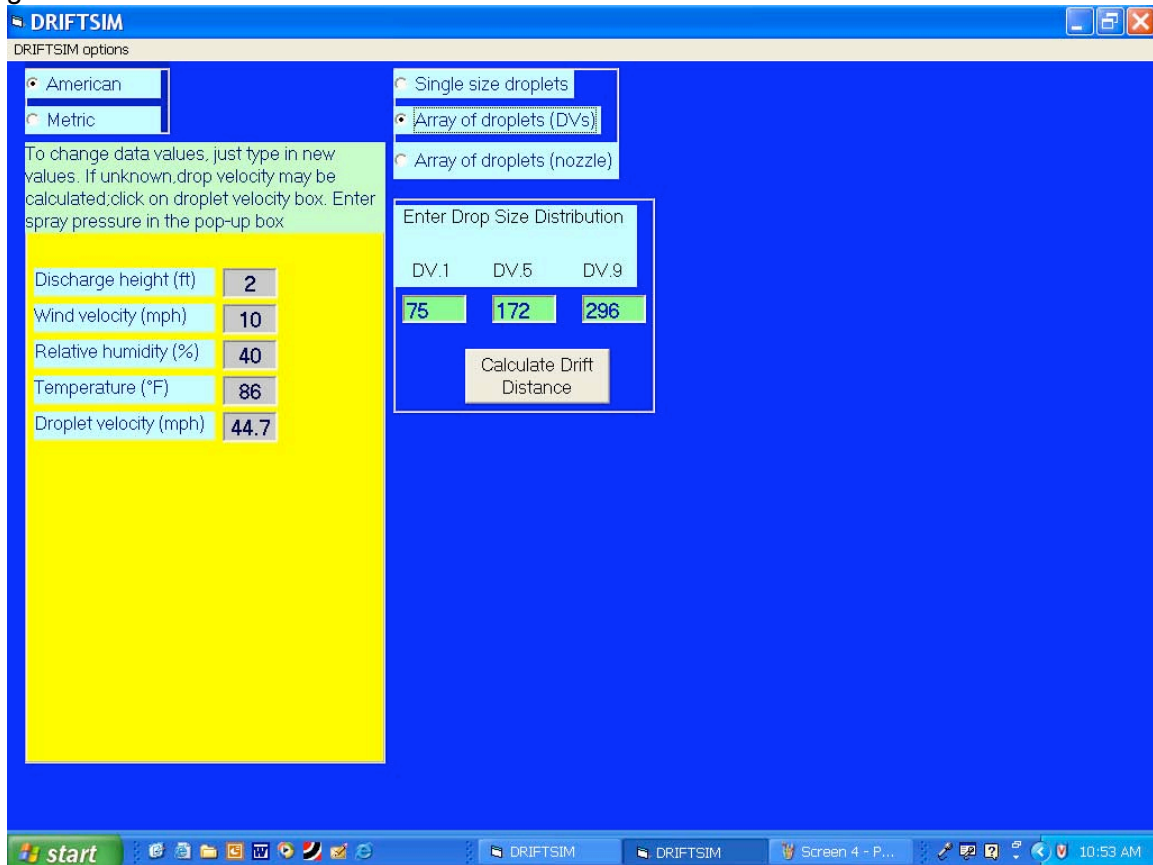


- (9) Click on "Print results" if you want to get a printout of input variables and the result.
- (10) To continue running DRIFTSIM with a new or revised set of inputs for the "single size droplet", repeat steps (7) to (10).
- (11) When you are done with all the simulations, exit DRIFTSIM by clicking on the **X** at the upper right corner of the window on the screen.

[Note: Steps (12) to (17) are for "Array of droplets (DVs)" only]

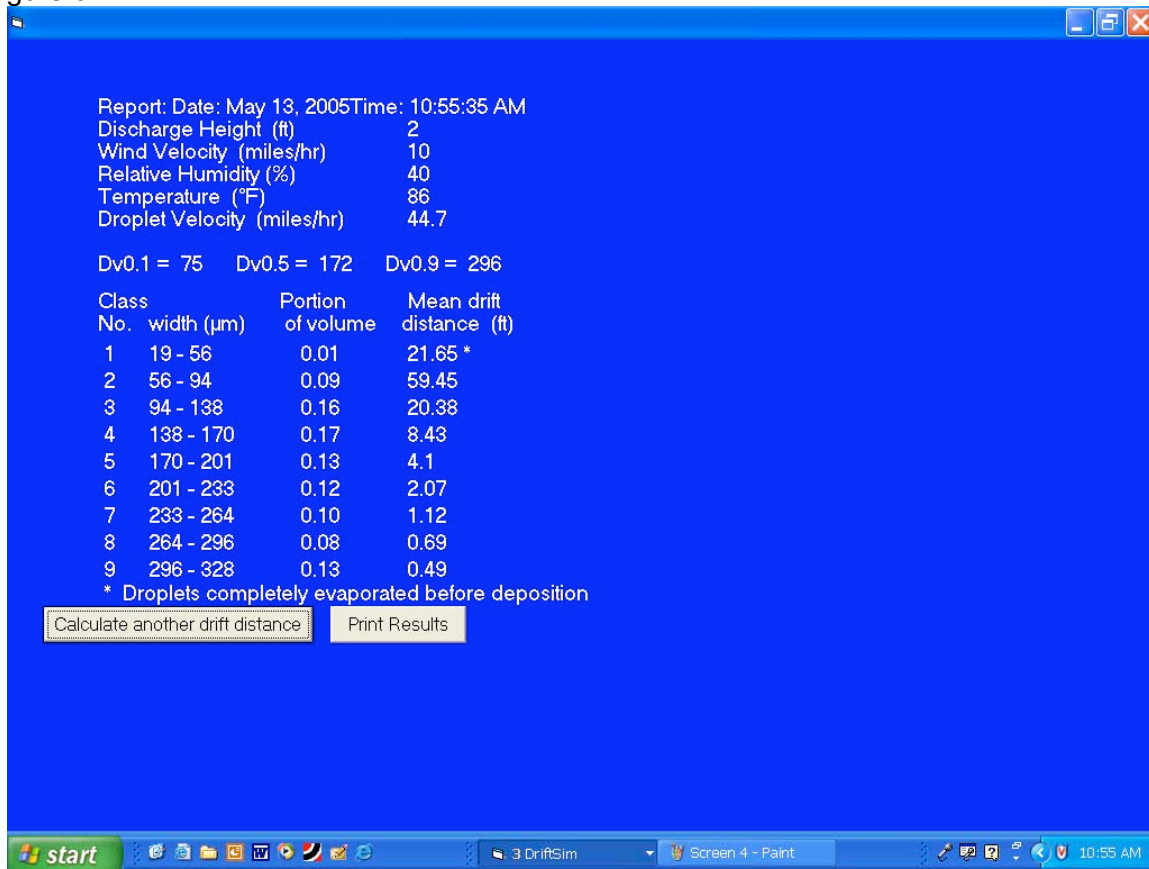
- (12) After choosing "Array of droplets (DVs)", a new box for droplet size distribution appears on the screen as shown in Figure 5.

Figure 5



- (13) Enter " $D_{v,1}$ ", " $D_{v,5}$ " and " $D_{v,9}$ " values in boxes.
- (14) Enter or change values for "Wind velocity", "Discharge height", "Droplet velocity", "Temperature" and "Relative humidity".
- (15) Click on "Calculate Drift Distance". Drift distances of 9 size classes of droplets along with the portion of the spray volume corresponding to each size class appear on the screen as shown in Figure 6. Error message appears on this screen if " $D_{v,1}$ ", " $D_{v,5}$ " and " $D_{v,9}$ " values are not reasonable.

Figure 6

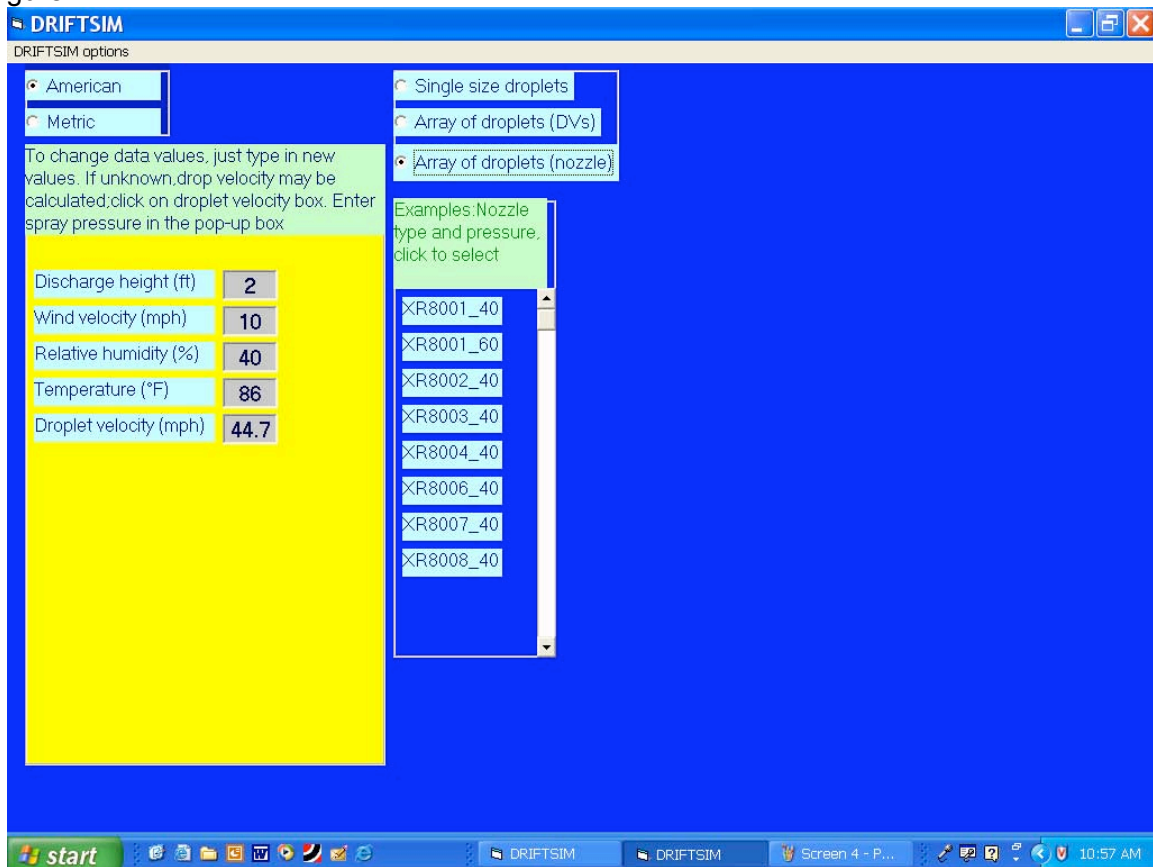


- (16) Click on either “*Print Results*” to get a printout of the results, or “*Calculate another drift distance*” to repeat steps (13) to (16) for a revised or new set of inputs.
- (17) When you are done with all the simulations, exit DRIFTSIM by clicking on the **X** at the upper right corner of the window on the screen.

[Note: Steps (18) to (23) are for “*Array of droplets (nozzle)*” only]

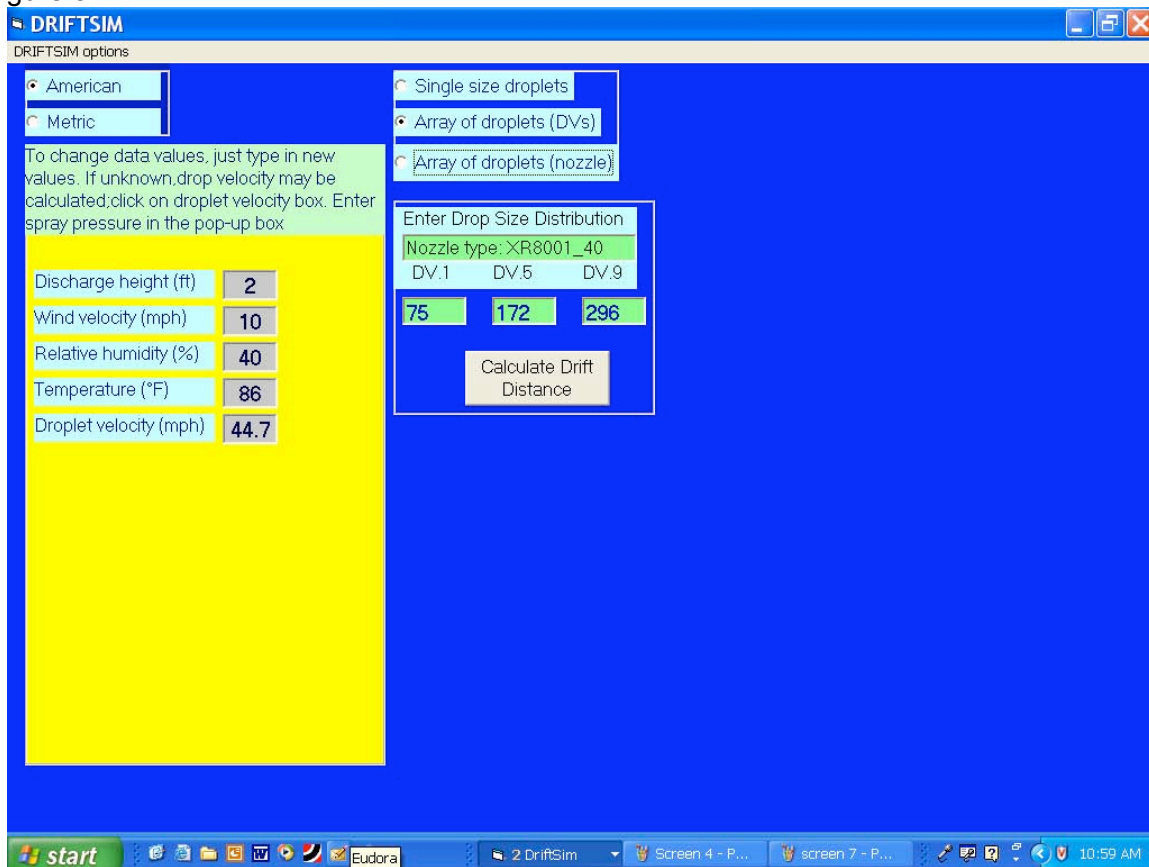
- (18) After choosing “*Array of droplets (nozzle)*”, a new box with a list of several nozzles appears on the screen as shown in Figure 7.

Figure 7



- (19) Click on one of nozzle choices, then " $D_{v,1}$ ", " $D_{v,5}$ " and " $D_{v,9}$ " values automatically appear in boxes for the nozzle chosen, as shown in Figure 8.

Figure 8



- (20) Enter or change values for “*Wind velocity*”, “*Discharge height*”, “*Droplet velocity*”, “*Temperature*”, and “*Relative humidity*”.
- (21) Click on “*Calculate Drift Distance*”. Drift distances of 9 size classes of droplets along with the portion of the spray volume corresponding to each size class appear on the screen as the same as step (15). Error message appears on this screen if “ $D_{v,1}$ ”, “ $D_{v,5}$ ” and “ $D_{v,9}$ ” values are not reasonable.
- (22) Click on either “*Print Results*” to get a printout of the results, or “*Calculate another drift distance*” to repeat steps (18) to (22) for a revised or new set of inputs.
- (23) When you are done with all the simulations, exit DRIFTSIM by clicking on the **X** at the upper right corner of the window on the screen.

Steps to run DRIFTSIM from a computer hard drive

To operate DRIFTSIM from a hard drive, the user should copy both DRIFTSIM subdirectory and all contents in the subdirectory, except AUTORUN.INF and Browsercall.exe, from the CD to the hard drive [**Note:** the subdirectory name must be DRIFTSIM; otherwise, the program will not work]. After the copying process is completed, go to DRIFTSIM subdirectory in the hard drive and click on DriftSim.exe file. DRIFTSIM introductory page should appear on the screen. Then follow steps (3) to (23) above to run the program.

References

- Goering, C.E. and D.B. Smith. 1978. Equations for droplet size distributions in sprays. Transactions of ASAE 21(2): 209-216.
- Reichard, D.L., H. Zhu, R.D. Fox and R.D. Brazee. 1992. Wind tunnel evaluation of a computer program to model spray drift. Transactions of the ASAE 35(3):755-758.
- Zhu, H., D.L. Reichard, R.D. Fox, R.D. Brazee and H.E. Ozkan. 1994. Simulation of drift of discrete sizes of water droplets from field sprayers. Transactions of the ASAE 37(5):1401-1407.
- Zhu, H., D.L. Reichard, R.D. Fox, H.E. Ozkan and R.D. Brazee. 1995. DRIFTSIM, a program to estimate drift distances of spray droplets. Applied Engineering in Agriculture 11 (3): 365-369.

This manual, as well as other information on spray drift, is available at Ohio State University Extension's web site "Ohioline" (<http://ohioline.osu.edu>) by clicking on "Search" and entering "DRIFTSIM" or "spray drift" in the search box.

OSU Extension embraces human diversity and is committed to ensuring that all educational programs conducted by Ohio State University Extension are available to clientele on a nondiscriminatory basis without regard to race, color, age, gender identity or expression, disability, religion, sexual orientation, national origin, or veteran status.

Keith L. Smith, Associate Vice President for Agricultural Administration and Director, OSU Extension

TDD No. 800-589-8292 (Ohio only) or 614-292-1868

**APPLICATION FOR PERMIT
OWL LANDFILL SERVICES, LLC**

**VOLUME III: ENGINEERING DESIGN AND CALCULATIONS
SECTION 9: WAVE ACTION CALCULATIONS**

TABLE OF CONTENTS

Section No.	Title	Page
1.0	INTRODUCTION	III.9-1
1.1	Description	III.9-1
2.0	DESIGN CRITERIA	III.9-2
3.0	CALCULATION	III.9-2
4.0	SUMMARY	III.9-3

LIST OF ATTACHMENTS

Attachment No.	Title
III.9.A	<i>LOW COST SHORE PROTECTION: A GUIDE FOR ENGINEERS AND CONTRACTORS</i> (U.S. ARMY CORPS OF ENGINEERS 2004)
III.9.B	<i>WATER-RESOURCES ENGINEERING</i> (LINSLEY & FRANZINI 1979)

**APPLICATION FOR PERMIT
OWL LANDFILL SERVICES, LLC**

**VOLUME III: ENGINEERING DESIGN AND CALCULATIONS
SECTION 9: WAVE ACTION CALCULATIONS**

1.0 INTRODUCTION

OWL Landfill Services, LLC (OWL) is proposing to permit, construct, and operate a “Surface Waste Management Facility” for oil field waste processing and disposal services. The proposed OWL Facility is subject to regulation under the New Mexico (NM) Oil and Gas Rules, specifically 19.15.36 NMAC, administered by the Oil Conservation Division (OCD). The Facility has been designed in compliance with the requirements of 19.15.36 NMAC, and will be constructed, operated, and closed in compliance with a Surface Waste Management Facility Permit issued by the OCD.

The OWL Facility is one of the first designed to the new more stringent standards that, for instance, mandate double liners and leak detection for land disposal. The new services that OWL will provide fill a necessary void in the market for technologies that exceed current OCD requirements.

1.1 Description

The OWL Surface Waste Management Facility will comprise approximately 500 acres of the 560-acre site, and will include two main components: an oil field waste Processing Area and an oil field waste Landfill, as well as related infrastructure. Oil field wastes are anticipated to be delivered to the OWL Facility from oil and gas exploration and production operations in southeastern NM and west Texas. The Site Plan provided as **Figure II.1.2** identifies the locations of the Processing Area and Landfill facilities, which are further detailed on the **Permit Plans (Volume III.1)**. The proposed facilities are detailed in **Table II.1.2**, and are anticipated to be developed in four primary phases as described in **Table II.1.3**. The design of the OWL facilities shown on Figures and Permit Plans is preliminary; and construction plans and specifications for each major element will be submitted to OCD in advance of installation.

2.0 DESIGN CRITERIA

The purpose of the Wave Action Calculations presented herein is to provide the wave height and run-up for the evaporation ponds proposed for the OWL Processing Area. The OWL Processing Area is planned to include up to 12 evaporation ponds, approximately 420 feet (ft) in length and 200 ft in width, each with a capacity of approximately 9.5 acre-ft. These calculations assume a pond length of 420 ft and a conservative wind speed of 75 miles per hour (mph). Wave height and run-up must be less than the 3.5 ft of freeboard provided in the pond design. The methodology applied for determining wave height and run-up in reservoirs for the Wave Action Calculations is provided in two documents, *Low Cost Shore Protection: A Guide for Engineers and Contractors* (U.S. Army Corps of Engineers 2004; (**Attachment III.9.A**); and *Water-Resources Engineering* (Linsley & Franzini 1979; **Attachment III.9.B**).

3.0 CALCULATION

The fastest mile wind speed for a 25-year return period was obtained from Figure 16, **Attachment III.9.A**. The fastest mile wind speed is approximately 75 mph for the OWL site vicinity.

Wave height in a pond is estimated using the following equation (i.e., page 166, Equation 7-4, **Attachment III.9.B**):

$$Z_w = 0.034 (V_w)^{1.06} F^{0.47}$$

Where: Z_w = height of wave (feet)
 V_w = wind speed (mph) = 75 mph
 F = fetch length (miles) = 420 feet/5,280 feet/mile = 0.080 miles

Therefore: $Z_w = 0.034 (75 \text{ mph})^{1.06} (0.080 \text{ miles})^{0.47}$

$$Z_w = 0.034 (97.2) (0.30)$$

$$Z_w = 0.99 \text{ feet} = \text{height of wave in pond due to a 75 mph wind}$$

The height of wave runup for a smooth (i.e., HDPE liner) surface can be obtained from Table 11, **Attachment III.9.A**. On Table 11, $R = 1.75H$ for a 2.5H:1V smooth slope and $R = 1.50H$

for a 4.0H:1V smooth slope. Interpolating between these two values a value of $R = 1.68H$ is obtained for a 3.0H:1V smooth slope. Therefore:

Wave Runup = $1.68H = 1.68 (0.99 \text{ feet}) = 1.66 \text{ feet}$ for a 3H:1V smooth sideslope.

Total: Wave height + Wave run-up = $0.99 \text{ feet} + 1.66 \text{ feet} = 2.65 \text{ feet}$

4.0 SUMMARY

When considering a conservative 75 mph wind across the length of the pond, a wave height of 0.99 ft is calculated. This wave will run-up approximately 1.66 ft up the sideslope of the pond. The ponds have been design with a minimum freeboard of 3.5 ft which will provide adequate protection against the combined potential impact of waves, wave run-up, and simultaneous rainfall event (i.e., 25 year, 24 hour rainfall = 4.31”) with a sufficient Factor of Safety (FS) of over 0.5 ft. In addition, the berm to be constructed west of the entire pond area is lined to an additional height of at least 10 ft, providing additional potential drift protection (see **Permit Plans, Volume III.1**)

**APPLICATION FOR PERMIT
OWL LANDFILL SERVICES, LLC**

**VOLUME III: ENGINEERING DESIGN AND CALCULATIONS
SECTION 9: WAVE ACTION CALCULATIONS**

ATTACHMENT III.9.A

***LOW COST SHORE PROTECTION: A GUIDE FOR ENGINEERS AND
CONTRACTORS (U.S. ARMY CORPS OF ENGINEERS 2004)***

LOW COST SHORE PROTECTION

... a Guide for Engineers and Contractors

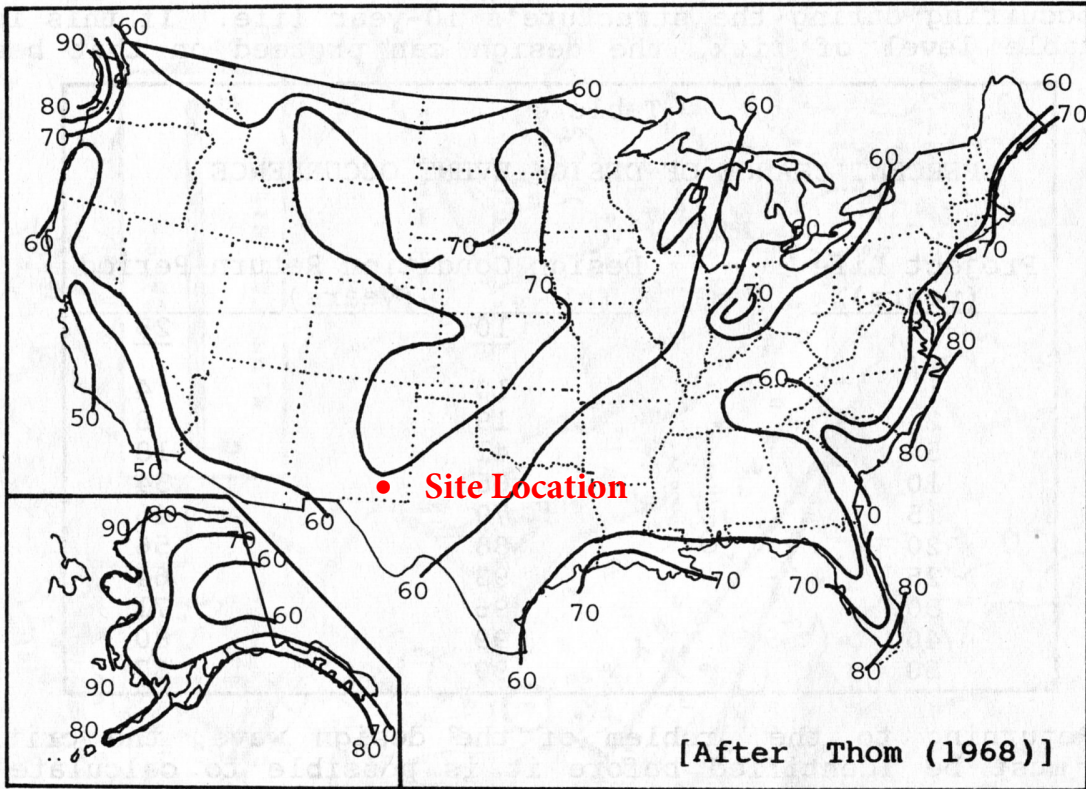


Figure 15 Fastest-Mile Wind Speeds: 10-year Return Period

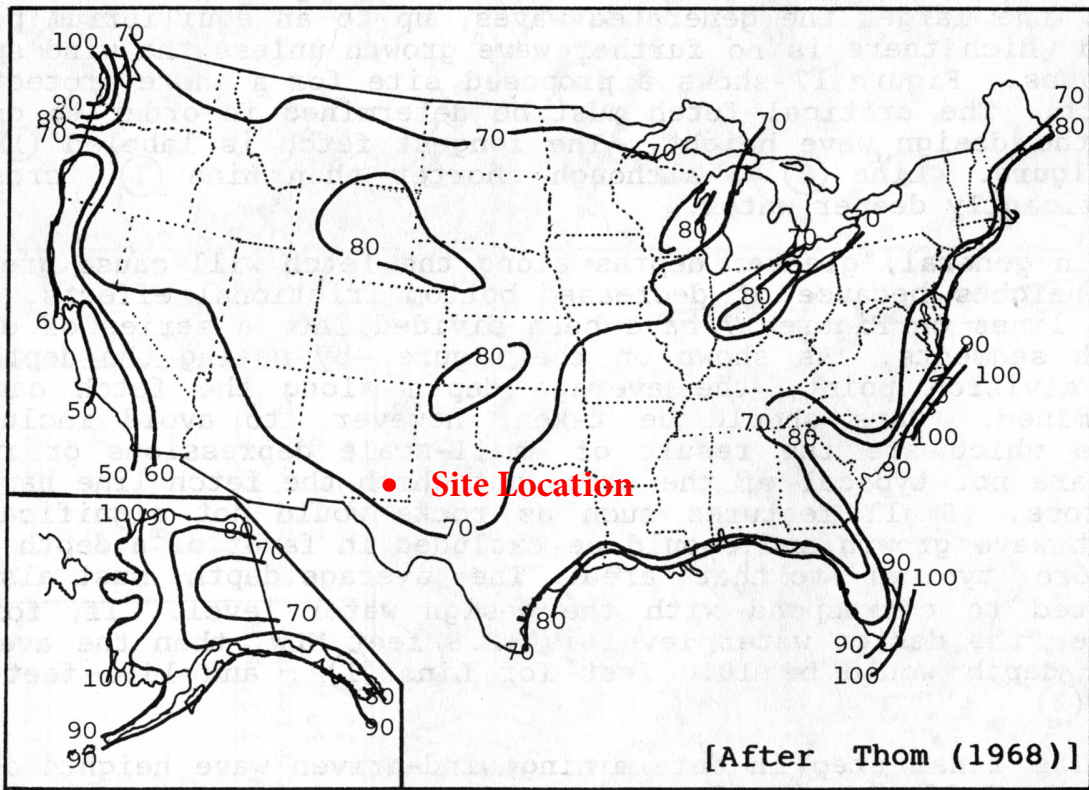


Figure 16 Fastest-Mile Wind Speeds: 25-year Return Period

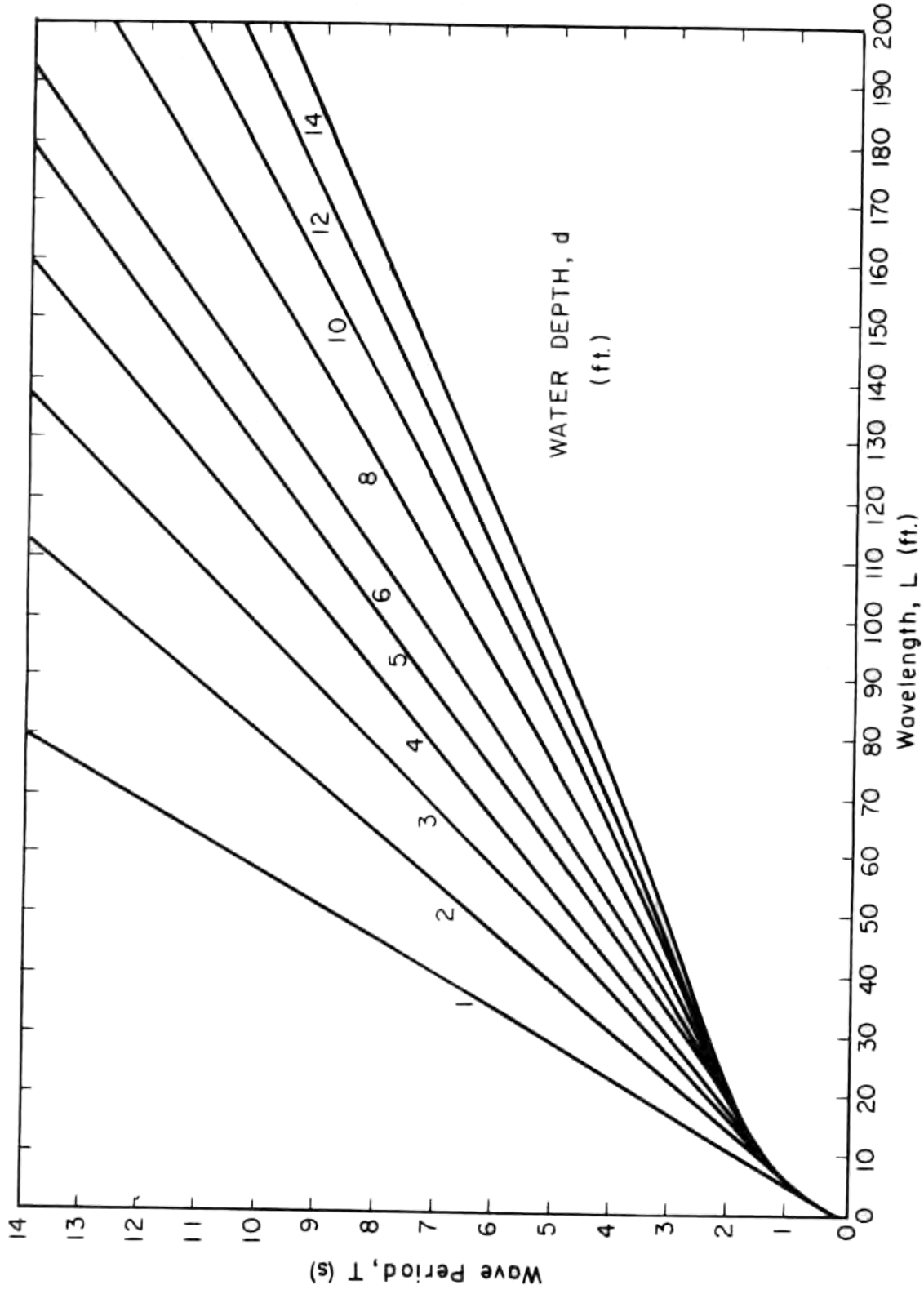


Figure 26 Local Wavelength Given Depth and Period
 [After Giles and Eckert (1979)]

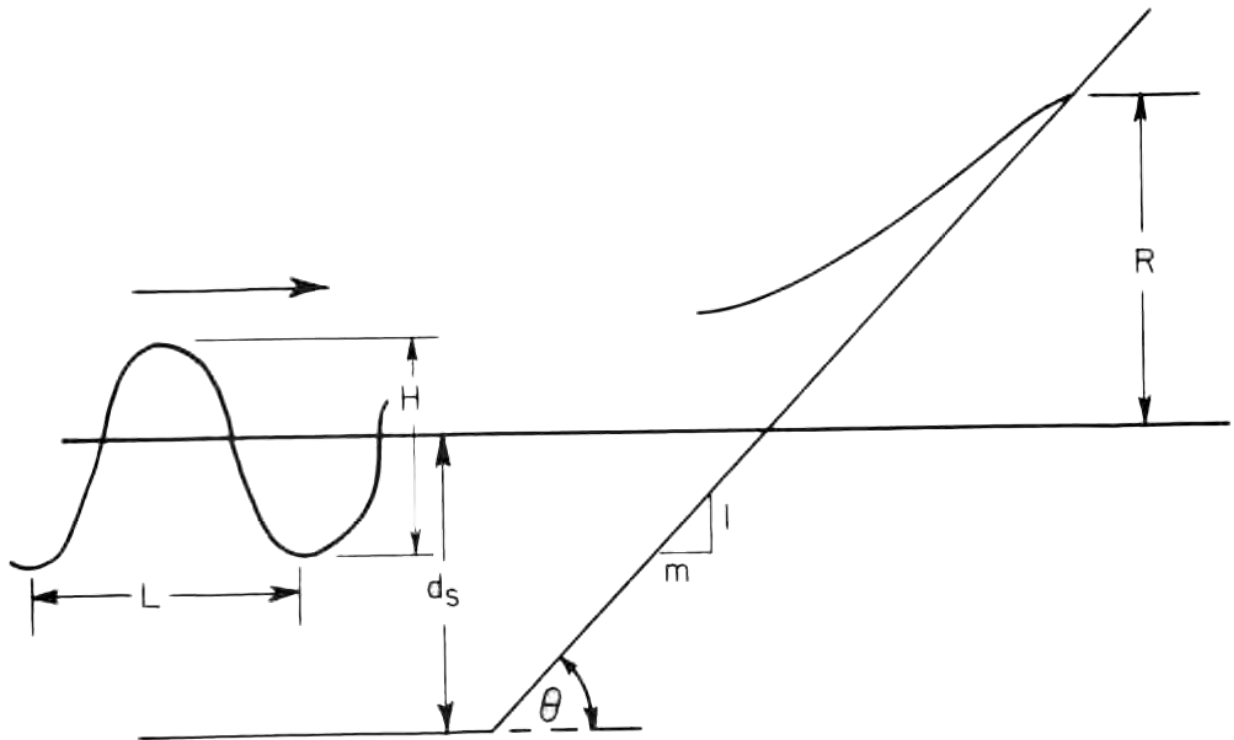


Figure 27 Wave Runup Definition Sketch

For STEPPED slopes, Stoa (1979) recommends using 70 to 75 percent of the smooth slope runup if the risers are vertical, and 86 percent if the edges are rounded.

A rough approximation of the runup height can be obtained from Table 11. However, the values in the table tend to represent the upper bound of the available data and may result in over design. Equations (13) and (14) or the methods given in Stoa (1978) and (1979) are recommended.

If it is impossible or undesirable to build a structure to the recommended height, a splash apron should be provided at the top of the structure. These are generally constructed of rock and they prevent the ground at the top from being eroded and undermining that portion of the structure.

Environmental Factors

Many different materials can be used to construct shore protection structures, including rock, concrete, timber, metal and plastics. The choice often depends on the desired permanence of the protection. Durable materials usually cost considerably more than shorter-lived materials used for temporary protection. The choice of materials is important because the coastal environment is a harsh testing ground for all man-made structures. Aside from wave forces, which are formidable in and of themselves, a host of chemical, biological and other factors can degrade structural materials. A brief review of these follows.

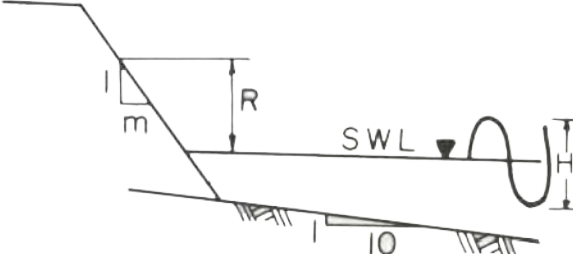
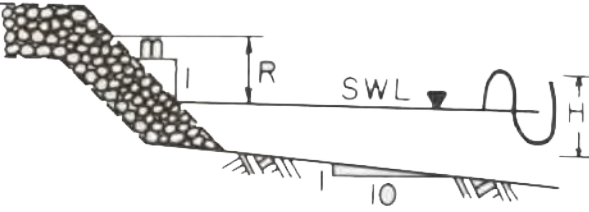
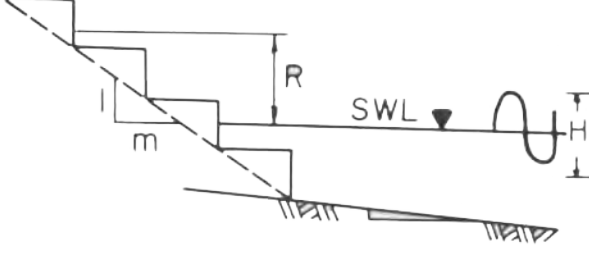
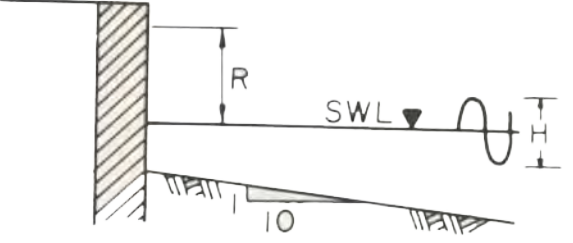
 <p>SMOOTH FACE</p>	<p><u>m</u></p> <p>1.5</p> <p>2.5</p> <p>4.0</p>	<p><u>R</u></p> <p>2.25H</p> <p>1.75H</p> <p>1.50H</p>
 <p>ROUGH FACE</p>	<p><u>m</u></p> <p>1.5</p> <p>2.5</p> <p>4.0</p>	<p><u>R</u></p> <p>1.25H</p> <p>1.00H</p> <p>0.75H</p>
 <p>STEPPED FACE</p>	<p><u>m</u></p> <p>1.5</p>	<p><u>R</u></p> <p>2.00H</p>
 <p>VERTICAL FACE</p>	<p><u>m</u></p> <p>—</p>	<p><u>R</u></p> <p>2.00H</p>

Table 11 Wave Runup Heights

**APPLICATION FOR PERMIT
OWL LANDFILL SERVICES, LLC**

**VOLUME III: ENGINEERING DESIGN AND CALCULATIONS
SECTION 9: WAVE ACTION CALCULATIONS**

**ATTACHMENT III.9.B
WATER-RESOURCES ENGINEERING
(LINSLEY & FRANZINI 1979)**

WATER-RESOURCES ENGINEERING

THIRD EDITION

Ray K. Linsley

*Professor Emeritus of Hydraulic Engineering
Stanford University*

Partner, Linsley, Kraeger Associates

Joseph B. Franzini

*Professor of Civil Engineering
Associate Chairman, Department of Civil Engineering
Stanford University*

McGraw-Hill Book Company

New York St. Louis San Francisco Auckland Bogotá Düsseldorf
Johannesburg London Madrid Mexico Montreal New Delhi Panama
Paris São Paulo Singapore Sydney Tokyo Toronto

by ordinary earth-moving methods would be expensive unless the excavated sediment has some sales value.

7-9 Wind setup and waves in reservoirs Earth dams must have sufficient freeboard above maximum pool level so that waves cannot wash over the top of the dam. Waves in reservoirs may also damage shoreline structures and embankments adjacent to the water and interfere with navigation. Part of the design of any reservoir is an estimate of wind setup and wave height.

Wind setup is the tilting of the reservoir water surface caused by the movement of the surface water toward the leeward shore under the action of the wind. This current of surface water is a result of tangential stresses between the wind and the water and of differences in atmospheric pressure over the reservoir. The latter, however, is, typically, a smaller effect. As a consequence of wind setup, the reservoir water surface is above normal still-water level on the leeward side and below the still-water level on the windward side. This results in hydrostatic unbalance, and a return flow at some depth must occur. The water-surface slope which results is that necessary to sustain the return flow under conditions of bottom roughness and cross-sectional area of flow which exist. Wind setup is generally larger in shallow reservoirs with rough bottoms.

Wind setup may be estimated from

$$Z_s = \frac{V_w^2 F}{1400d} \quad (7-3)$$

where Z_s is the rise in feet (meters) above still-water level, V_w is the wind speed in miles (kilometers) per hour, F is the *fetch* or length of water surface over which the wind blows in miles (kilometers), and d is the average depth of the lake along the fetch in feet (meters). In SI metric units, the constant in the denominator becomes 63,200.

Equation (7-3) is modified¹ from the original equation developed by Dutch engineers on the Zuider Zee. Additional information and techniques are given in other references.² Wind-setup effects may be transferred around bends in a reservoir and the value of F used may be somewhat longer than the straight-line fetch.

When wind begins to blow over a smooth surface, small waves, called capillary waves, appear in response to the turbulent eddies in the wind stream. These waves grow in size and length as a result of the continuing push of the wind on the back of the waves and of the shearing or tangential force between the wind and the water. As the waves grow in size and length, their speed increases until they move at speeds approaching the speed of the wind. Because growth of a wave depends in part upon the difference between wind speed and wave speed, the growth rate approaches zero as the wave speed approaches the wind speed.

¹ T. Saville, Jr., E. W. McClendon, and A. L. Cochran, Freeboard Allowances for Waves in Inland Reservoirs, *J. Waterways and Harbors Div., ASCE*, pp. 93-124, May, 1962.

² Shore Protection, Planning and Design, *Tech. Rept. 3*, 3d ed., U.S. Army Coastal Engineering Research Center, June, 1966.

The duration of the wind and the time and direction from which it blows are important factors in the ultimate height of a wave. The variability of the wind and the amazingly complex and yet to be fully understood response of the water surface to the wind lead to a wave pattern that is a superposition of many waves. The pattern is often described by its energy distribution or spectrum. The growth of wind waves as a function of fetch, wind speed, and duration can be calculated from knowledge of the mechanism of wave generation and use of collected empirical results.¹ The duration of the wind and the fetch play an important role because a wave may not reach its ultimate height if the wave passes out of the region of high wind or strikes a shore during the growth process. The depth of water also plays a key role, tending to yield smaller and shorter waves in deep water.

Wave-height data gathered at two major reservoirs² confirm the theoretical and experimental data for ocean waves if a modified value of fetch is used. The derived equation is

$$z_w = 0.034V_w^{1.06}F^{0.47} \quad (7-4)$$

¹ W. J. Pierson, Jr., and R. W. James, *Practical Methods for Observing and Forecasting Ocean Waves*, U.S. Navy Hydrographic Office Pub. 603, 1955 (reprinted 1960).

² T. Saville, Jr., E. W. McClendon, and A. L. Cochran, *Freeboard Allowances for Waves in Inland Reservoirs*, *J. Waterways and Harbors Div.*, ASCE, pp. 93-124, May, 1962.

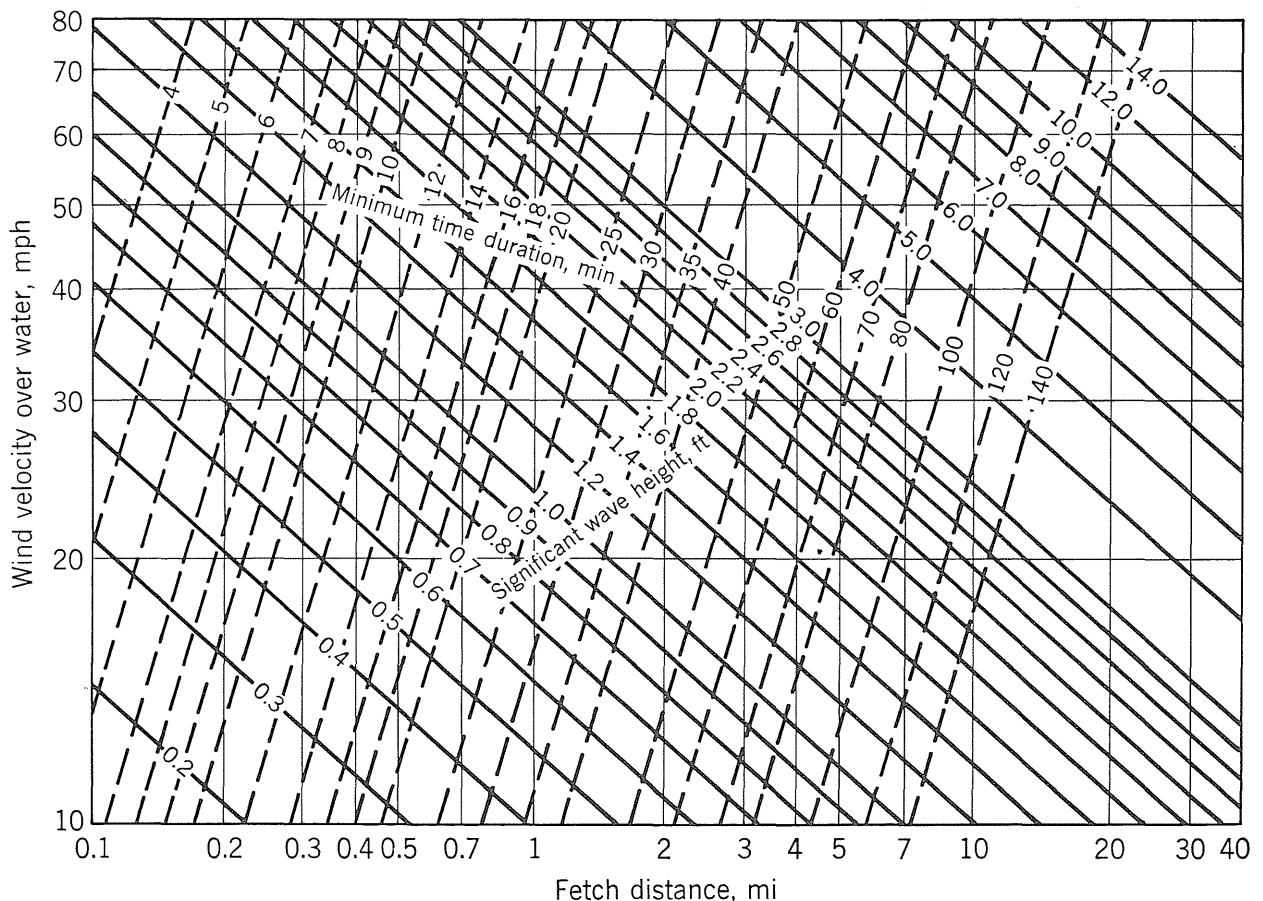


Figure 7-14 Significant wave heights and minimum wind durations (from Saville, McClendon, and Cochran). For metric version see Appendix B.

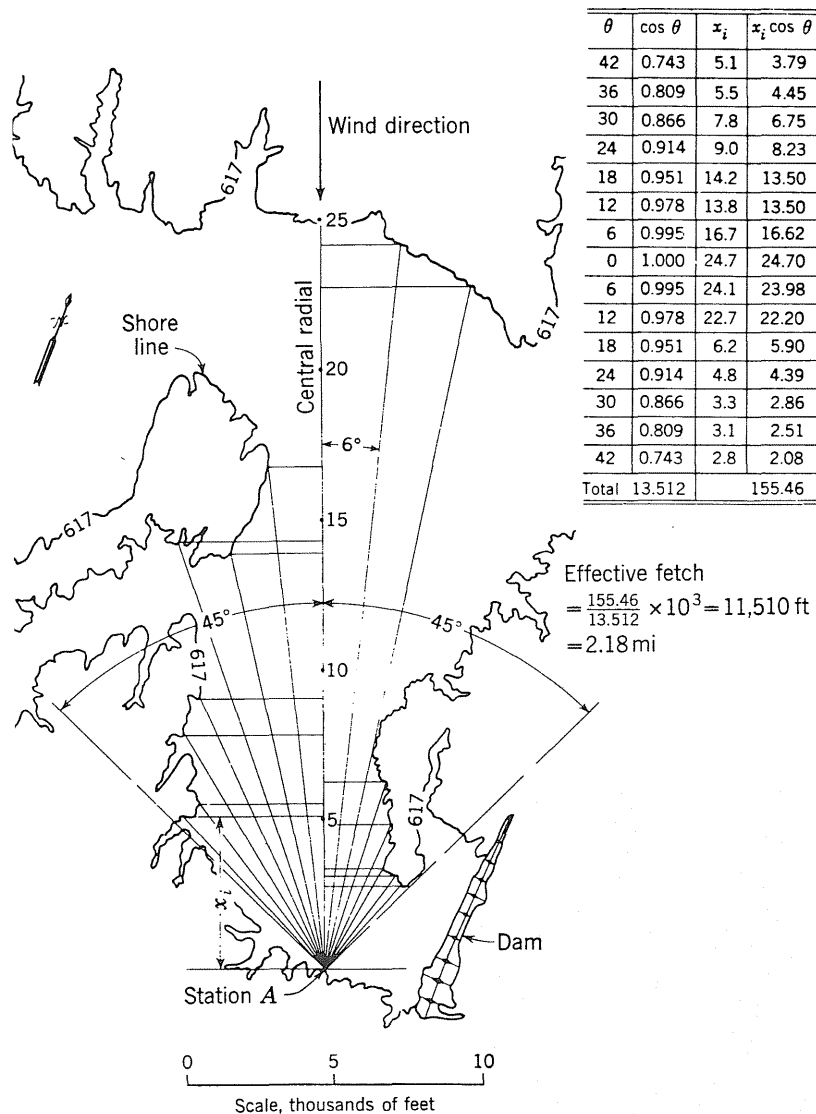


Figure 7-15 Computation of effective fetch. (Modified from Saville, McClendon, and Cochran)

where z_w is the average height in feet (meters) of the highest one-third of the waves and is called the *significant wave height*, V_w is the wind velocity in miles (kilometers) per hour about 25 ft (7.6 m) above the water surface, and F is the fetch in miles (kilometers). In SI metric units the coefficient becomes 0.005. The equation is shown graphically in Fig. 7-14¹ together with lines showing the minimum duration of wind required to develop the indicated wave height. Figure 7-15 shows the method of computing the effective fetch for a narrow reservoir.

Since the design must be made before the reservoir is complete, wind data over land must generally be used. Table 7-2 gives ratios of wind speed over land to those over water and may be used to correct observed wind to reservoir conditions. Waves are critical only when the reservoir is near maximum levels. Thus in selecting the critical wind speed for reservoirs subject to seasonal fluctuations,

¹ A graph for the solution of Eq. (7-4) in SI metric units is given in Appendix B-1.

Table 7-2 Relationship between wind over land and that over water. (After Saville, McClendon, and Cochran)

Fetch, mi (km)	0.5 (0.8)	1 (1.6)	2 (3.2)	4 (6.5)	6 (9.7)	8 (12.9)
$V_{\text{water}}/V_{\text{land}}$	1.08	1.13	1.21	1.28	1.31	1.31

only winds which can occur during the season of maximum pool levels should be considered. The direction of the wind and the adopted fetch must also be the same.

The height of the significant wave is exceeded about 13 percent of the time. If a more conservative design is indicated, a higher wave height may be chosen. Table 7-3 gives ratios of z'/z_w for waves of lower exceedance.

When a wave strikes a land slope, it will *run up* the slope to a height above its open-water height. The amount of run-up depends on the surface. Figure 7-16 shows the results of small-scale experiments¹ on smooth slopes and rubble mounds. Height of run-up z_r is shown as a ratio z_r/z_w and is dependent on the ratio of wave height to wavelength (wave steepness). Wavelength λ for deep-water waves may be computed from

$$\lambda = 5.12t_w^2 \text{ ft} \quad \text{or} \quad \lambda = 1.56t_w^2 \text{ m} \quad (7-5)$$

where the wave period t_w is given by

$$t_w = 0.46V_w^{0.44}F^{0.28} \quad (7-6)$$

For shallow-water waves other length relations are appropriate.² In metric units the coefficient of Eq. (7-6) becomes 0.32. The curves for rubble mounds represent extremely permeable construction, and for more typical riprap on earth embankments the run-up may be somewhat higher, depending on both the permeability and the relative smoothness of the surface.

¹ T. Saville, Jr., Wave Run-up on Shore Structures, *Trans., ASCE*, Vol. 123, pp. 139–158, 1958; R. Y. Hudson, Laboratory Investigation of Rubble-mound Breakwaters, *Trans. ASCE*, Vol. 126, Part IV, pp. 492–541, 1962.

² Shore Protection, Planning and Design, *Tech. Rept. 3*, 3d ed., U.S. Army Coastal Engineering Research Center, June, 1966.

Table 7-3 Percentage of waves exceeding various wave heights greater than z_w . (After Saville, McClendon, and Cochran)

z'/z_w	1.67	1.40	1.27	1.12	1.07	1.02	1.00
Percentage of waves $> z'$	0.4	2	4	8	10	12	13

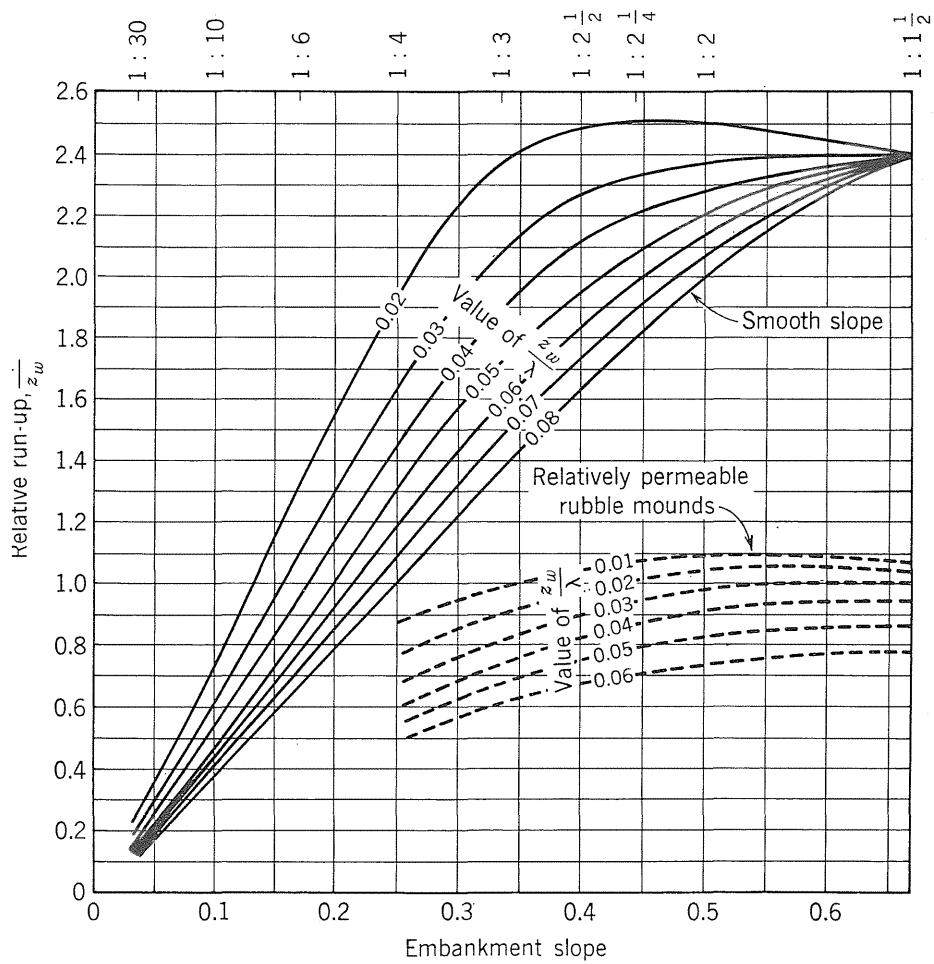


Figure 7-16 Wave run-up ratios versus wave steepness and embankment slopes. (From Saville, McClendon, and Cochran)